5-2021

Metamaterial Inspired Multi-Band Antenna for MM-Wave 5G Wireless Communication

Mohammad Ashif Hossain Chowdhury
The University of Texas Rio Grande Valley

METAMATERIAL INSPIRED MULTI-BAND ANTENNA

FOR MM-WAVE 5G WIRELESS COMMUNICATION

A Thesis

by

MOHAMMAD ASHIF HOSSAIN CHOWDHURY

Submitted to the Graduate College of
The University of Texas Rio Grande Valley
In partial fulfillment of the requirements for the degree of

MASTER OF SCIENCE IN ENGINEERING

May 2021

Major Subject: Electrical Engineering

METAMATERIAL INSPIRED MULTI-BAND ANTENNA FOR MM-WAVE 5G WIRELESS COMMUNICATION

A Thesis
by
MOHAMMAD ASHIF HOSSAIN CHOWDHURY

COMMITTEE MEMBERS

Dr. Heinrich Foltz
Supervisor and Committee Chair

Dr. Nantakan Wongkasem
Co-Supervisor and committee member

Dr. Yong Zhou
Committee Member

May 2021

ABSTRACT

Chowdhury, Mohammad Ashif Hossain, Metamaterial Inspired Multi-band Antenna for mm-wave 5G Wireless Communication. Master of Science in Engineering (MSE), May 2021, 76 pp., 6 tables, 68 figures, references, 55 titles

Due to the constant demand for speed and capacity in wireless communication, mm-wave bands are getting special interest. Most of the high speed 5G bands are in mm-wave region. As the mm-wave signal is prone to absorption and faces a significant free space path loss, an antenna with narrow beam, high gain, and high efficiency is required. The antenna also need to be working in multiple frequencies, as there are multitude of mm-wave frequencies allocated by the regulator for 5G communication. In this study we designed an antenna capable of working in high 5G bands consisting of 25GHz,28GHz, and 38GHz. The idea of metasurface is used to make the antenna resonant for multiple frequencies of mm-wave operation. The structure is tapered and curved in multiple places to funnel the flow of surface current, thereby generating a very sharp beam. In numerical analysis using CST microwave studio, the efficiency is found to be around 90% and the average gain is approximately 4dB,combining all three bands.

DEDICATION

I dedicate my master's thesis to my loving mother FAIZUN NESSA, without whose struggles I wouldn't have reached this point in my life. I also dedicate this thesis to the people who brought me up since my childhood, gave me a home after my father's death, and took care of me as their own child. They are my honorable maternal grandmother FAZILUTUN NESSA, my honorable maternal grandfather Dr. SHOFIUL ALAM CHOWDHURY, and all my maternal uncles. I am eternally indebted to them for each and every success of my life.

ACKNOWLEDGEMENTS

First of all, I would like to acknowledge all the opportunities ALLAH had given me throughout my life. I strongly believe that it is only with his blessings I came this far in life.

Secondly, I will be always grateful to my honorable supervisor Dr. Heinrich Foltz for his continuous guidance throughout my MS studies. His faith in me, while I was questioning my abilities, is a testament to how great a mentor he is. His motivations amidst my many failures were a beacon of hope for me. Without his continuous support it would have been a rough journey throughout my MS study. Along with his mental and academic support, he provided me with financial support during the period I needed it most. I will be forever grateful to him for everything he did for me. I must also mention the name of Dr. Nantakan Wongkasem, because of whom I am now a sound user of the electromagnetic simulation software CST. Her continuous effort in teaching the basics of electromagnetic metamaterials greatly helped my thesis, which is based on a metamaterial design. It will be an injustice not to mention my roommates Sk Ali Zaker Shawon, Md Shakil Arman, and S M Zia Uddin . They were my family away from family. I will never forget those long nights of discussions ranging from politics to religion, long drives in Austin and Houston, and all the marathon cooking runs we went through together. I will miss them forever. I will be doing wrong if I don’t mention Dr. Hasina Huq’s name in my acknowledgement. She had been helping me with my MS studies, since I started in the summer

of 2019. I am forever indebted to here for the troubles she went through for me. Lastly, I would like to acknowledge the immense mental support I got, and we all continue to get from the Bangladeshi community in the valley. I thank each and every one of the Bangladeshi students and families for being there to support us mentally. I must also thank Dr. Parwinder Grewal for initiating the PGRA program, without which it would've been a dream for me to achieve an MS degree from an US institution.

TABLE OF CONTENTS

Page

LIST OF TABLES

Page

LIST OF FIGURES

Page

CHAPTER I

INTRODUCTION

1.1: Background and Motivation for Study

Since the dawn of wireless communications, the need for speed inspired all the research and development in this field. We have come a long way from the first-generation analog voice call to fourth generation mobile broadband internet, due to these developments. But, as more and more devices are getting added to the Internet, the existing Wi-Fi, GSM,3G, and 4G bands are getting crowded and more capacity is needed to serve all the customers. Compared to 2010, demand for wireless data traffic is projected to increase 3000-30000 times by 2030[11]. All this extra demand for capacity and speed cannot be served by current technologies such as Long Term Evolution- advanced(LTE-A) and Wi-Fi, due to their design limitations[12]. To tackle these problems fifth generation radio access technology(5G) is introduced. It is a significantly faster system with a data rate requirement of 10Gbps, latency of approximately 1ms, and at least twice the spectral efficiency of the 4G technology [13]. To accommodate this high speed and high capacity system, less congested portions of the spectrum are required. This is where millimeter wave(mm-wave) bands play an important role in increasing the speed of the 5G system[14] . Studies have shown that, gigabit-per-second data rates were possible with indoor

and fixed outdoor mm-wave wireless systems[15]. Moreover, advances in mm-wave hardware technology and the availability of the spectrum in frequencies higher than the regular sub 6 GHz have motivated companies and regulators alike to move towards mm-wave spectrum for wireless communication channels with more speed and capacity[16][14]. For example, Federal Communications Commission (FCC) has designated the 24GHz, 28GHz, 37GHz,39GHz, and 47GHz bands as the frequencies for 5G communications in the higher-band. They are also planning to designate two extra bands at 26GHz, and 42 GHz for 5G communications. There are also mid-bands and low-bands for more wide area of 5G coverage. But, most of the spectrums allocated are in the higher centimeter wave or mm-wave range. Concentration of these many 5G allocations in the mm-wave band is indicative of the importance of it for high speed wireless communications.

With all its potential, the mm-wave spectrum has its fair share of disadvantages. As the Free Space Path Loss of RF signals increase with increasing frequency of operation[17], signals at mm-wave frequencies will cover lot less area than the current wireless communication channels at and below 6GHz frequency. Signals at these frequencies also get absorbed by the ionosphere, building walls, atmospheric gases, and attenuated heavily by foliage and raindrops[18][19][20]. Measurement data from New York City and Austin, Texas is also indicative of those effects on mm-wave signals, suggesting that the communication using mm-wave technology will heavily rely on high gain directional antennas with Massive MIMO and beamforming [21].

1.2: Objective

The scope of this study is to design an small antenna element that could be integrated with a mm-wave 5G communication system, fulfilling all the major criteria such as high gain, ability to be used in massive MIMO, and beamforming capability. The concept of this antenna is based on the metamaterial structure. The objective is to design an antenna capable of working in multiple mm-wave bands such as 24GHz,28GHz, and 38GHz. In this thesis first we talk about previous work. Then we discuss our design and optimization procedure using EM simulation software CST(Computer Simulation Technology). Later we compare both simulated and experimental results, thereby drawing a conclusion on our final design.

CHAPTER II

LITERATURE REVIEW

2.1 Metamaterials

Since the antenna is based on the idea of metamaterial structures, it is only befitting to start the discussion with the description of metamaterial. These materials or structures are engineered artificially to exhibit electromagnetic properties, otherwise not present in nature. [22]. Physical properties related to Electric and Magnetic fields, which are permittivity(ε) and permeability(μ) respectively, are being manipulated to generate a negative refractive index. Pendry et. al. demonstrated that characteristics similar to that of a metal's plasma frequency could be produced in GHz frequency range by periodic placement of thin metal strips, which in turn will generate negative permittivity[23]. They also demonstrated that non-magnetic metallic strips placed in a split ring setup could be excited to magnetic resonance by an incoming EM wave, which in turn lets us manipulate permeability[24]. Smith et. al. [25] have shown that by combining findings from [23] [24] a passband could be generated where both permittivity and permeability are negative, for certain ranges of lattice parameter in the periodic arrangement of SRRs and thin metal strip. This way negative index of refraction could be generated for a certain frequency band in the GHz range. Now these special features of metamaterials make them suitable for various applications like sensor[26][27][28][29][30], antenna[31][3][32][33],

optics[34][35][36][37], invisibility cloak[38][39], absorbers[40], and so on. Since our antenna is based on a metamaterial structure, we will primarily focus our discussion on antennas inspired by metamaterials in the next section.

2.2 Metamaterial Inspired Antennas

In this section we will discuss about the antennas inspired by metamaterial structures. There are all sorts of antennas at multiple of frequency bands, which are designed using the idea of metamaterial geometry. For instance, the work by Hasan et. al. [1] presented an antenna designed for traditional WiMAX, LTE, and Bluetooth bands inspired by a metamaterial structure. The design is based on an FR-4 substrate. They tested two configurations for the antenna, one with the modified radiating patch, and the other one with metamaterials on the side of the radiating patch. In both cases the ground is defected and slotted. Due to a defected ground plane, the antenna has an omni directional pattern. Based on the return loss response, the antenna is resonant at L band frequency range (0.645~0.689 GHz) and S band frequency ranges (2.75~3.38 GHz) and (3.45~3.56 GHz). The antenna exhibits peak gain of 3dB and 3.69dB at L and S bands respectively. Figure 2.2 clearly indicates the performance differences before and after the metamaterials are added.

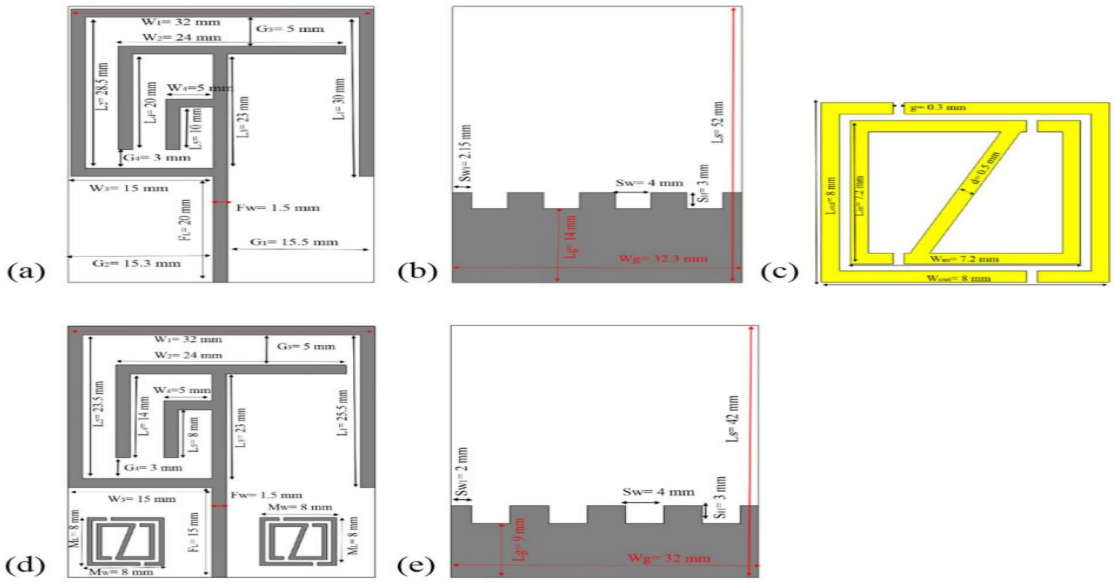

Figure-2.1: (a) Antenna without metamaterials, front view (b) Antenna without metamaterials, back view (c) Metamaterial Unit Cell (d) Antenna with metamaterials, front view (e) Antenna with metamaterials, back view.[1]

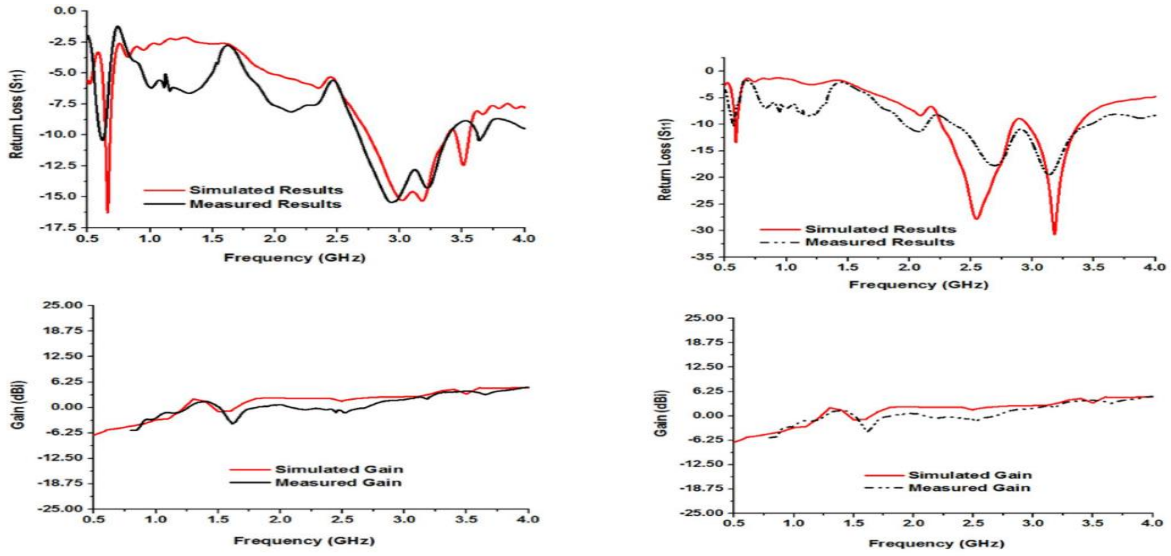

(a) (b)

Figure-2.2: (a)S11 and gain with Metamaterial (b) S11 and gain without Metamaterial[1]

He et. al.[2] reported a compact metamaterial inspired monopole antenna that resonates at 2.3GHz. Their design achieved a bandwidth of 220 MHz and radiation efficiency of 73%. The antenna is designed by modifying the geometry of a circular patch as shown below (figure 2.3). For substrate they used low cost FR-4 laminate. The defected ground plane of the antenna made it possible to obtain an omnidirectional radiation pattern as shown by the gain plot in figure 2.3(c).

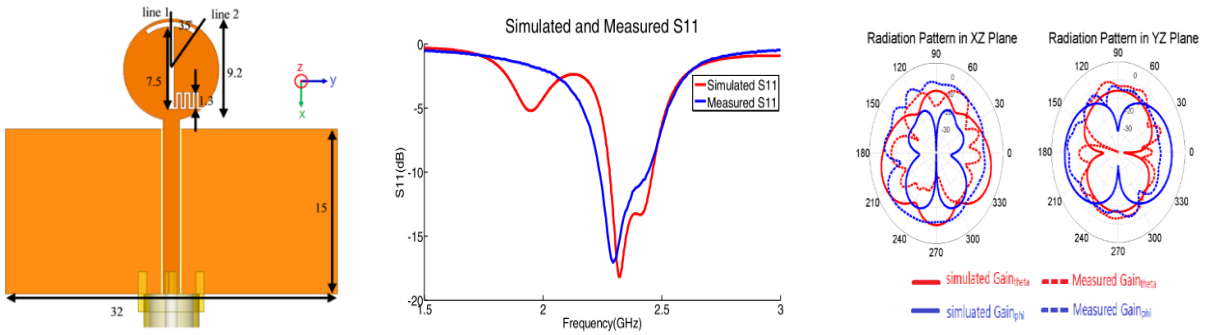

(a) (b) (c)

Figure2.3: (a) Designed Antenna (b) Return Loss of the Antenna(S11) (c) Gain plot [2]

Liu et. al.[3] proposed a metamaterial based broadband mushroom antenna. The antenna has an average gain of 9.9 dBi, an operating bandwidth of 25% (which is equivalent to almost 1.5GHz) at the 5GHz band, and radiation efficiency around 80-90%. It consists of multiple rectangular patches, which are spaced periodically over the substrate and placed symmetrically in a 4 X 4 matrix . Every patch is connected to the ground plane through a via hole in its center. To feed the antenna, a slot is cut onto the ground plane right beneath the center of the mushrooms. Physical design of the antenna and all the measurements are illustrated in figure 2.4 and 2.5.

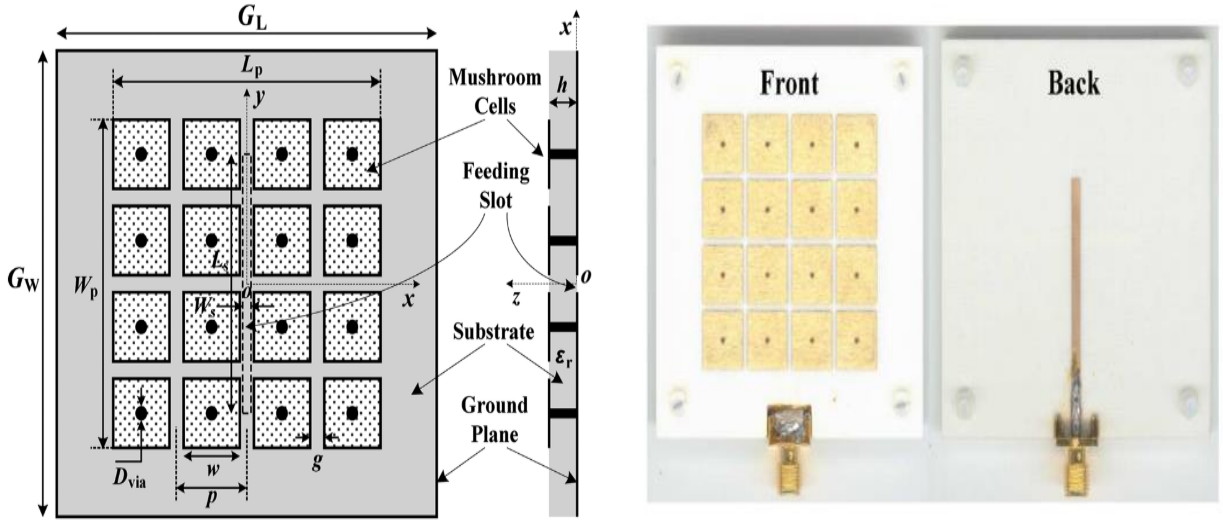

(a) (b)

Figure-2.4: (a) Geometry of the proposed antenna (b) Fabricated prototype [3]

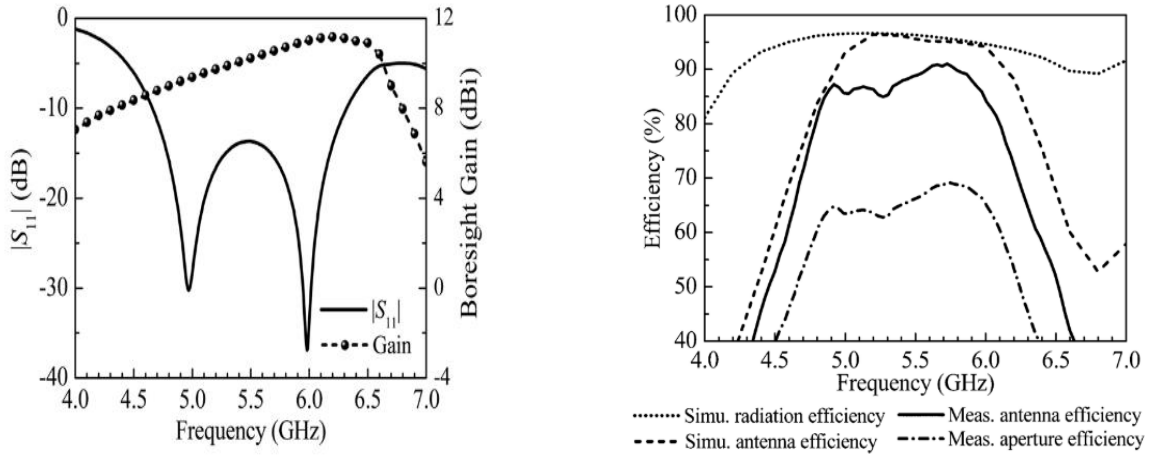

(a) (b)

Figure-2.5: (a) Return Loss(S11) and Gain Plot (b) Plot of the antenna efficiency [3]

An antenna proposed by Latha et. al. [4] shown that metamaterial inspired antennas could perform well in a wearable setup. The substrate used for their antenna simulation is polydimethylsiloxane (PDMS) substrate. The partial ground plane in the design makes the antenna omnidirectional when it is off body. In the simulation they placed the antenna on the jeans textile and placed 4 metamaterial unit cells behind the jeans as shown in figure 2.6. The proposed antenna resonates at 2.45GHz while simulated in an off body condition. It shows almost exact return loss(S11) bandwidth while simulated in an on body condition, as shown in figure 2.7(a). The antenna resonates omnidirectionally when it is off body. But, when it is on body, the antenna shows a somewhat directive radiation pattern compared to its original one, as shown in figure 2.7(b).

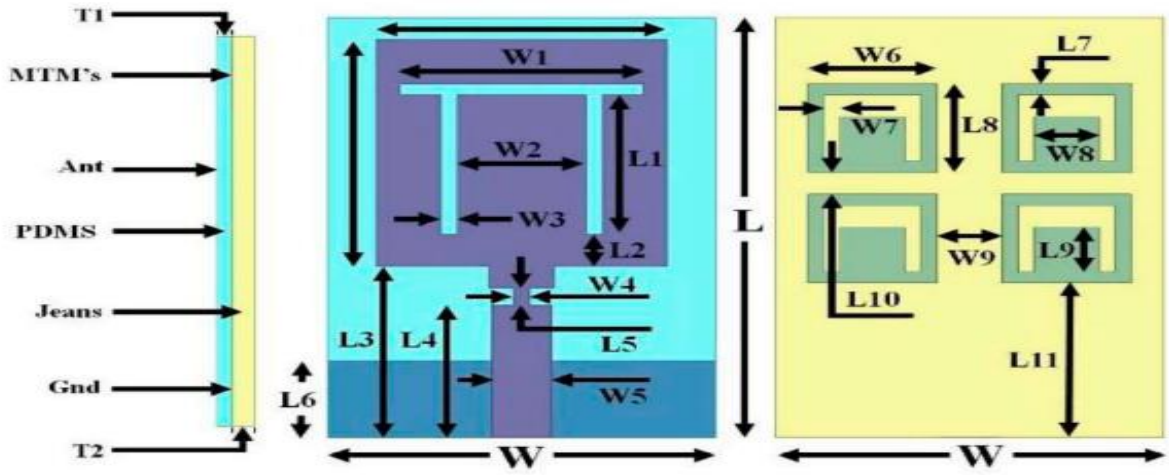

(a) (b) (c)

Figure-2.6: (a) Sideview of the various layers present in the antenna (b) Geometry of the radiating patch of the proposed antenna (c) Placement of metamaterial behind the antenna(Yellow color denotes jeans textile) [4]

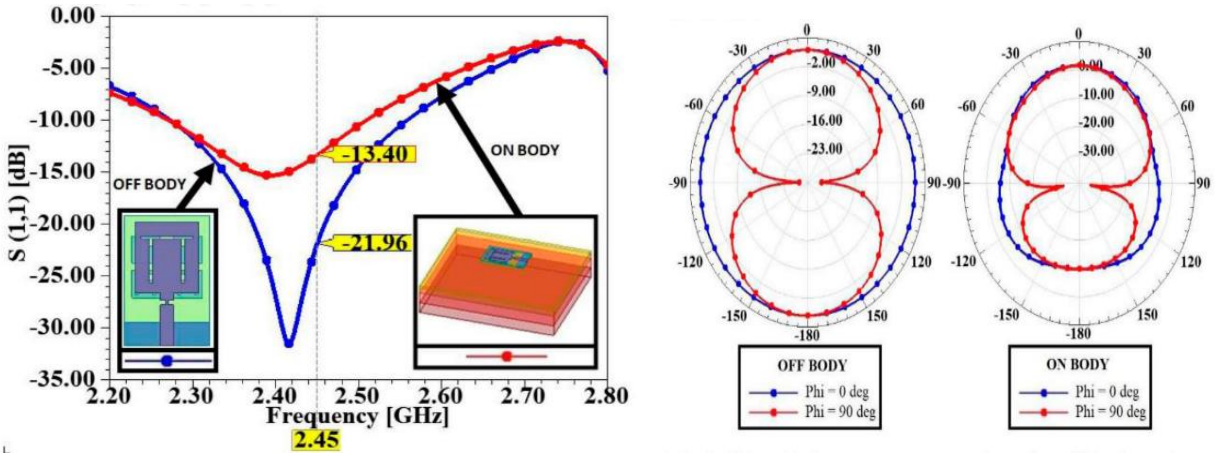

(a) (b)

Figure-2.7: (a) On Body and off body S11 response of the proposed antenna (b) On body and off body radiation pattern of the proposed antenna [4]

Cheng et. al. [5] reported a metamaterial half lens to control the beam direction of a compact antipodal Vivaldi antenna. The proposed antenna has a huge bandwidth of 143.6%(2.3-14 GHz) and three different beam forms at 3-9GHz, 12GHz, and 13GHz. In this design, a metamaterial half lens array is placed beside the radiating element to control the beam direction. The beam shaping is clearly visible in the electric field distribution of the antenna, as shown in figure- 2.9. The ground plane in this design is an antipode to the radiating element, hence we can say that the design employed a partial ground with a modified shape. The placement of metamaterial half lens also increases the gain in operating frequency by 2dB. Physical dimensions and responses of the antenna is shown below in figure-2.8 and 2.10.

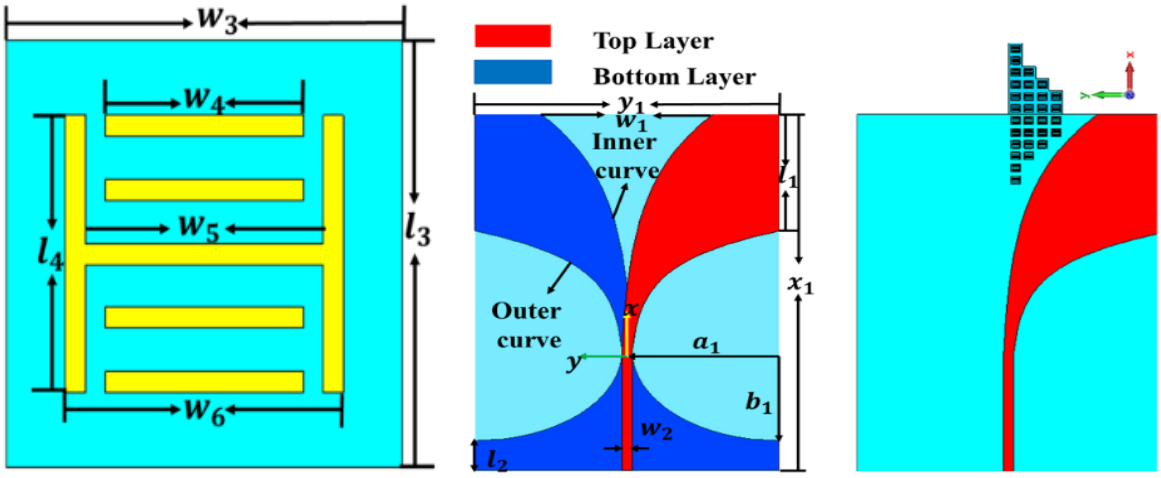

(a) (b) (c)

Figure-2.8: (a) Metamaterial Half Lens unit cell (b) Geometry of the Proposed antenna (c) Front view of the proposed antenna with Metamaterial Half Lens array. [5]

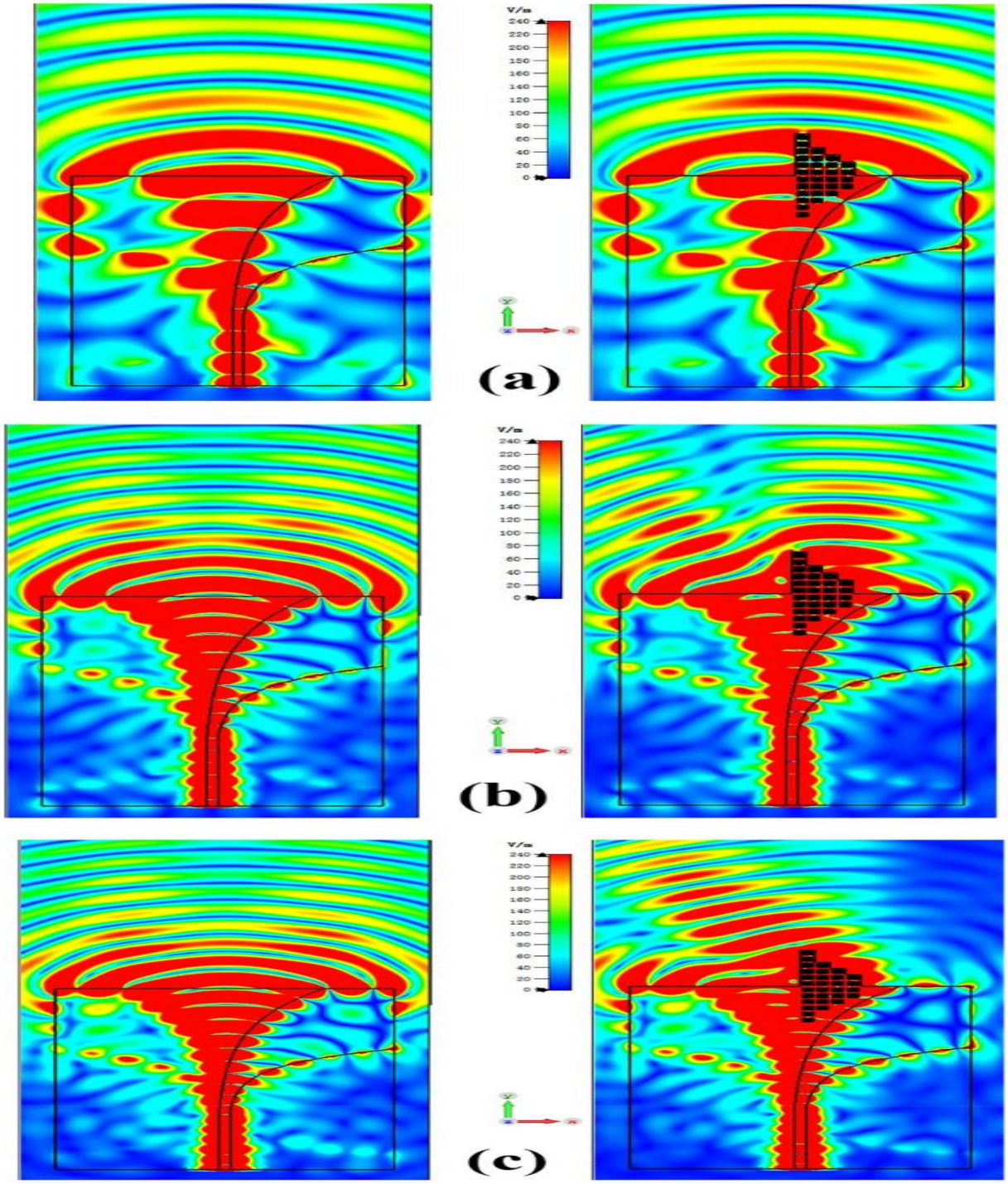

Figure-2.9: Comparison of electric field distribution of the antenna with and without metamaterial half lens (a) 7 GHz, (b) 12.2 GHz, and (c) 13 GHz [5]

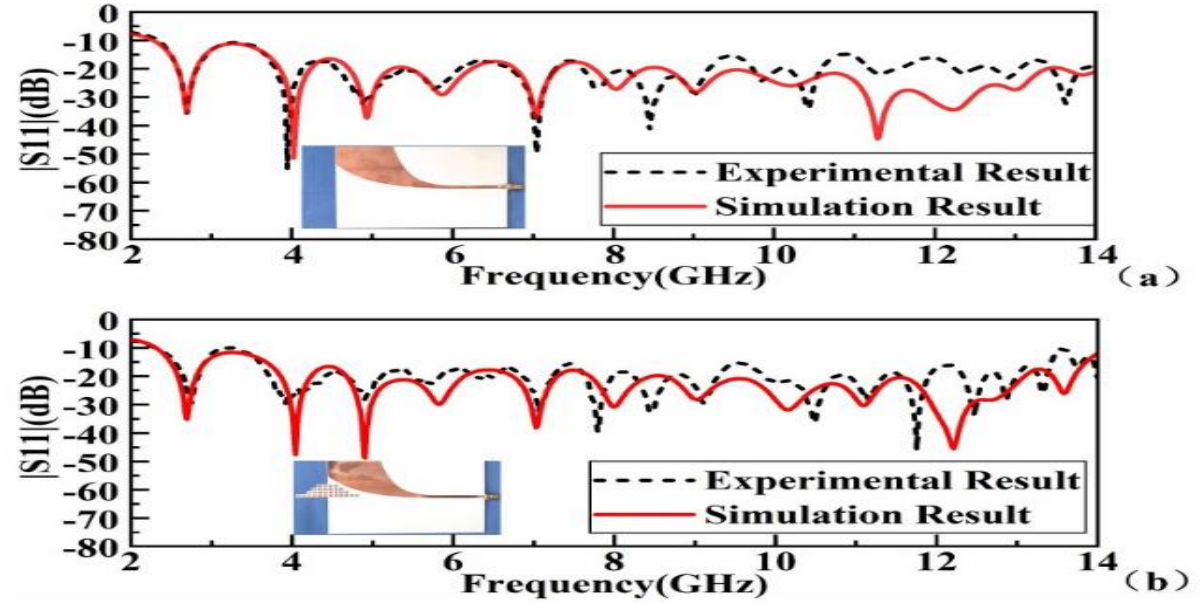

Figure-2.10: Simulated and measured S11 response (a) Without the Metamaterial half lens (b) With the metamaterial Half lens [5]

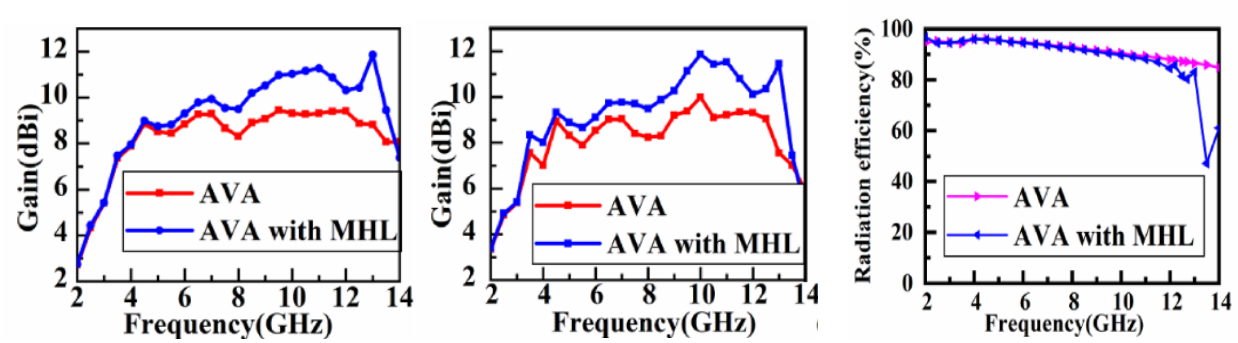

(a) (b) (c)

Figure-2.11: (a) Simulated Gain (b) Measured Gain (c) Efficiency of the antenna with and without metamaterial half-lens [5]

2.3: 5G Antennas

From the literatures of sub section 2.1, we can see that metamaterials are widely used either as an antenna or to enhance the performance of the antenna for a specific application. In this subsection we will discuss some prominent planar 5G antennas reported in various publications.

Hasan et. al. [6] proposed an antenna for mm wave 5G communication in 28GHz and 38GHz bands. Their antenna is the result of geometric modification of a regular patch. The geometric dimension of the antenna is shown in figure- 2.12. The design employs hemispherical contours to intensify the surface current of the radiating element, as shown in the surface current distribution plot in fig-2.13. It also employs a partial ground, which results in an omnidirectional radiation pattern. The proposed antenna covers frequencies at 26.65–29.2GHz and 36.95–39.05 GHz , corresponding to a -10dB impedance bandwidth. At 28GHz, the antenna has a peak gain of 1.27dBi, and at 38GHz it has a peak gain of 1.83dBi. As this antenna is proposed for MIMO application, it shows a good isolation (S_{21} less than -20dB) in the operating frequency range. We can say that this antenna will be a good receiving antenna for 5G application, as it has a nice omnidirectional radiation pattern for both frequencies. Since, mm-wave signals suffer from free space path loss and absorption [19], it is good to have an antenna with high gain to compensate for the loss of the signal in the channel. Overall, the antenna has an efficiency of 60-80% throughout the operating frequency. All the measurements of the proposed antenna is shown below in figures 2.14-2.15.

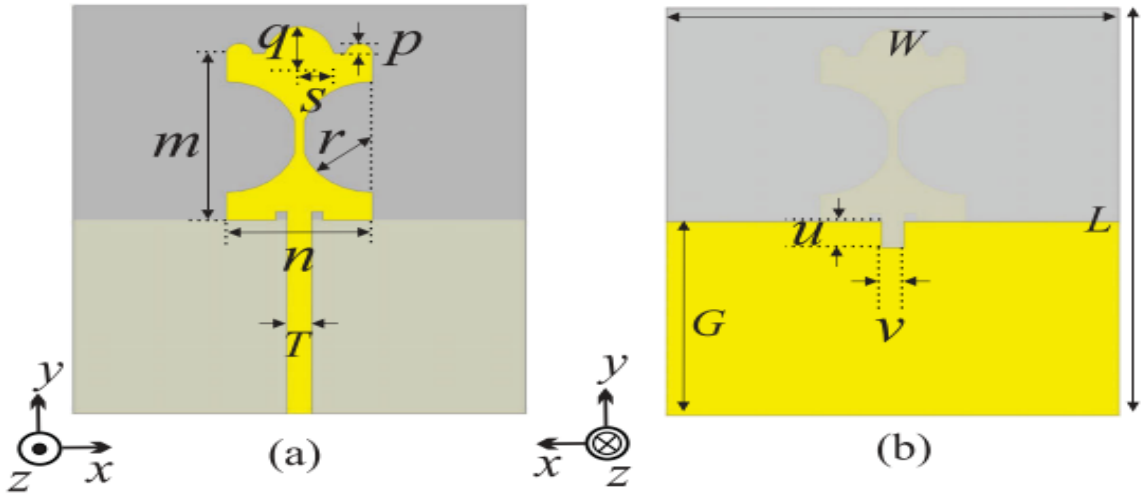

Figure-2.12: (a) Front view of the proposed antenna (b) Back view of the proposed antenna[6]

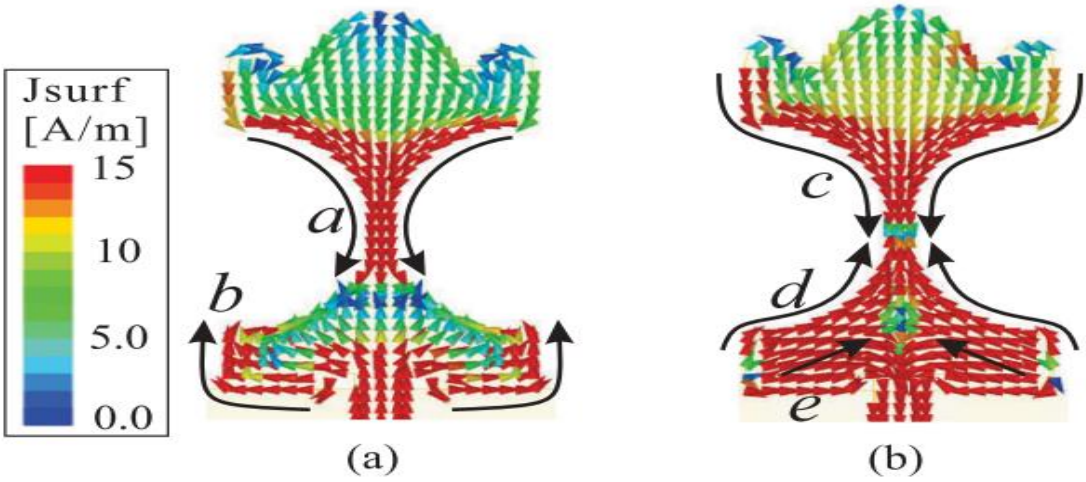

Figure-2.13: (a) Surface current density at 28GHz resonance frequency (b) Surface current density at 38GHz resonance frequency[6]

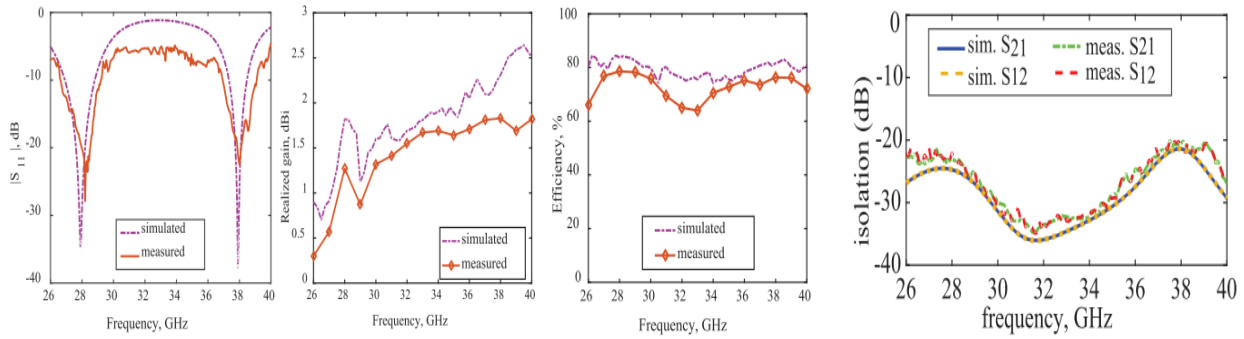

(a) (b) (c) (d)

Figure-2.14: (a) Return loss(S11) (b) Realized gain(in dBi) (c) Efficiency of the antenna (d) Isolation of two antennas while arranged in a MIMO setup.[6]

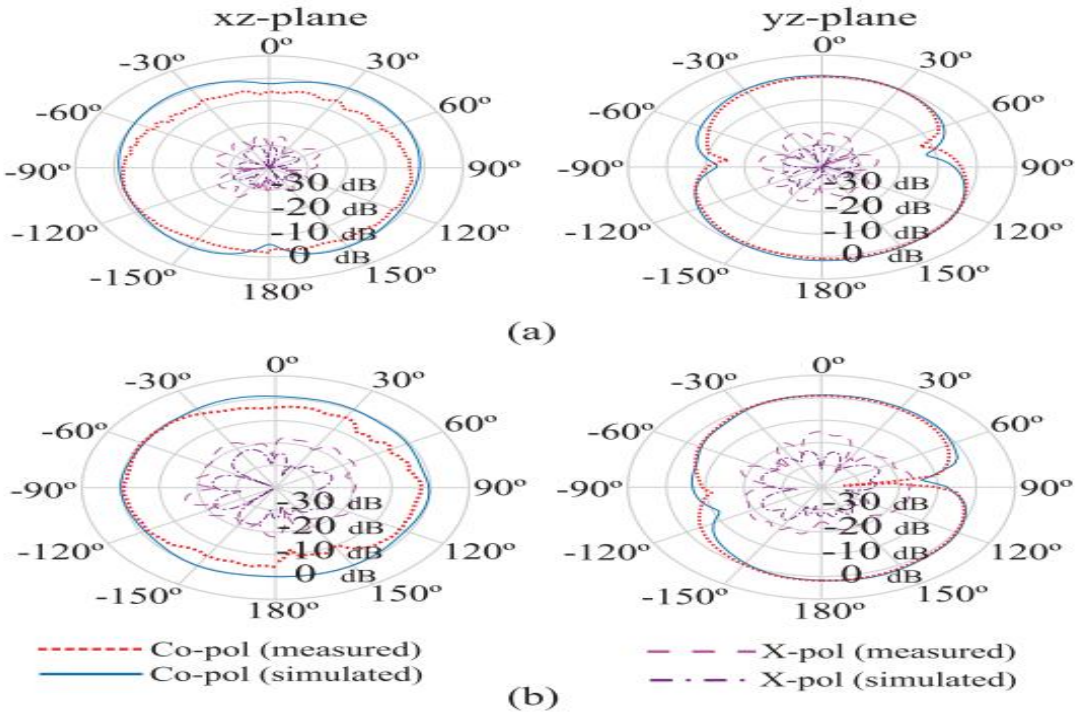

Figure-2.15: Radiation patterns at (a) 28GHz (b) 38GHz [6]

An antenna proposed by Ullah et.al. [7] achieved a wide operating bandwidth of 23.41-33.92 GHz. This antenna resembles a bowtie antenna in a sense. It is built upon Rogers RT Duroid 5880 substrate with a thickness of 0.254mm. Both front and backside of the antenna has the same radiating element, except in the back the structure is part of the ground plane and flipped horizontally. The geometry is shown in figure-2.16. From the surface current density in figure—2.17, we can see intensified surface current in the center than in the edges. This results in a very high gain for the antenna. By placing 4 individual antenna elements in an array which is fed by same input, average gain 10.7dBi is achieved by this antenna. The antenna also attains a very narrow directional beam with a beamwidth of 14.6° in its H- plane. Throughout the operating band, it has an efficiency over 90%. With all its characteristics, it is definitely a good design. However, in certain applications, narrower bands may suit the purpose than the very high band designs. In other aspects of the performance, it is a good antenna. Antenna dimensions, measurement results etc. are shown in figure 2.15-2.21

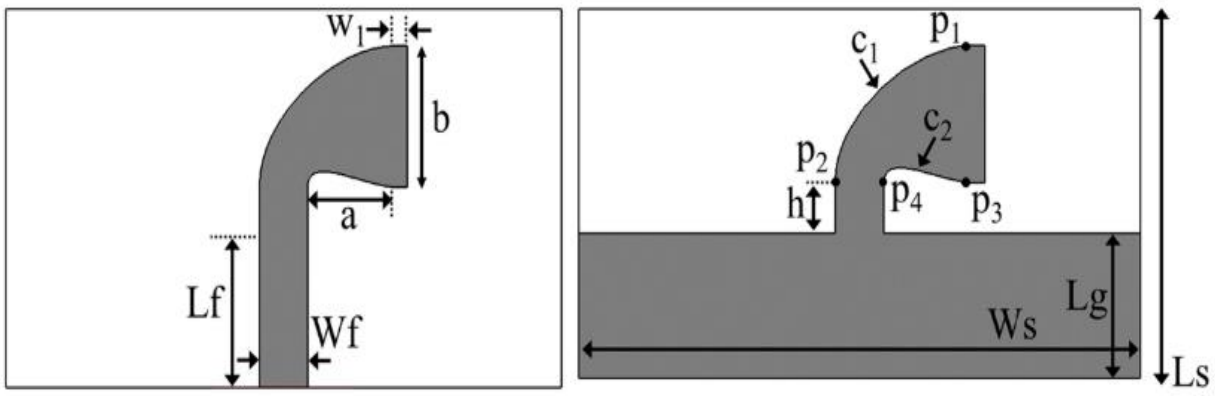

(a) (b)

Figure-2.16: (a) Front view of the antenna (b) Back view of the antenna[7]

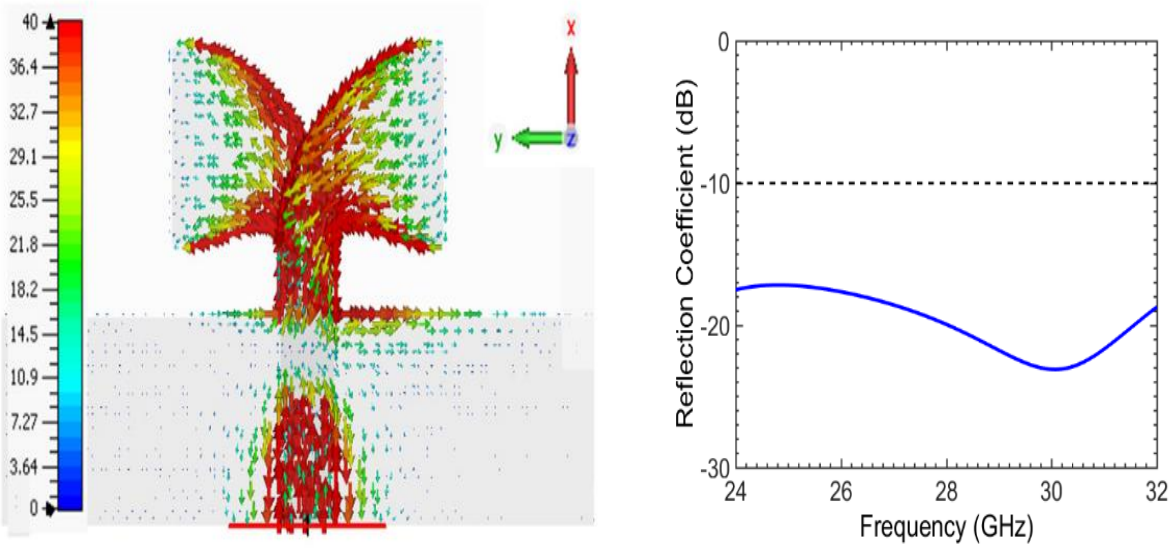

(a) (b)

Figure-2.17: (a) Surface current distribution (b) Return loss (S11) of the antenna[7]

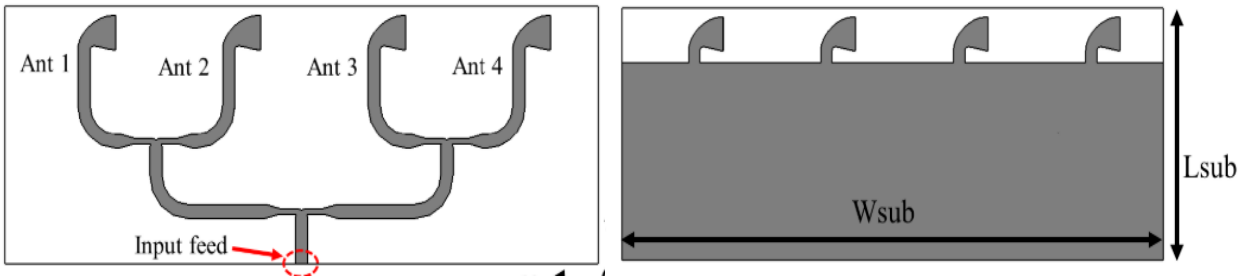

(a) (b)

Figure-2.18: 4 X 4 antenna array (a) Front view (b) Back view[7]

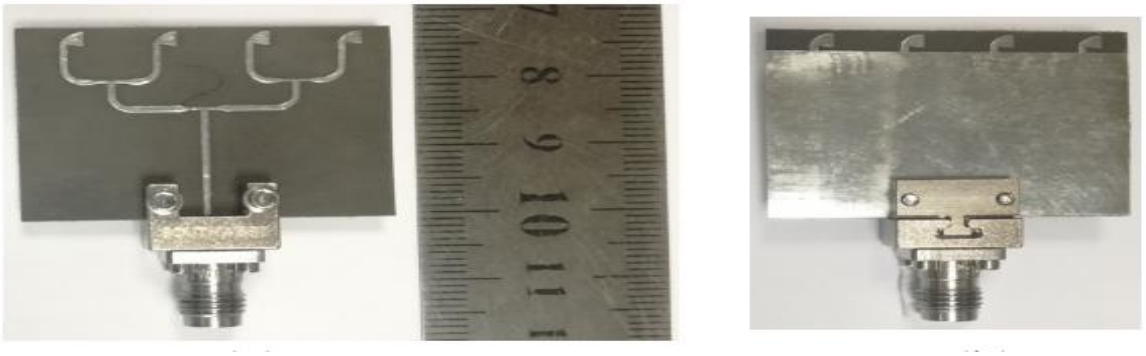

Figure-2.19: Fabricated antenna array prototype[7]

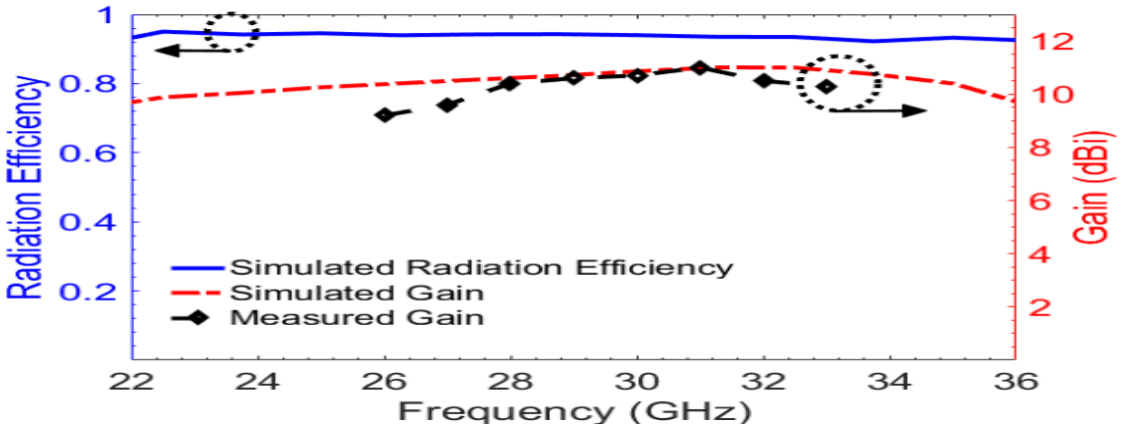

Figure-2.20: Efficiency and gain plot of the antenna array[7]

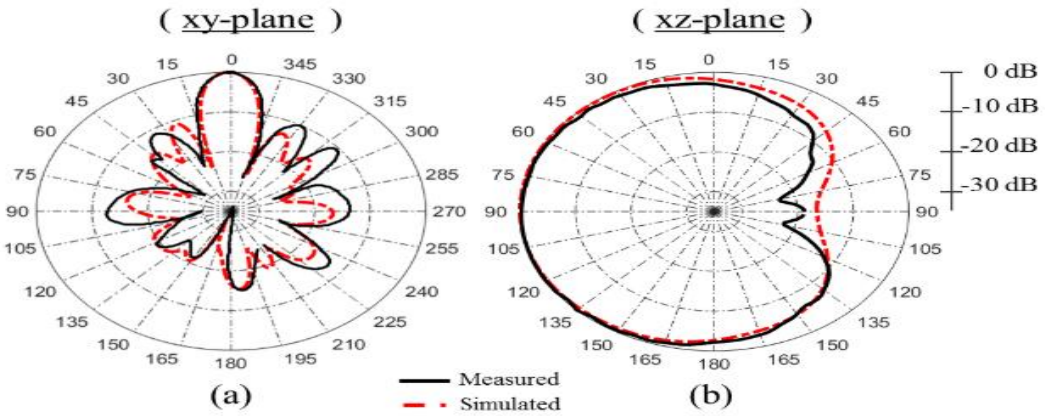

Figure-2.21: Measure and simulated radiation pattern of antenna array at 28GHz (a) XY-plane (b) XZ-plane.[7]

Chen et. al. [8] reported a grid array antenna designed on a low cost FR-4 substrate. This antenna has a dimension of 15 X 15 mm^2 and it covers 10 dB impedance bandwidth in the frequency range 23.86- 31.02 GHz. It radiates a fixed beam and has a peak realized gain of 12.66dBi at 29.2 GHz. This antenna has a mesh like structure in the radiating element, which is fed by a probe from underneath the ground plane. The authors have simulated the antenna in a setup much like a real cell phone. The performance of the antenna remains practically unchanged with the increase in substrate length and decrease in ground length. Radiation efficiency of this antenna is 88.8% at 28GHz. Even though this antenna has overall good performance and low cost, the probe feeding of the antenna could be a challenge for practical applications. Antenna geometry and measurement results are shown below in figures 2.22-2.25.

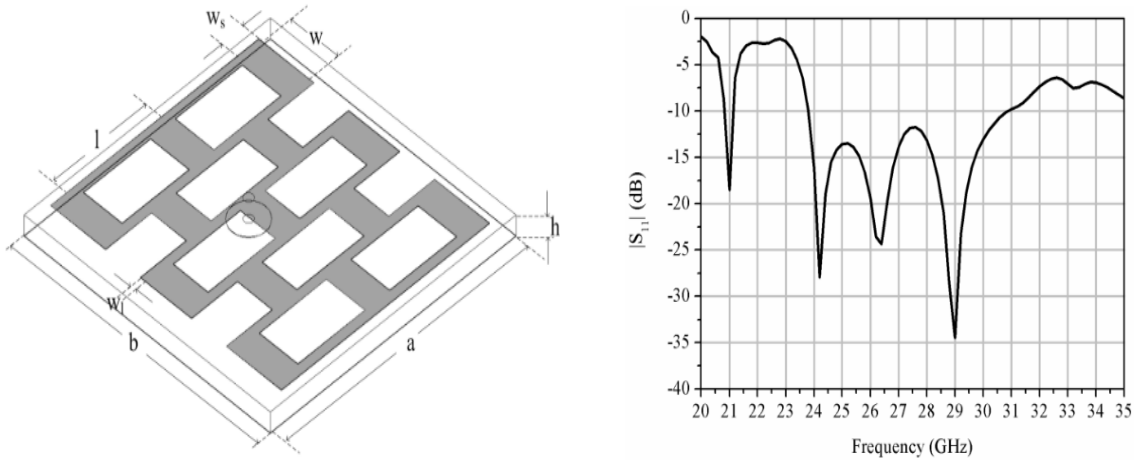

(a) (b)

Figure-2.22: (a) Geometry of the proposed antenna (b) Return loss(S11) response of the antenna[8]

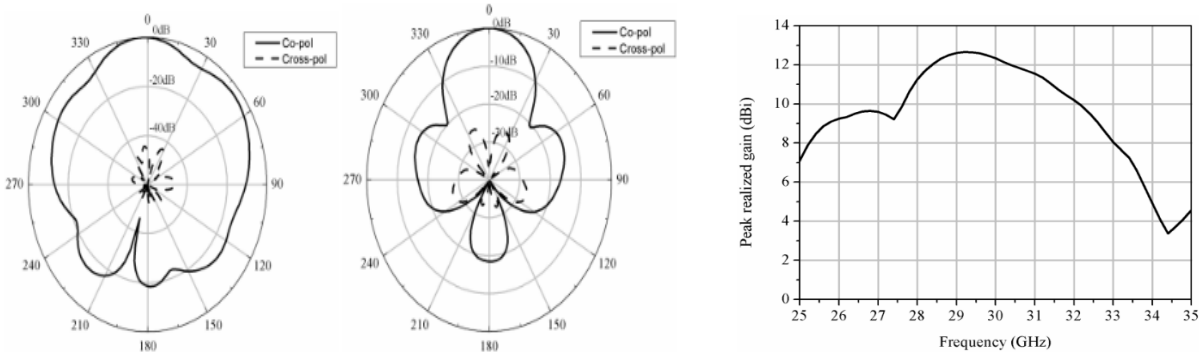

(a) (b) (c)

Figure-2.23: (a) Radiation pattern at 28GHz E-plane (b) Radiation pattern at 28GHz H-plane (c)Gain of the antenna in the operating band[8]

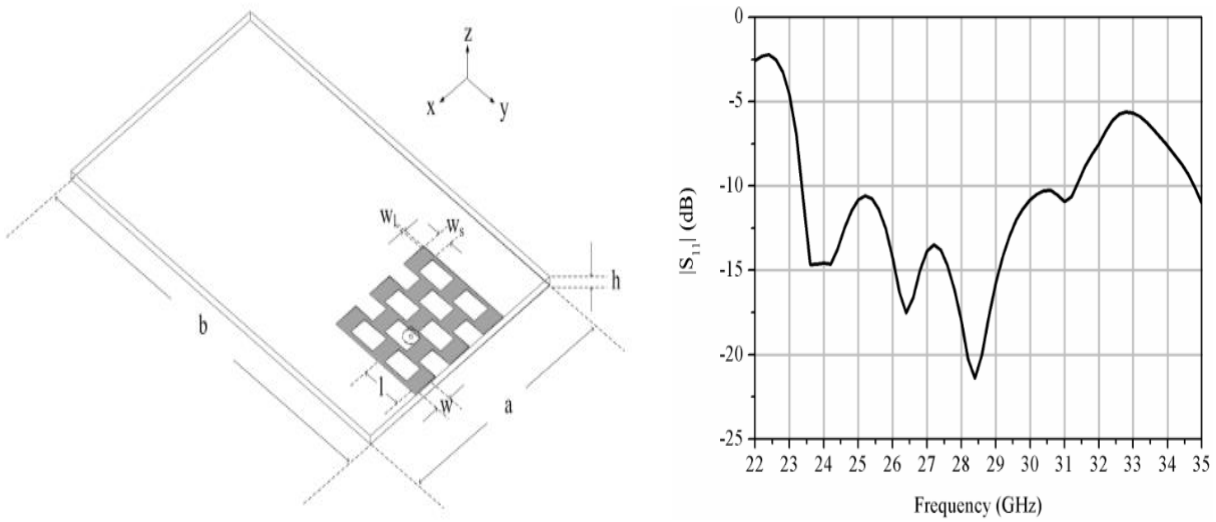

(a) (b)

Figure-2.24: (a) Antenna setup implying its position on a handset (b) S11 response of the test [8]

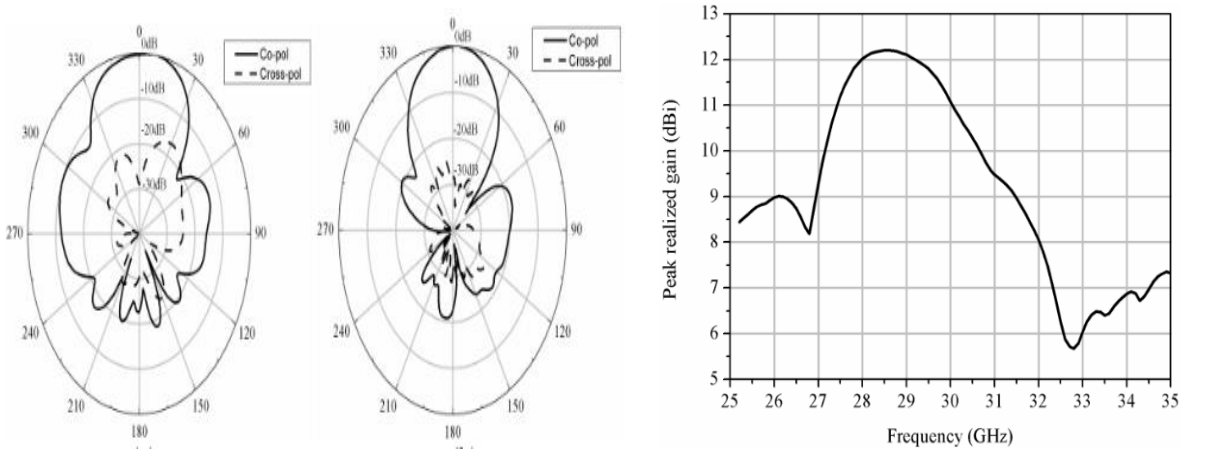

(a) (b) (c)

Figure-2.25: (a) Radiation pattern at 28GHz(After the antenna put to test in a handset like setup) E-Plane (b) Radiation pattern at H-plane (c) Gain of the antenna in handset test. [8]

In another work Alsaif et. al. [9] designed a 2 X 2 MIMO antenna with super wide bandwidth of 46.8GHz in the frequency range 15.2 GHz - 62 GHz. The authors characterized the antenna as a MIMO antenna, even though there is only a single source of excitation in the antenna. All the radiating elements in this antenna are interconnected to each other. It is printed on a low loss Rogers Duroid RT 5880 substrate with εr = 2.2 and loss tangent δ = 0.0009. Radiating elements of this antenna are basically rectangular patches with two slots cut at the center of each patch. It also has a modified partial ground plane, which gives this antenna an omnidirectional radiation pattern. The presence of multiple interconnected radiating elements give this antenna a peak gain of 13.5 dBi, as found in simulations using CST and HFSS software. Very high bandwidth of 46.8 GHz makes this antenna suitable for wide range of mm wave applications, including 5G. Overall it is a good antenna suitable for 5G and other mm wave communication. Geometric dimension and measurements for this antenna are shown in figure 2.25-2.26.

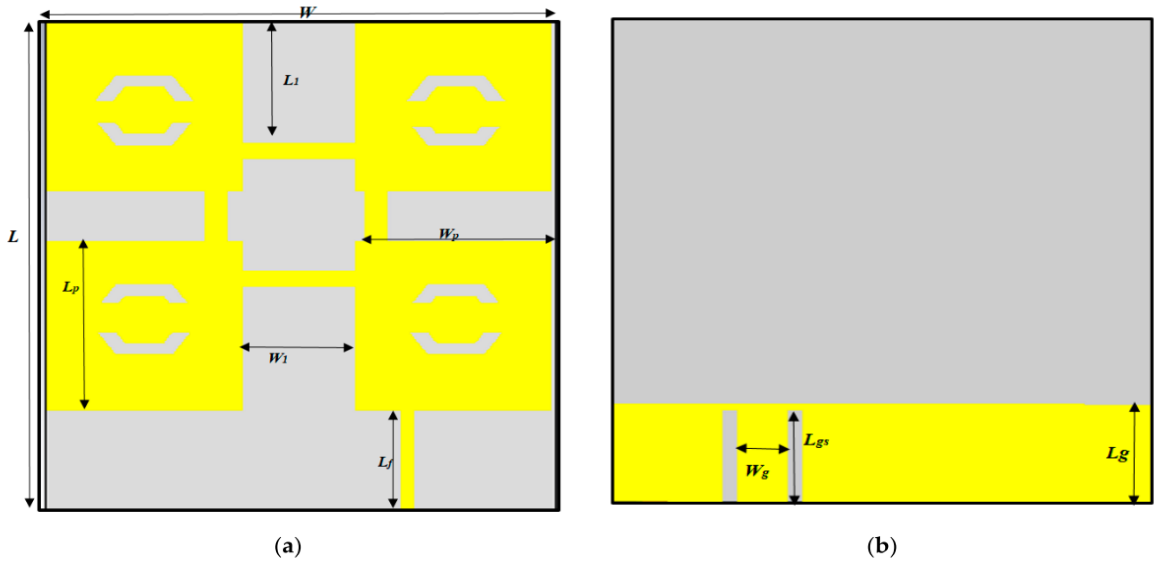

Figure-2.26: (a) Front view of the proposed antenna (b) Back view of the proposed antenna[9]

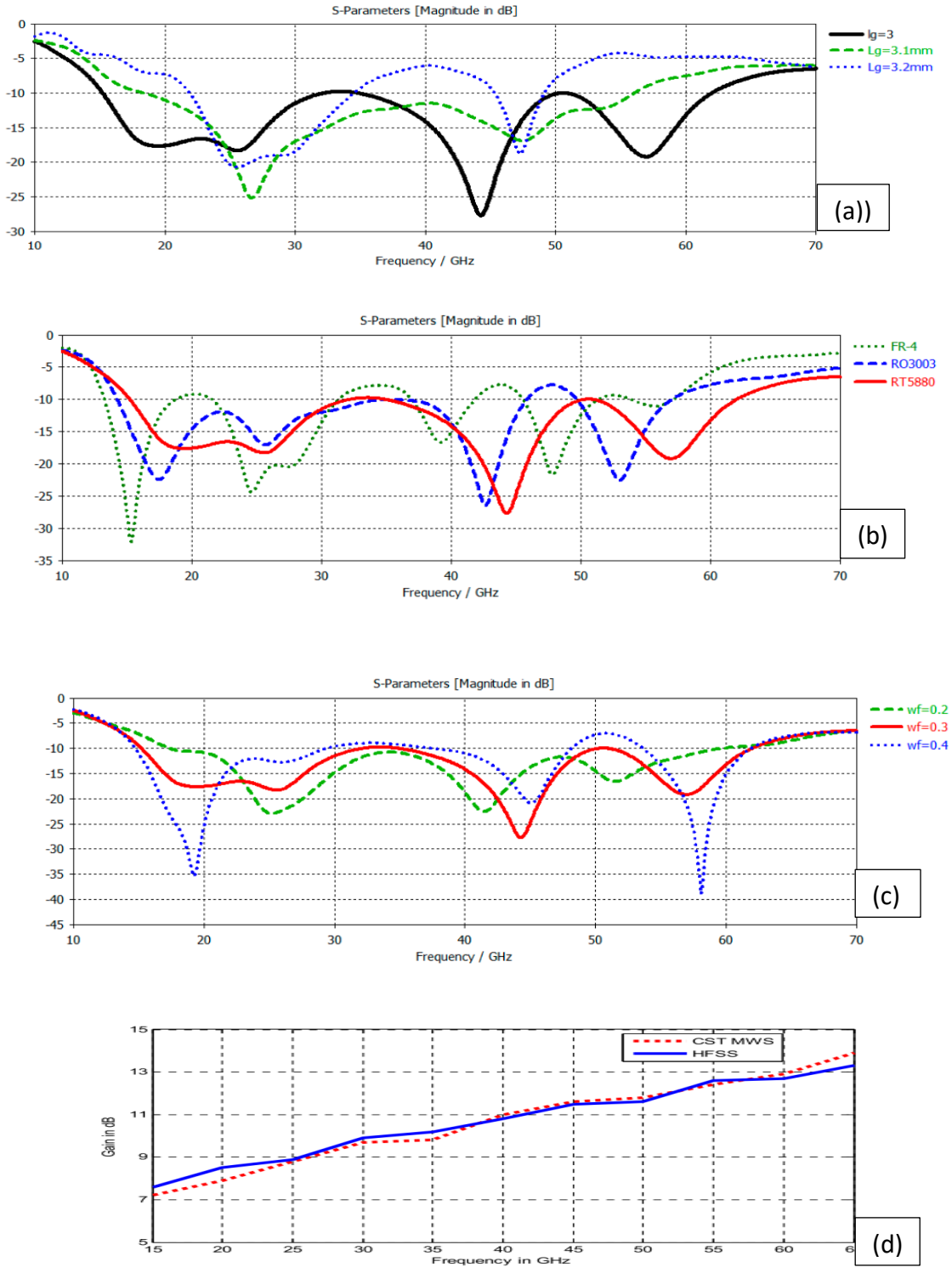

Figure-2.27: (a) Change of S11 with respect to length of ground (b) Change in S11 due to substrate materials (c) Change in S11 with respect to width of the feedline (d) Gain of the antenna[9]

Khalily et. al. [10] proposed an array antenna, which is fed by multiple sources. This antenna is designed and tested for 28GHz frequency, and it has beam steering capability in the operational band. Radiating elements of this antenna consist of interconnected rectangular patches placed symmetrically over a ground plane. The authors have proposed two configurations for this array antenna. One has a 2 X 2 array configuration and another one has a 3 X 3 array configuration. The configuration with 2 X 2 array has been tested with four excitation ports, and the configuration with 3 X 3 array has been tested with 4 and 6 excitation ports. By exciting the ports with signals containing a certain phase difference, the beam of the 2 X 2 array is being steered left and right as shown in figure 2.30(a). By increasing the port number from 4 to 6 in the 3 X 3 array, the beamwidth, gain, efficiency, and homogeneity of the radiation is increased. The proposed antenna has a bandwidth of 820MHz in the frequency range 27.61-28.43 GHz, making it suitable for 5G communication in the 28GHz band. All the dimension and measurements of the proposed antenna are shown in figure 2.27- 2.30.

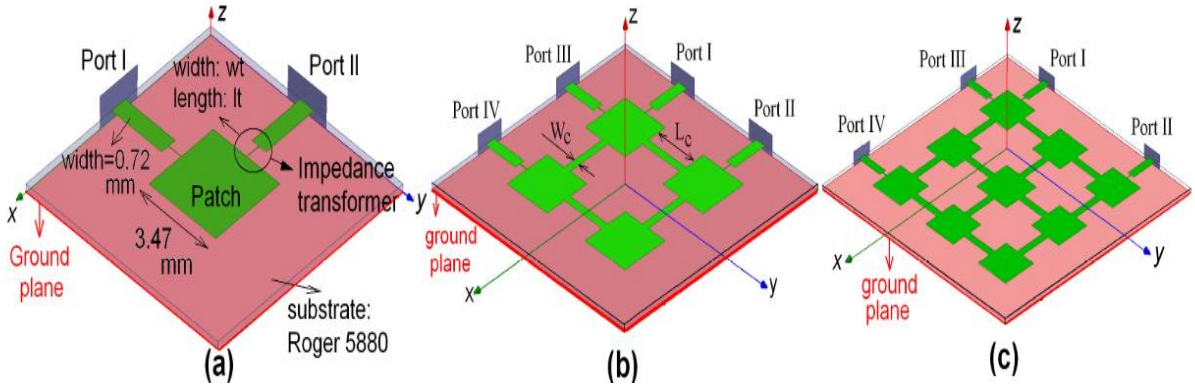

Figure-2.28: (a) Two port connection of single patch (b) Proposed 2 X 2antenna with four ports (c) proposed 3 X 3 antenna with 4 ports.[10]

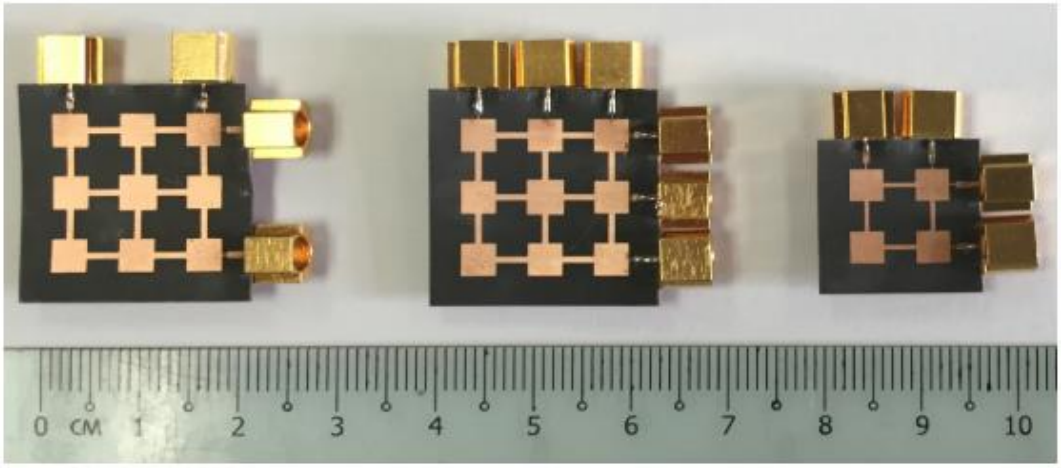

Figure-2.29: Fabricated prototype of the proposed antenna with different array configurations[10]

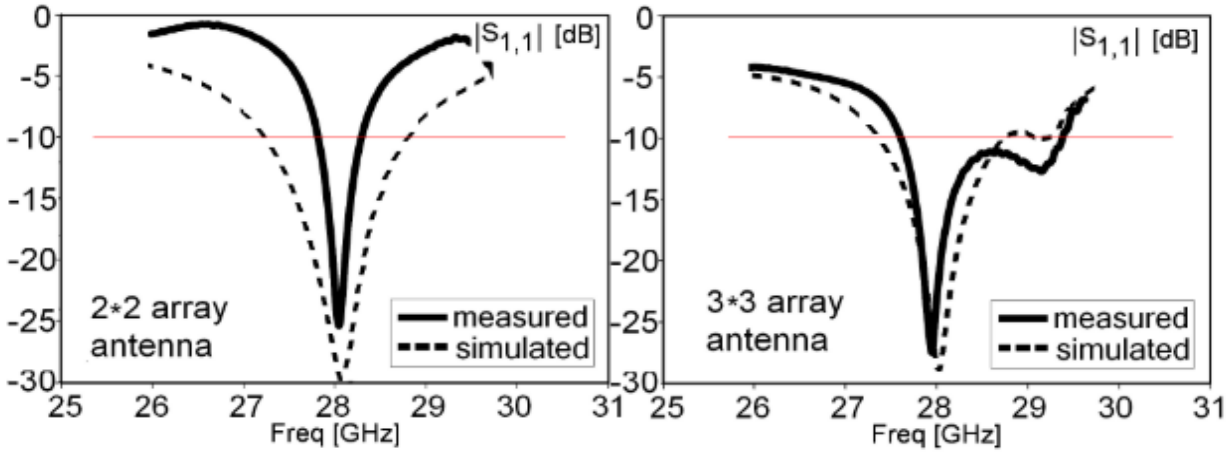

(a) (b)

Figure-2.30: (a) S11 response of the proposed 2X 2 array (b) S11 response of the proposed 3X 3 array[10]

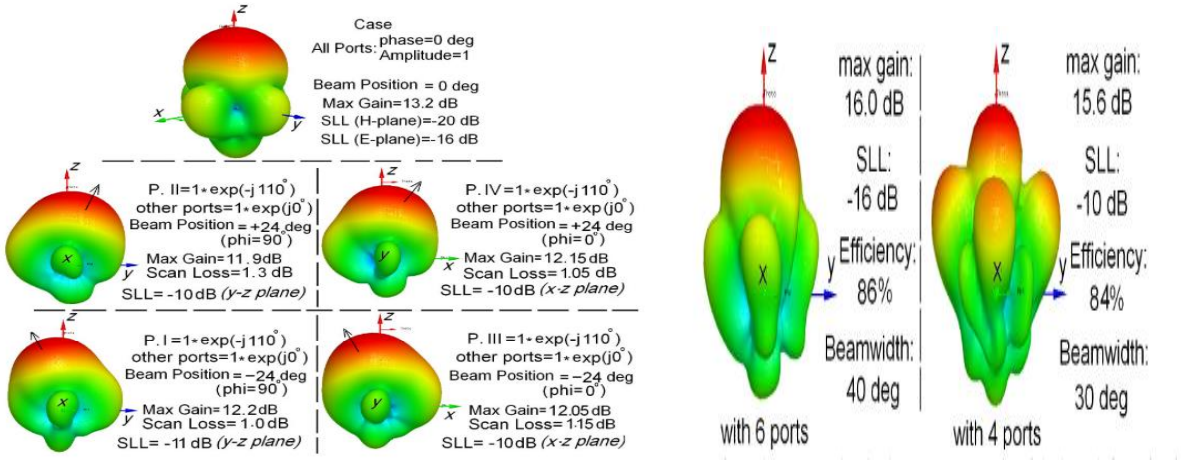

(a) (b)

Figure-2.31: (a) Beam steering due to phase shift in 2 X 2 array (b) Effect of 6 and 4 ports in the proposed 3 X 3 antenna gain, beamwidth, and efficiency[10]

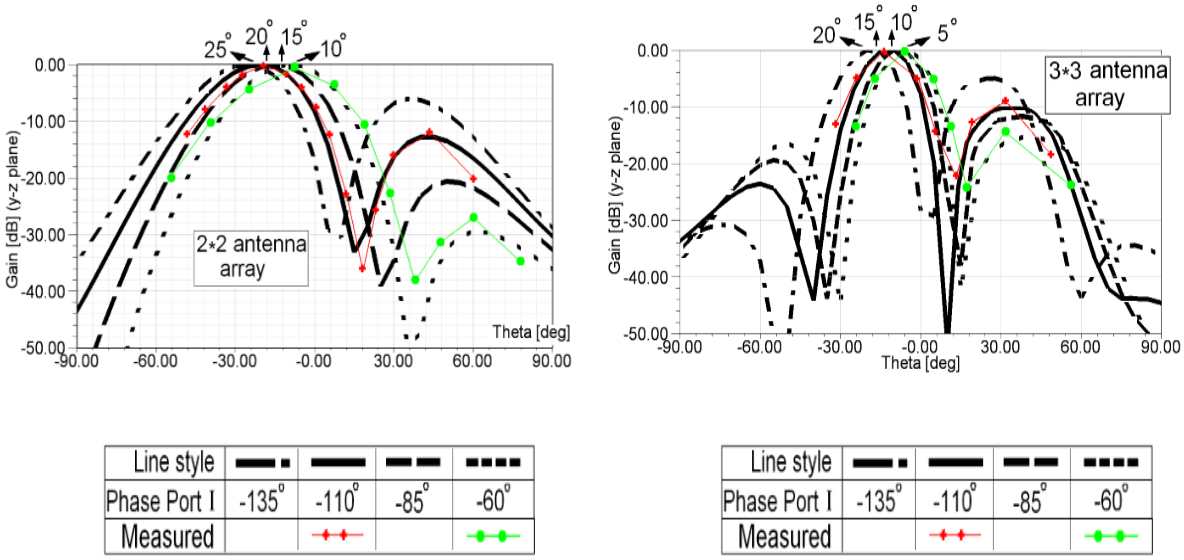

(a) (b)

Figure-2.32: (a) Gain of the proposed 2 X 2 array antenna (b) Gain of the proposed 3X 3 Array antenna [10]

From above discussion on different types of 5G antennas, we can see that bandwidth, gain, beamwidth plays an important role in 5G mm wave antenna designs. Another noticeable characteristic of most of those discussed antennas are modified geometry of the radiating patch and ground plane. There are many other works on mm wave 5G antennas [41][42][43][44][45][46][47], which is based on the motivations just mentioned and most of those are antennas with modified geometry. We can also notice from the discussion of general metamaterial inspired antennas that, inclusion of metamaterial structures in the radiating path or using the structure itself as a radiating patch could increase the gain, bandwidth, beamwidth of an antenna. So, in the next chapter we will discuss our design of 5G antenna based on a metamaterial structure.

CHAPTER III

DESIGN METHODOLOGY

3.1: Design of Negative Index Metamaterial

Metamaterials are composite structures consisting of periodic arrangements of numerous unit cells. The dimension of an unit cell is significantly smaller than the wavelength we are trying to interact with[24]. The unit cell is generally comprised of a Split Ring Resonator (SRR) and a thin wire. SRRs are made of non-magnetic thin metallic sheets, and they respond to the microwave radiation as if they have an effective magnetic permeability[24]. The periodic thin wire structure exhibits electromagnetic properties in the GHz range which are only possible in UV range for normal metals[23]. The combined structure of SRR and thin wire has self-inductance and capacitance within. With the presence of an incident wave the capacitance and inductance create a resonance which interacts strongly with an applied magnetic field (via SRR) and electric field (via the thin wire)[48]. The interaction with magnetic field gives rise to net effective permeability and the interaction with electric field gives rise to a net effective permittivity. By changing the dimensions of the structures a negative permittivity and permeability can be achieved, which in turn gives us the negative refractive index (NRI) according to the equation $n=\sqrt{(\varepsilon\mu)}$ [48].

By taking into account all the design considerations, we have designed a unit cell which has both wire structure and SRR incorporated within it. The structure is shown in figure 3.1. The central bar works as the wire element of the structure and the concentric rings with splits work as the SRR. The structure is designed for a frequency of 24GHz. Hence the overall dimension of the structure is approximately λ/5. The simulation for the structure is performed in CST Microwave Studio. It is designed on a Rogers RT 5880 substrate. From the simulation result of S_{21}, we can see that the primary resonance for the structure occurs right at the 24GHz mark. To retrieve permittivity and permeability data from the S_{11} and S_{21} data, we used the robust method proposed by MIT[49]. All the simulation results and retrieved parameters are shown in figures 3.2- 3.4.

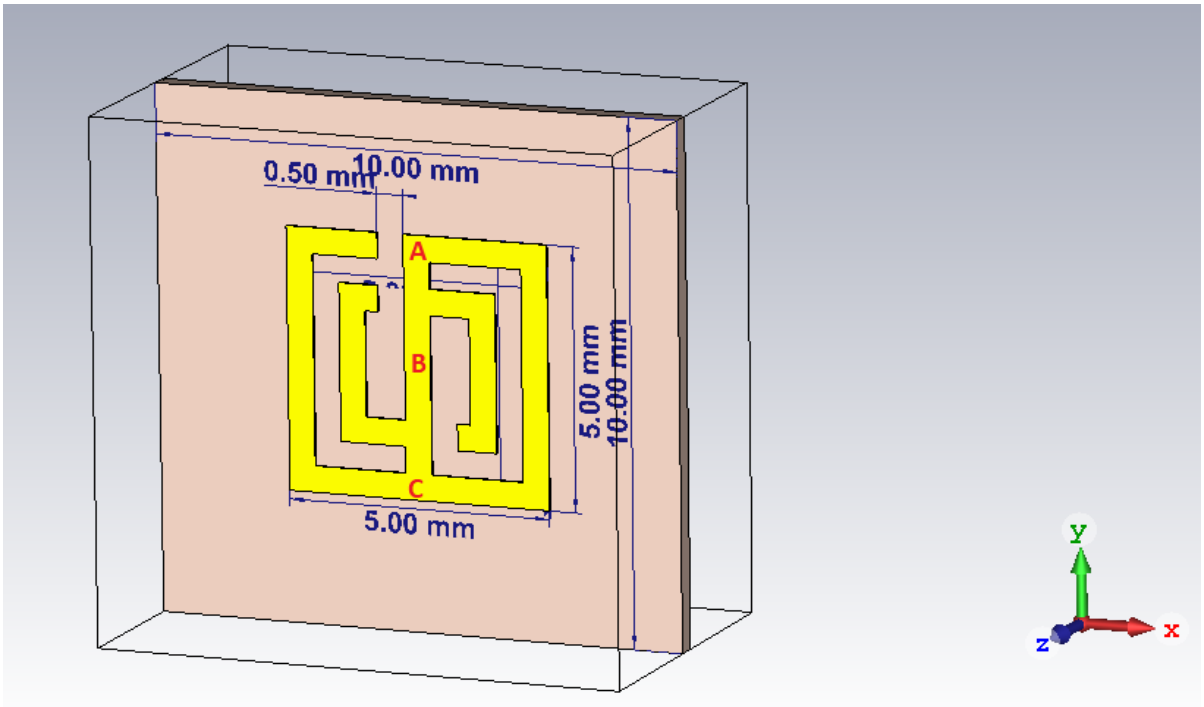

Figure-3.1: Proposed Metasurface (The bar marked by ABC represents the thin wire portion of the structure, rest of it are SRR.).

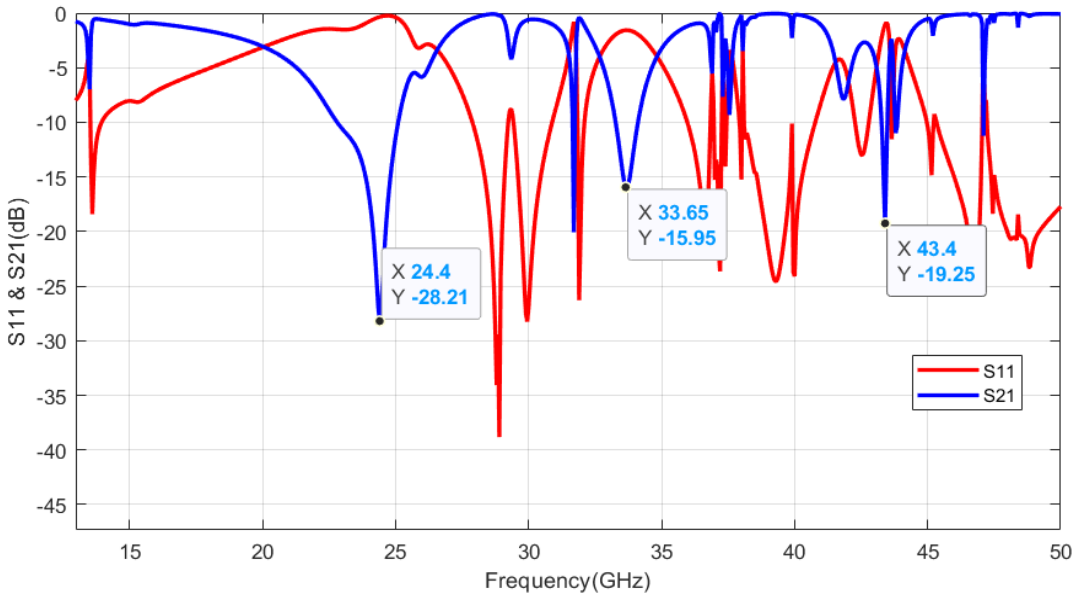

Figure-3.2: S_{11} and S_{21} response of the structure (The primary S_{21} resonance at the 24.4 GHz sits right at the 24 GHz band, as was designed. Also noticeable are secondary resonances).

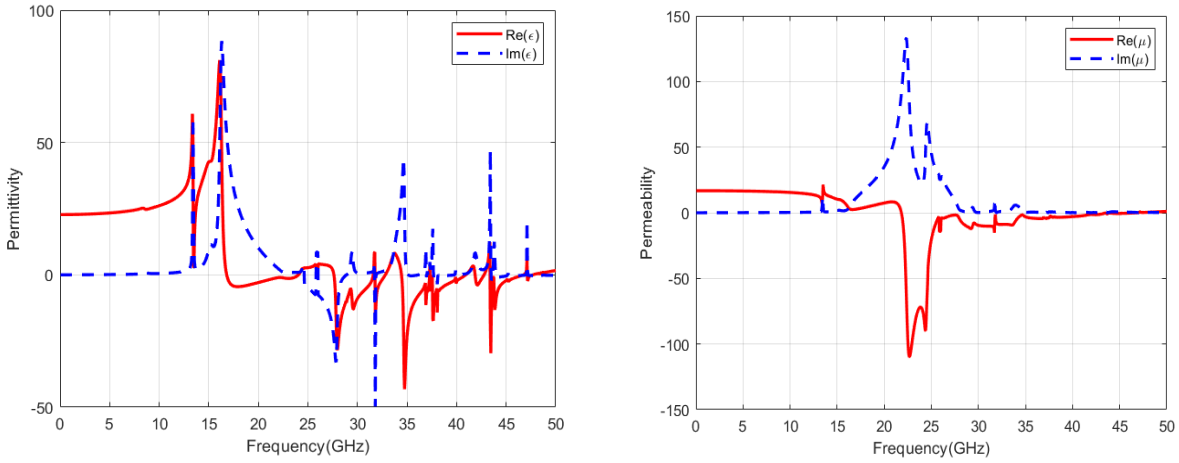

(a) (b)

Figure-3.3: (a) Extracted permittivity response of the structure (b) Permeability response of the structure

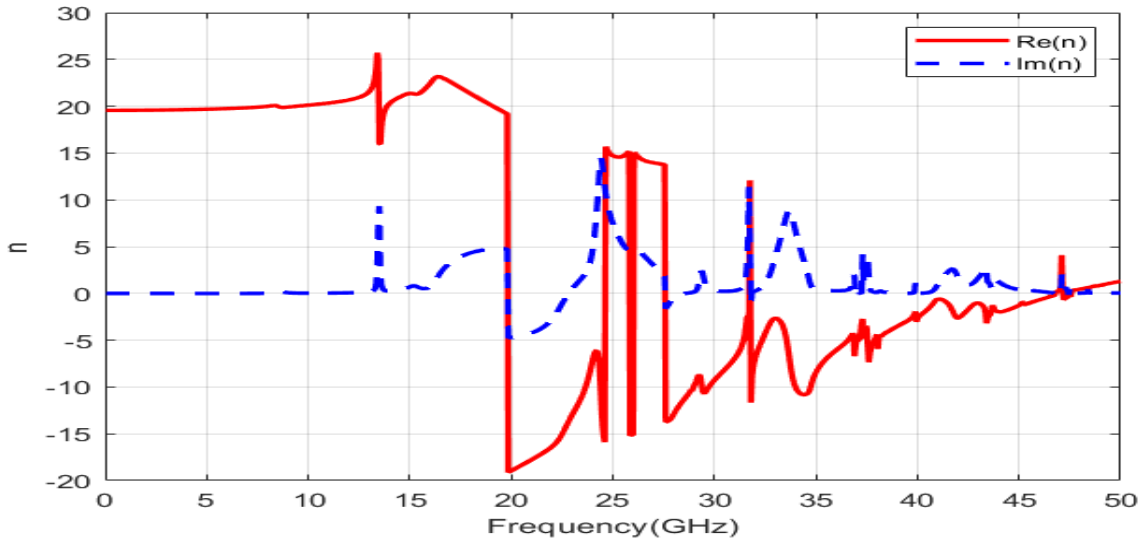

Figure-3.4: Extracted negative refractive index data (Noticeable NRI in the 20- 25 GHz band).

From the S_{21} plot of figure 3.2 we can see the primary resonance at around 24GHz, and multiple secondary resonances around 30GHz and 40GHz ranges. These interactions of the structure with mm-wave frequencies makes it suitable for antenna design in mm-wave frequencies. A similar method of antenna design could be found in the work by Roy et. al. [50], where they first designed a metamaterial, observed and extracted its parameters, then used the metamaterial itself as a patch for wideband wearable antenna.

From the figure 3.3 we can see that the real part of permittivity and permeability of the structure is negative throughout a wide range of frequencies, ranging from 20GHz- 40GHz. As a result we achieved negative index of refraction in that wide frequency range, as shown in figure 3.4. As we have achieved the expected metamaterial response from the structure and also resonances at higher mm wave frequency, we will describe how we used the structure as a patch antenna in the next subsection.

3.2: Antenna Design

We started the antenna design with the numerical analysis of the structure in CST microwave studio. Since we reached our expected S_{11} response through the optimization of physical dimension of the metamaterial patch, we will present here 10 cases out of numerous simulations we performed in CST. There are multiple ways to observe the changes in S_{11} through simulations. One way is parameter sweep, another one is the use of optimization algorithm, and the final one is running each simulation separately based on the trend. Since the employment of an optimization algorithm will require heavy computing power and space, we used parameter sweep and running simulations based on calculated guess. We have also taken into account the shape of the radiation pattern, radiation efficiency, and generation of multiple bands during our simulations.

Let's start with some equations that best describes the impedance of the antenna. From [51][52] we know that input impedance Z_{in} of a transmission line is given by

$$Z_{\text{in}} = Z_0 \frac{Z_L + j Z_0 \tan \beta l}{Z_0 + j Z_L \tan \beta l} \qquad \text{---------- (3.1)}$$

where

Z_0 = Characteristics Impedance of the microstrip

Z_L = Antenna impedance

Z_{in}= Input impedance at the excitation port= Z_{11}

$\beta = (2\pi f * \sqrt{\varepsilon_{eff}}) / C_0$

l= length of the microstrip line

$$\varepsilon_{eff} = \frac{\varepsilon_r + 1}{2} + \frac{\varepsilon_r - 1}{2}\left[\frac{1}{\sqrt{1+12\frac{H}{W}}} + 0.04\left(1-\frac{W}{H}\right)^2\right] \quad \text{----------(3.2)}$$

$$Z_0 = \frac{60}{\sqrt{\varepsilon_{eff}}} \ln\left(\frac{8H}{W} + \frac{W}{4H}\right) \quad \Omega \quad \text{----------(3.3)}$$

- W= Width of Microstrip Line
- H = thickness of the substrate
- ε_r =Dielectric constant of substrate

Now we will start with the first antenna model

Model-1:

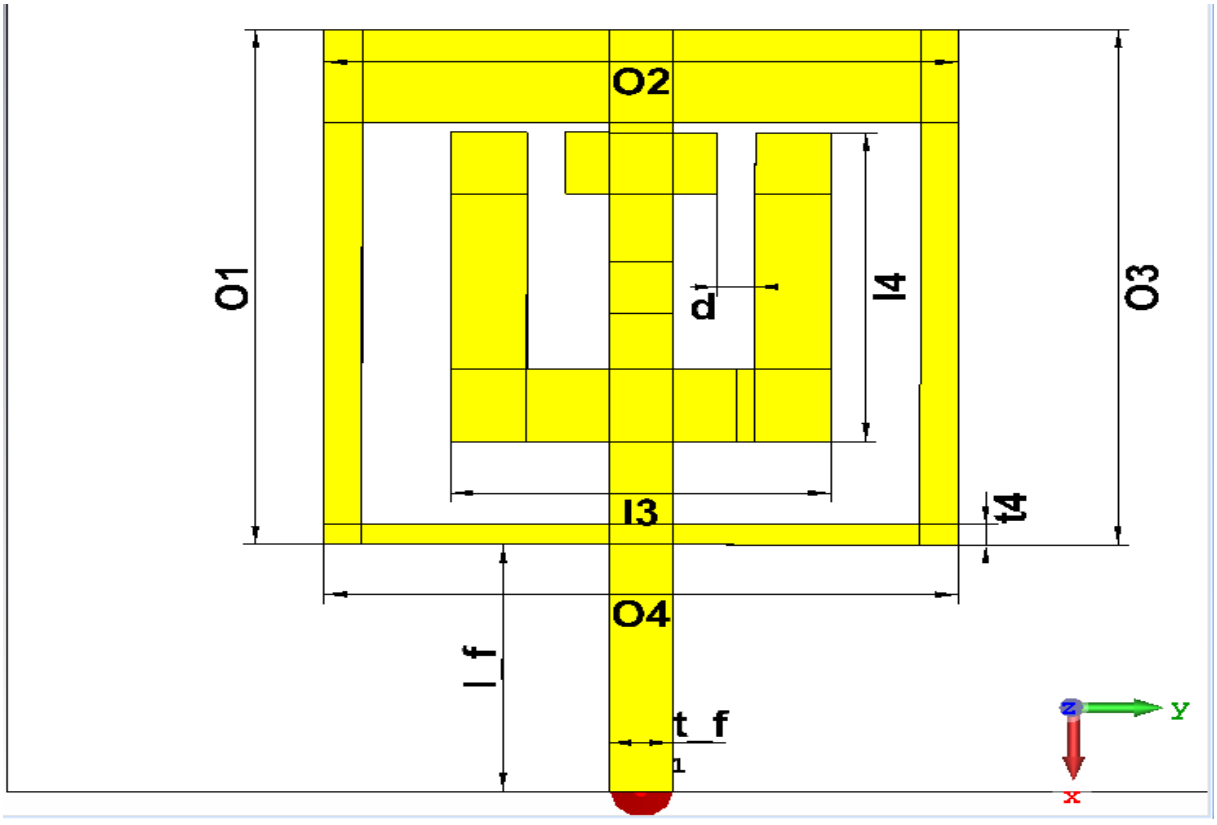

Figure-3.5: Labeled top view of the model-1

Table-3.1

Notable Dimensions of Model-1

Antenna Parameters	Descriptions	Value(mm)
ls	Substrate length	10
ws	Substrate width	10
l_f	Length of microstrip	2.4
t_f	Thickness of microstrip	0.5
O1,O2,O3,O4	Length of each arm of the outer ring	5
t4	Width of the O4 arm of outer ring	0.2, 0.3, 0.9

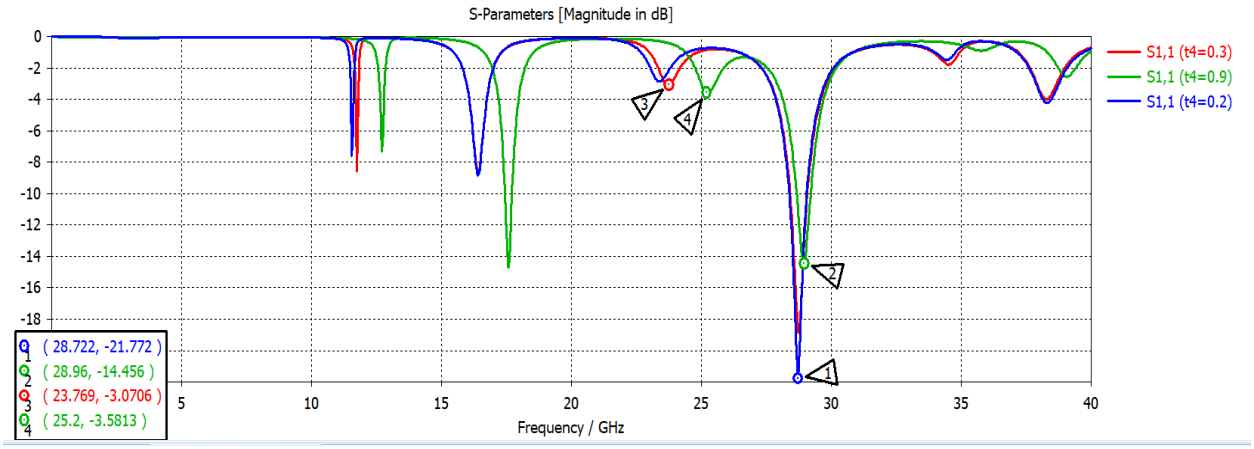

Figure-3.6: S_{11} response of the model-1 antenna due to change in the thickness t4 of O4 arm

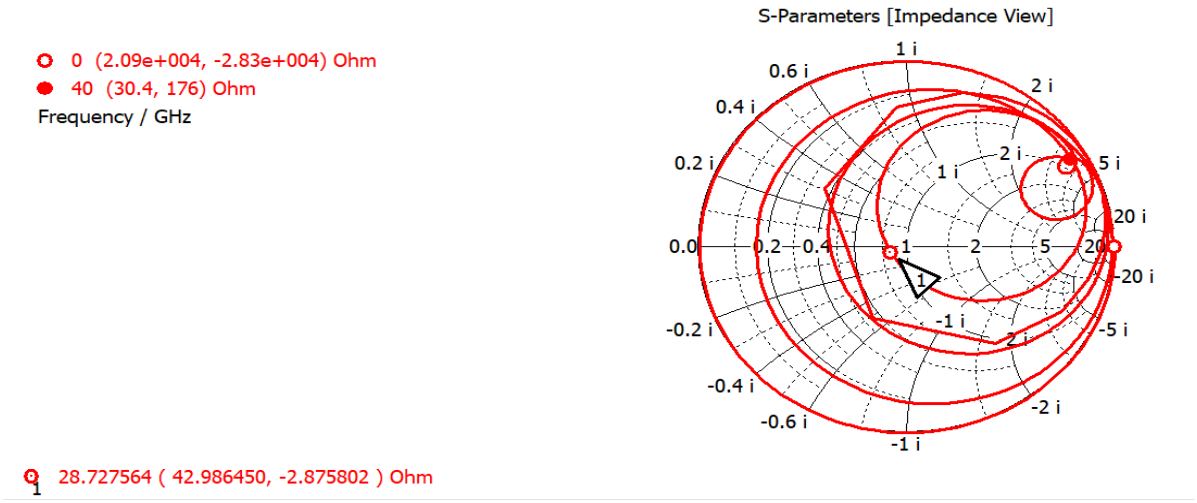

Figure-3.7: Smith chart representation of antenna input impedance

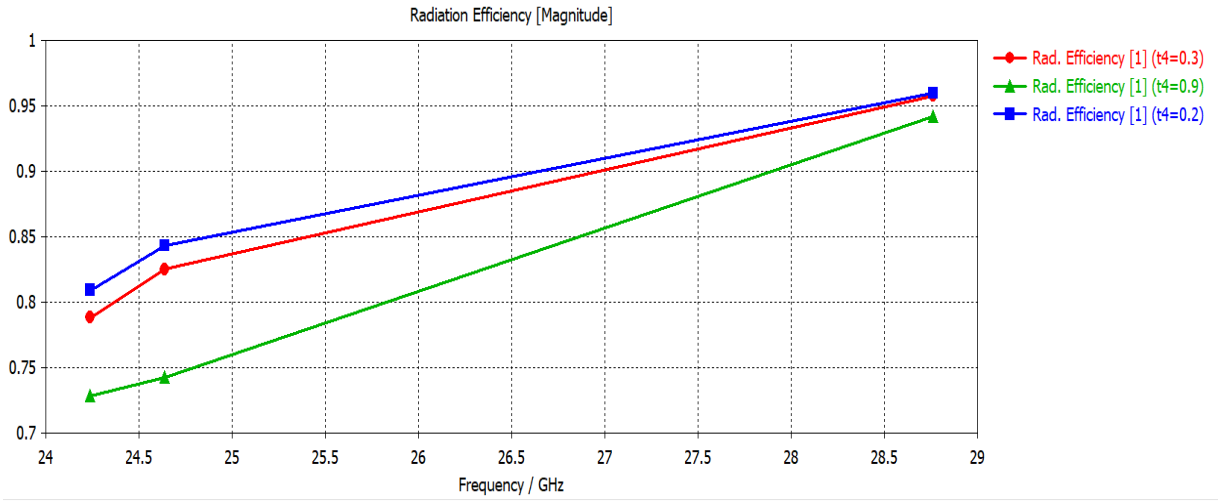

Fig-3.8: Radiation efficiency of the model-1 antenna

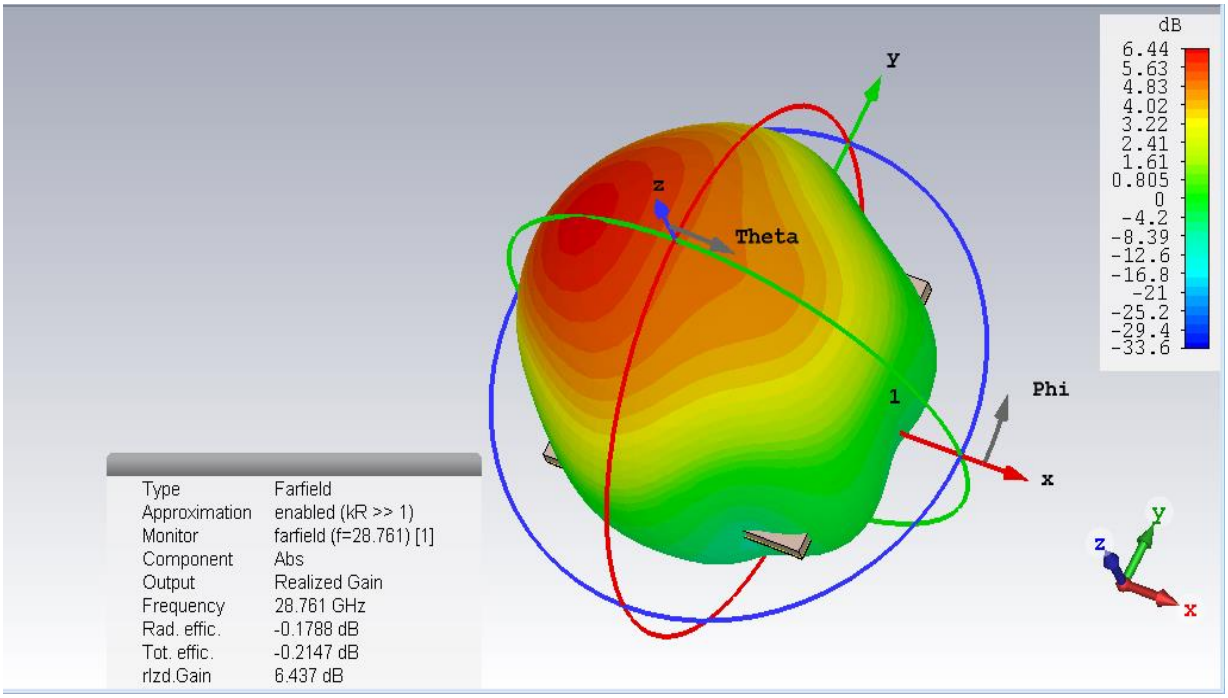

Fig-3.9: 3D Radiation pattern (Realized Gain) at 28.761 GHZ

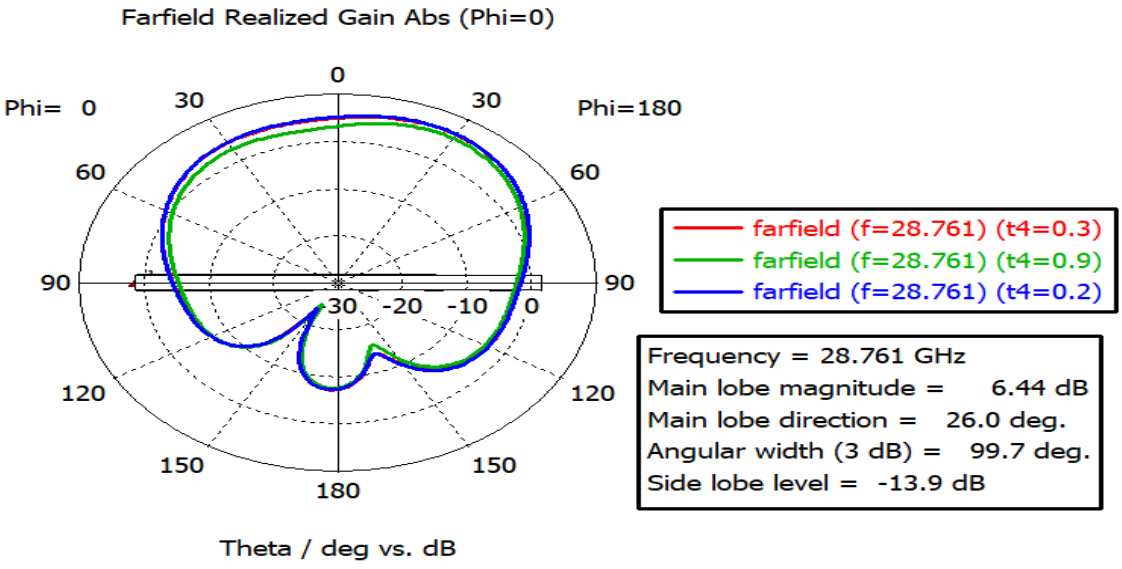

Figure-3.10: Polar plot of the radiation pattern (Realized Gain)

The very first of our antenna models, which we named Model-1, is a result of many simulations that preceded this design. In terms of all mm-wave considerations, this is not a high performing design. We started with this case to show the continuous progression towards expected result. As can be seen from the figure, this antenna doesn't reflect the original metamaterial structure described in subsection 3.1. It is a modification of the metamaterial design in terms of dimensions. The antenna is based on the substrate Rogers RT Duroid 5880 with a dielectric constant of ε_r =2.2. We selected this substrate for its low loss tangent and high efficiency performance in many other mm wave designs[6][7]. By using equations 3.1, 3.2, and 3.3 we found out that for a microstrip feed of width 0.5mm and characteristics impedance of 94.91Ω the antenna impedance Z_L stands out to be 43.10-2.5j =43.17Ω, which is almost similar to the antenna input impedance as shown in the smith chart of figure 3.7. This antenna's return loss performance could be seen from figure-3.6, which shows the evolution of S_{11} response with respect to the change in the thickness t4 of the O4 arm of the antenna. From S_{11} we can see that, the antenna has a resonance at 28.7GHz, but it is not exactly at the 5G band designated by FCC. With a few more tunings we could get there, but the multi band performance of this antenna is very poor with only one band present. The antenna radiation efficiency is in the range of 85-90% for all three cases, and the radiation looks homogeneous throughout the XY- plane. The realized gain at 28.76 GHz is also a good 6.43dB. So, it is a fair design for a single band, but far from achieving our multi band objective. Also, with a very wide beam, this could be useful for beamforming, but in case of massive MIMO the isolation(S_{12} and S_{21}) may require more physical space. So, we move onto our next design which we designate as Model-2.

Model-2:

The Model 2 is not an immediate outcome from the results of Model-1. Rather we went through multiple simulations and prior publications to make a narrow beam multi band antenna. In this model we've applied a design idea presented by Hasan et. al.[6]. The idea is to skew the path of surface current distribution, thereby creating a local high intensity point in the antenna. This high intensity points of the surface current in terms shaped the radiation pattern of the antenna. The physical design and characteristics of this antenna is shown in figures below.

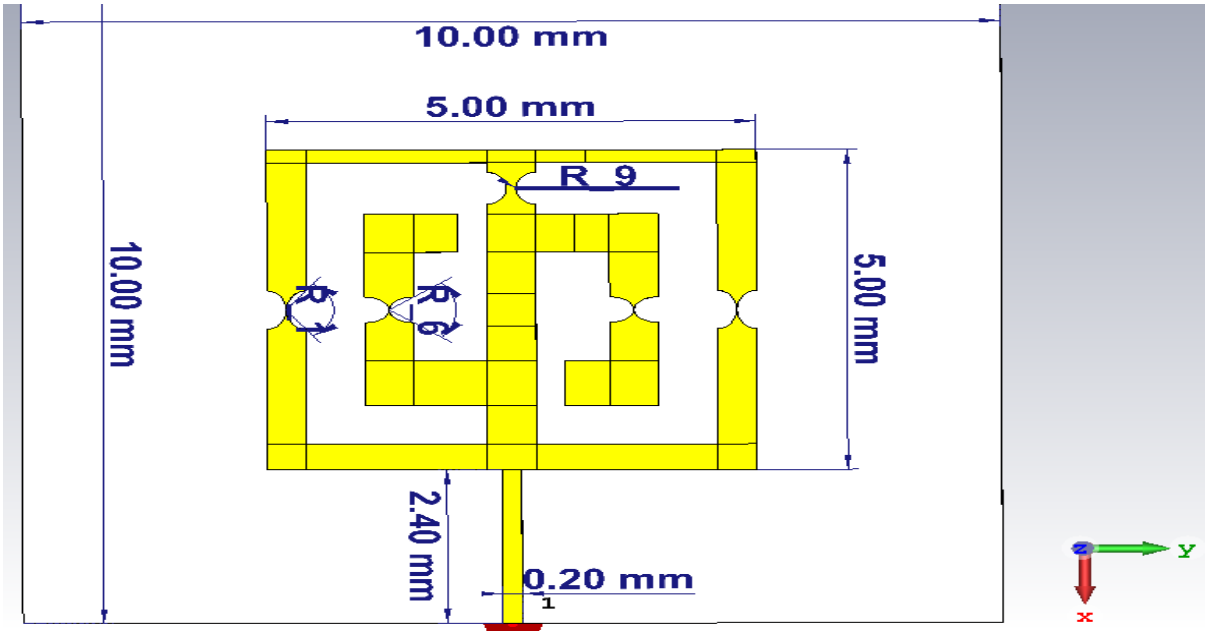

Figure-3.11: Geometrical design of the proposed model-2 antenna

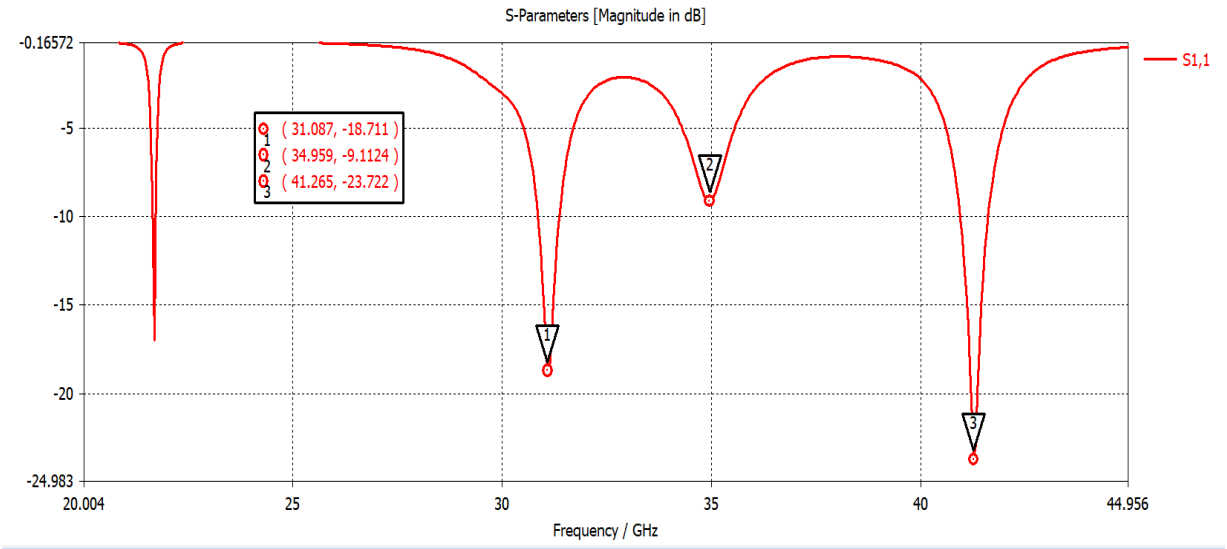

Figure-3.12: S11 response of the antenna over the frequency range 20GHz-45GHz

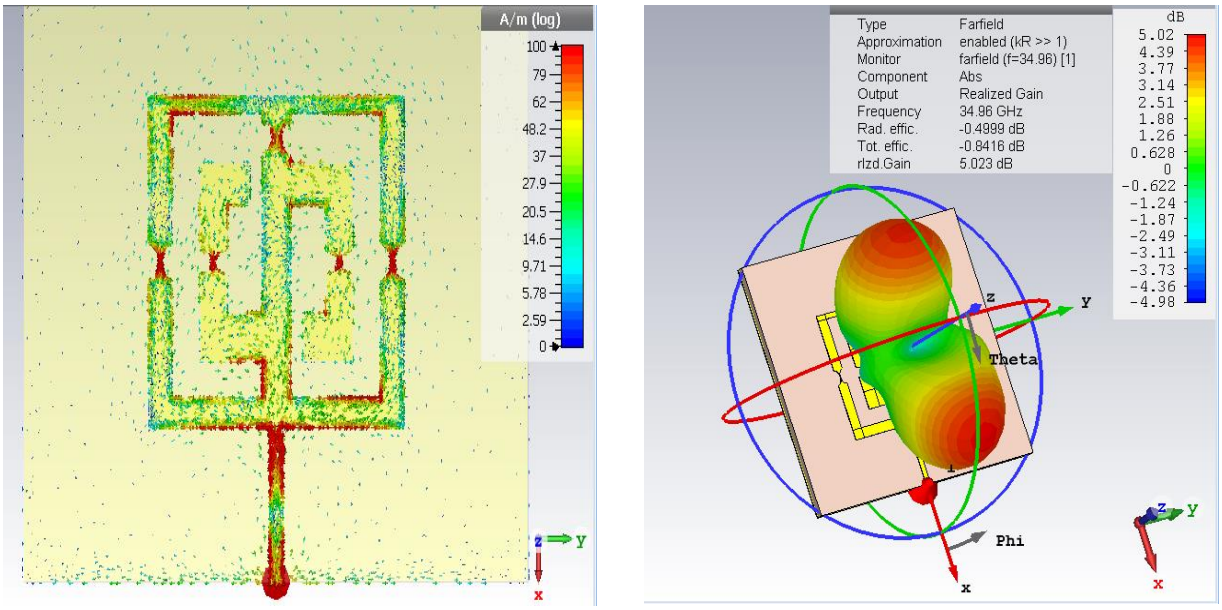

(a) (b)

Figure-3.13: (a)Surface current distribution at 34.96GHz (b) 3D Radiation pattern at 34.96GHz

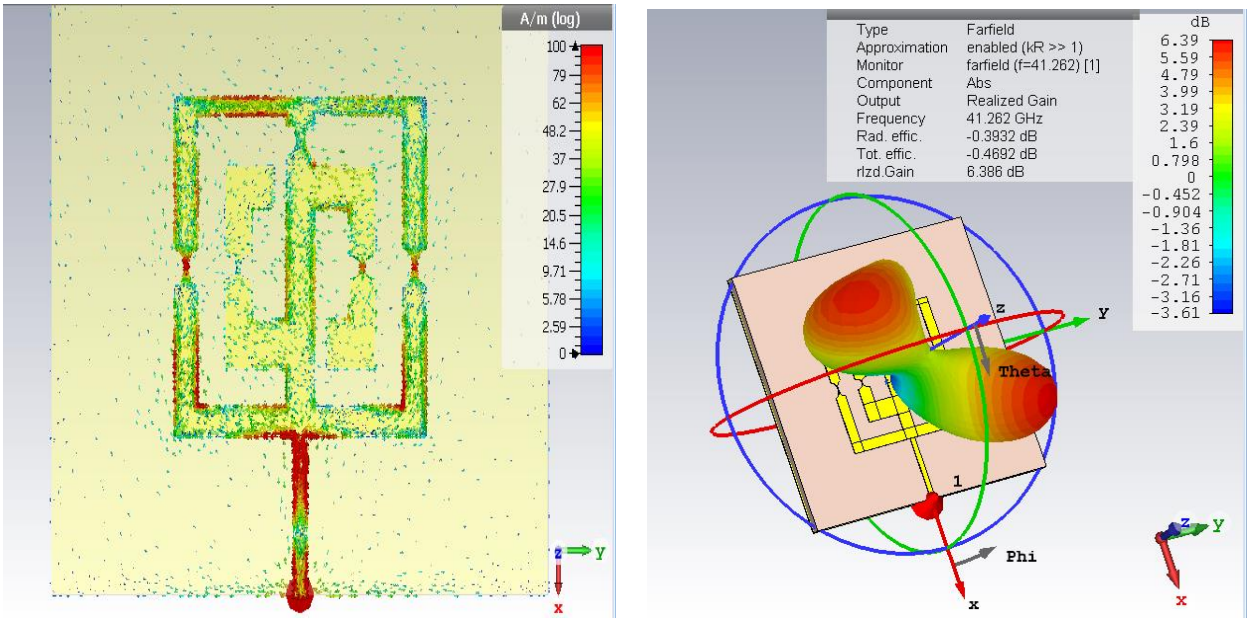

(a) (b)

Figure-3.14: (a) Surface current distribution at 41.26 GHz (b) 3D radiation pattern at 41.26GHz

Table-3.2

Notable Dimensions of Model-2

Antenna Parameters	Descriptions	Value(mm)
R_1	Radius of all skewed points in the outer ring	0.3
R_6	Radius of all skewed points in the inner ring	0.25
l_f	Length of microstrip	2.4
w_f	Thickness of microstrip	0.25
R_9	Radius of all skewed points in the center bar	0.2

The antenna in this case has a dimension of 5mm X 5mm in the radiating structure, as shown in figure-3.11 . The overall dimension considering the substrate is 10mm X 10mm. Notable dimensions of the antenna are shown in table 3.2 . The feedline of this antenna is 2.4mm in length, which is equivalent to lambda/4 or quarter wavelength in 31GHz frequency. Since we have an objective to achieve multiple bands, the quarter wavelength is set to an intermediate frequency instead of a certain 5G band. From the S11 response of figure 3.12, we can see that the antenna is resonant at 31.087 GHz, 34.959 GHz, and 41.265GHz in the mm wave range. All these resonances are very near to the resonance frequencies of our objective. By comparing surface current distribution and radiation pattern data, we can see a pattern in the shaping of the main lobe of radiation. For instance at figure 3.13(a) we can see that all of the curved arms of the antenna have a high surface current intensity point. Since the current intensities along the horizontal Y axis cancels each other, the current intensity along X axis is prevailing here, and hence the pattern is in X axis as shown in figure- 3.13(b). In figure-3.14(a) we can see that the current distribution is not prevalent in any one single skewed point. Overall it is distributed unevenly throughout the various arms of the antenna and also the curved choke points. So, as a result the antenna radiates diagonally in between X and Y axes. The curving of the antenna arms also gave rise to very narrow sidelobes. From both the patterns we can see that this antenna has high gain(in the range of 5dB and 6dB) at both frequencies of operation shown here. With the good results from this simulation we tried a different way in the next model, which we will name Model-3. Afterwards we combined results from both Model-2 and Model-3 to achieve a better antenna.

Model-3:

This antenna is not exactly the manifestation of results we came up with the antenna at model-2. This is rather a detour to test the possibility of a new design idea which was used by another work of Hasan et. al.[53] for a UWB monopole antenna. In this model we kept the regular rectangular structure of the antenna, without adding any curve in either arms. Apart from that we added an inverted U stub at the far end of the radiating patch. We also fed the antenna with an inset microstrip feed to get a better impedance matching. The geometry and results are shown below.

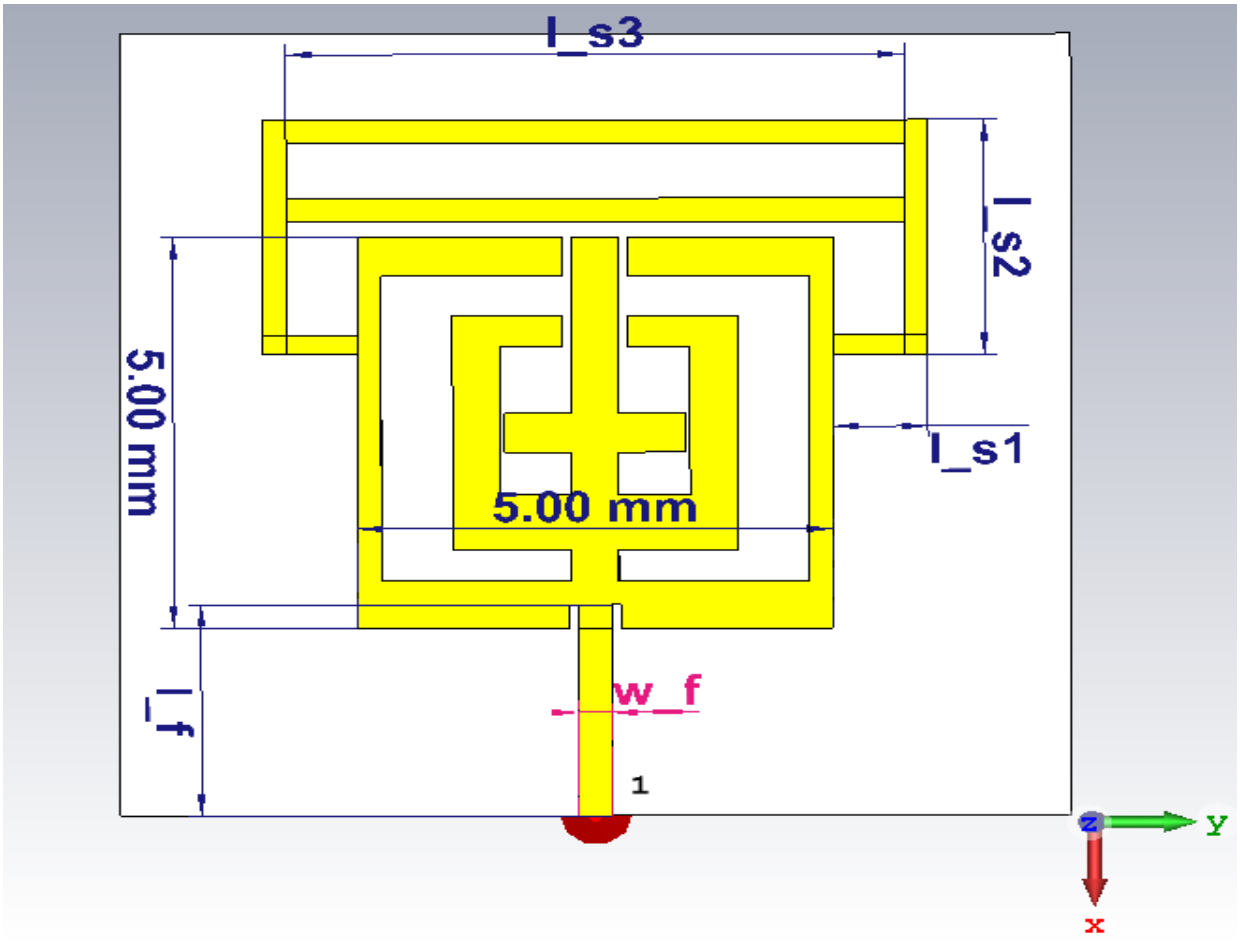

Figure-3.15: Geometry of the antenna with U stub

Table-3.3

Notable Dimensions of Model-3

Antenna Parameters	Descriptions	Value(mm)
l_s1	Stub support length	1
L_s1	Stub support length	3
L_s2	Stub length	6.5
l_f	Length of microstrip	2.7
w_f	Thickness of microstrip	0.35

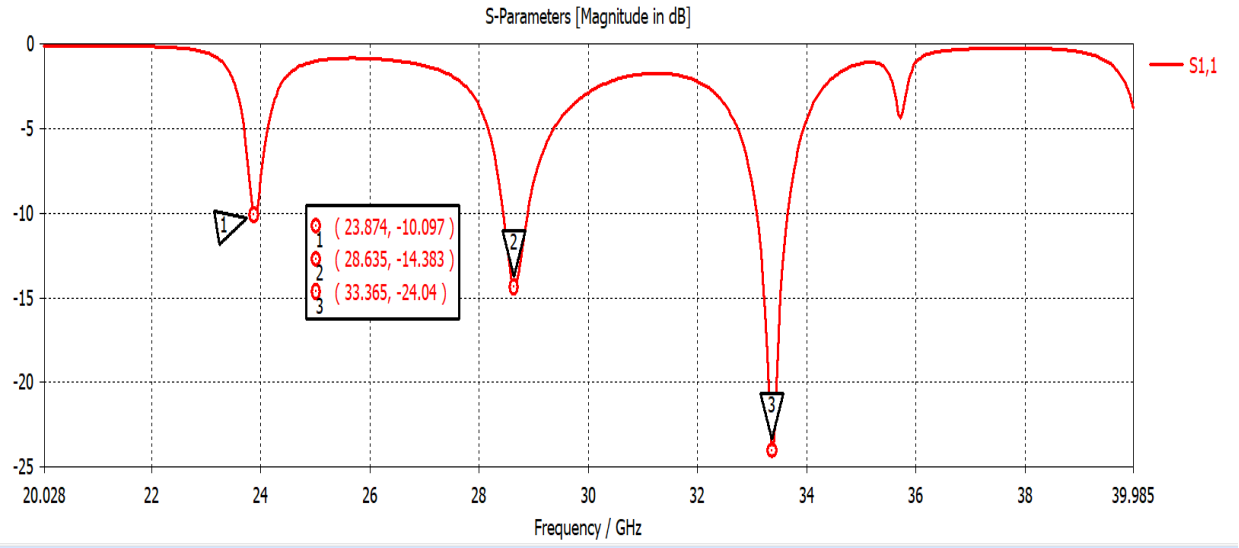

Figure-3.16: S_{11} response of the model-3 antenna

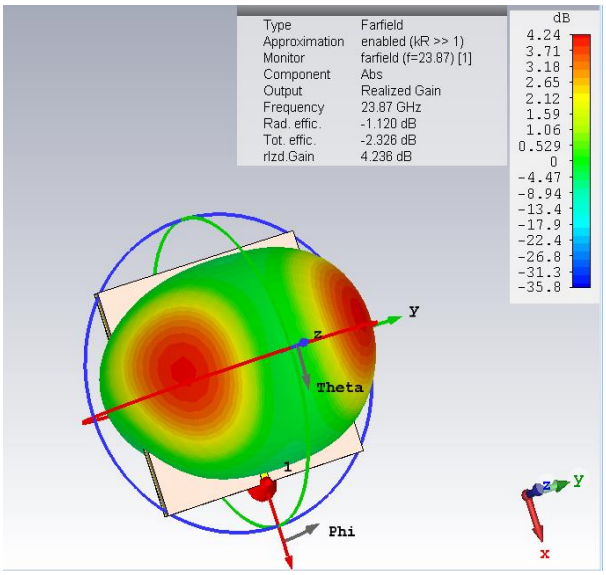

(a)

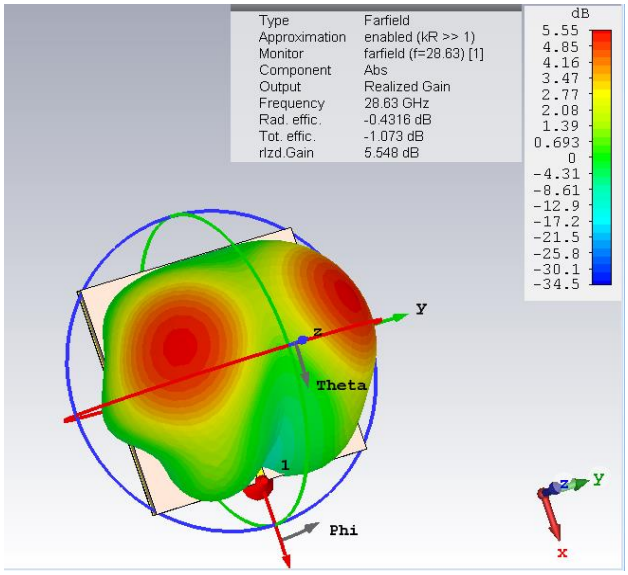

(b)

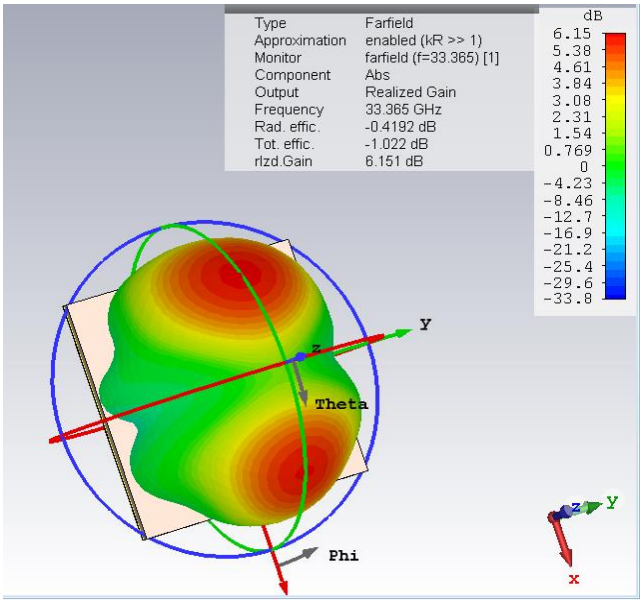

(c)

Figure-3.17: Radiation pattern (Realized Gain) at (a) 23.87GHz (b) 28.63 GHz (c) 33.36 GHz

From figure 3.15 we can see that there are basically two stubs along the width of the antenna at the far end. We kept one stationary and moved the second one to control the impedance and thereby controlling the return loss. From the return loss(S_{11}) response we can see that there are three distinct resonances at 23.8GHz, 28.635 GHz, and 33.36GHz. First two resonances are at the 5G band with both having -6dB bandwidth (50% transmission) of 344 MHz and around 1GHz at 23.8GHz and 28.63 GHz respectively. The third resonance at 33.36GHz also has a -6dB bandwidth (50% transmission) of 1GHz . By tuning the antenna further there is a real chance to make it a tri band antenna at this point. The far field radiation pattern for mdel-3 antenna is shown in figure-3.17. We can see from figure 3.17(a) and 3.17(b) that, at frequencies 23.8 GHz and 28.63 GHz the radiation is along Y axis with two main lobes along the Z axis. For 33.365 GHz the radiation is along Y axis with same two distinct main lobes. One notable factor in this model is the presence of significant sidelobe at the back of the antenna. Even though it is a full ground antenna, there is a sidelobe for each of the simulated frequencies. This and the wide beamwidth of the antenna will require more spacing between adjacent antenna elements in a massive MIMO system to stop coupling between two antennas. So, we combined the design idea of Model-3 and the narrow beam design idea of Model-2 in a new design we will name Model-4. In the next section we will describe the hybrid antenna we came up with, which performs better.

Model-4:

In this step of the design process we combined our knowledge from previous cases and designed an antenna which is loaded with a U shaped stub and also has skewed arms for surface current intensity. We were also bound by the physical fabrication parameters such as gap width, minimum width, minimum length etc. So the design is optimized according to the requirements of the fabrication company. All the physical dimensions and results for mode-4 antenna are shown below in figure 3.18-3.25 .

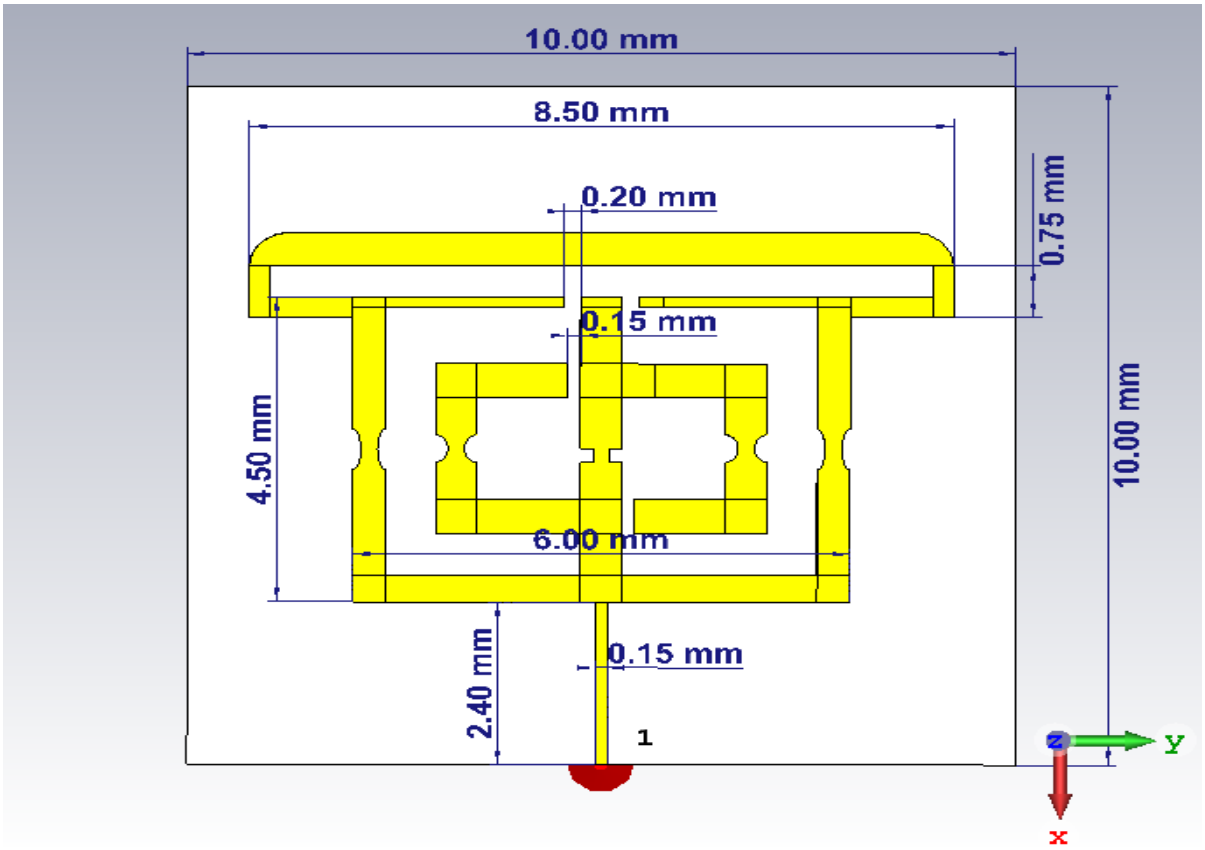

Figure-3.18: Geometry of the Model-4 Antenna

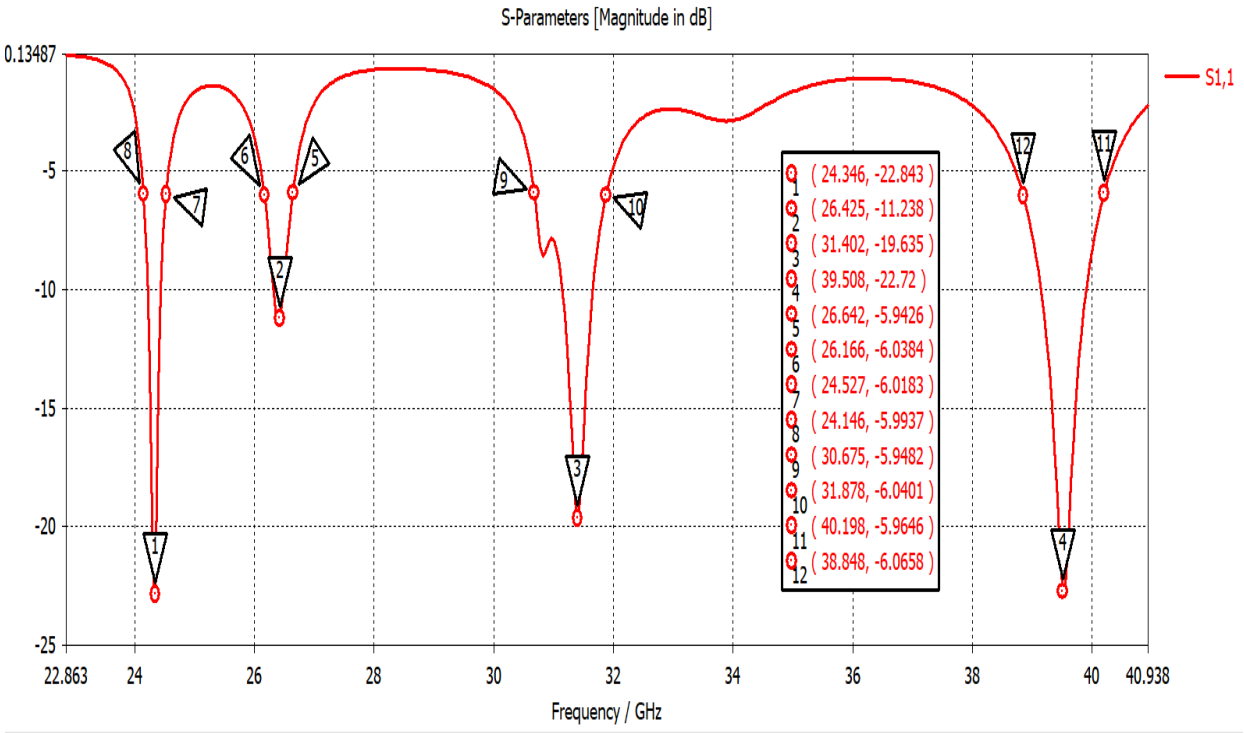

Figure-3.19: S11 response of the Model-4 Antenna

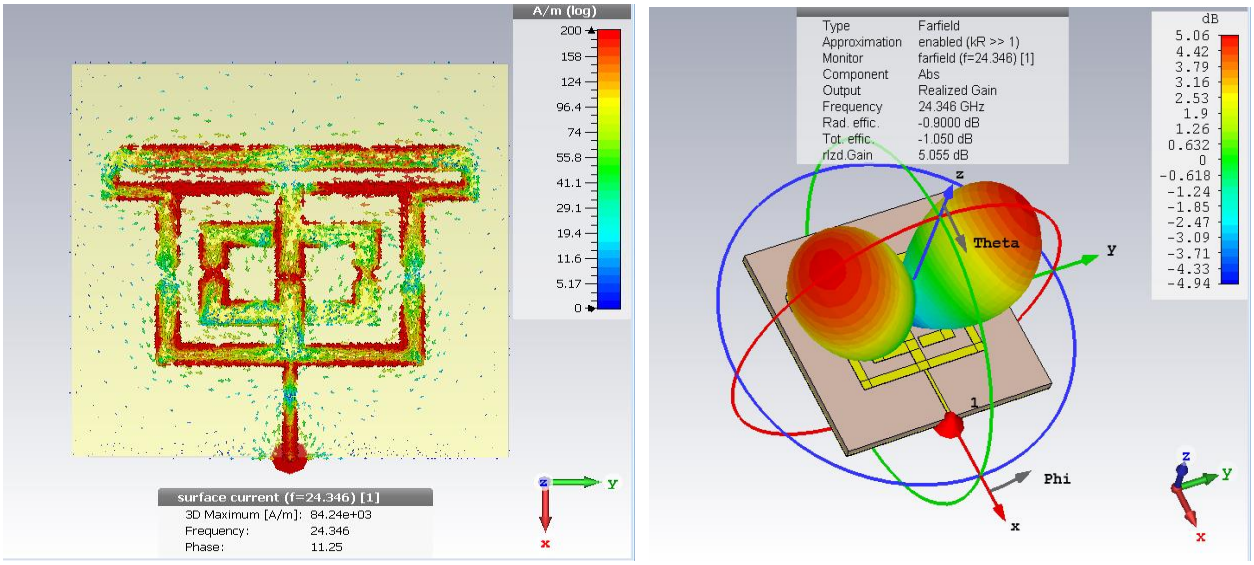

(a) (b)

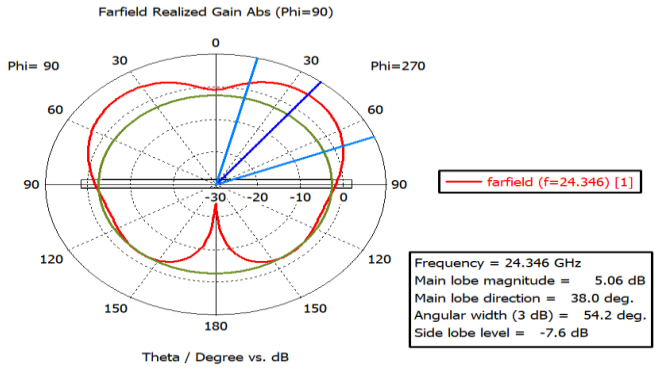

(c)

Figure-3.20: (a) Surface current density (b) 3D radiation pattern (c) polar plot of the radiation pattern at 24.346 GHz

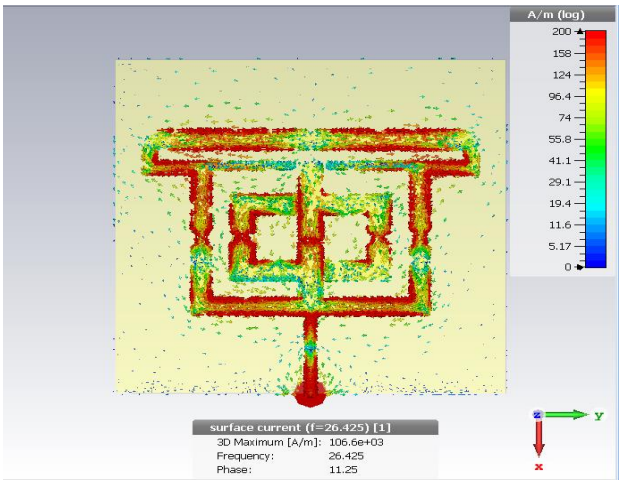

(a)

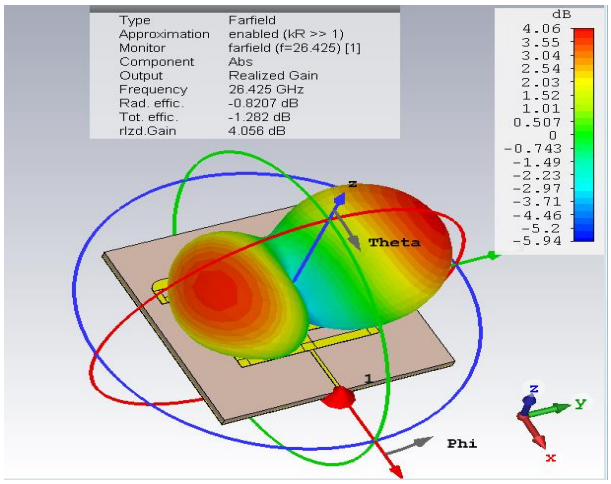

(b)

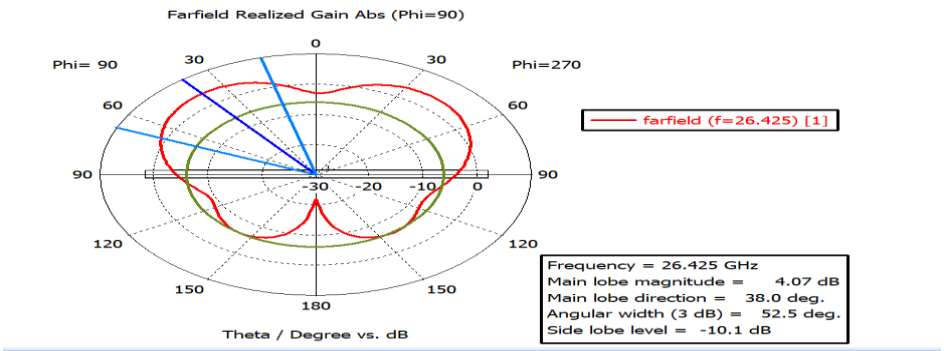

(c)

Figure-3.21: (a) Surface current density (b) 3D radiation pattern (c) polar plot of the radiation pattern at 26.425 GHz

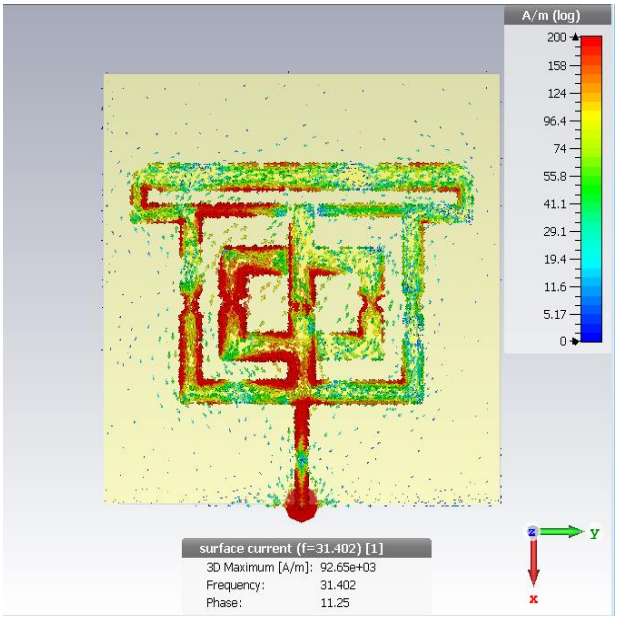

(a)

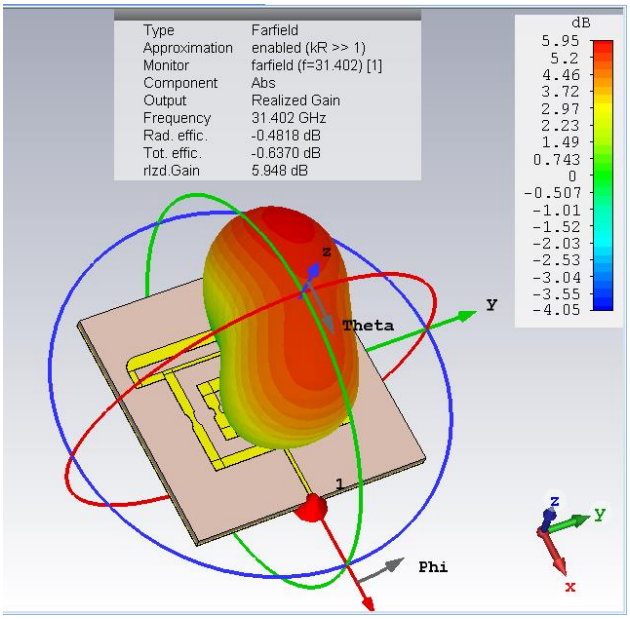

(b)

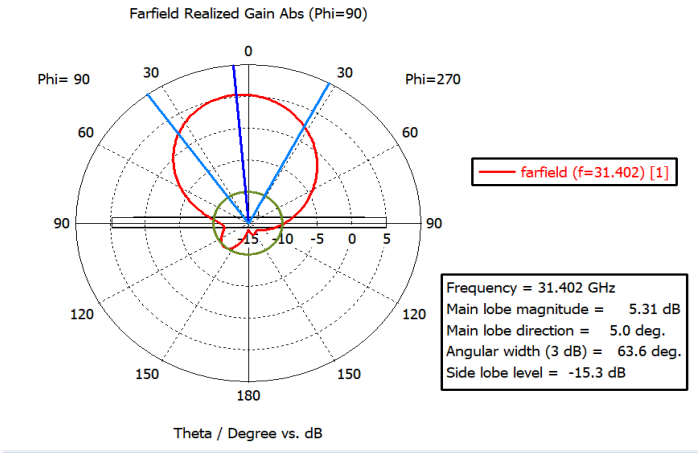

(c)

Figure-3.22: (a) Surface current density (b) 3D radiation pattern (c) polar plot of the radiation pattern at 31.402 GHz

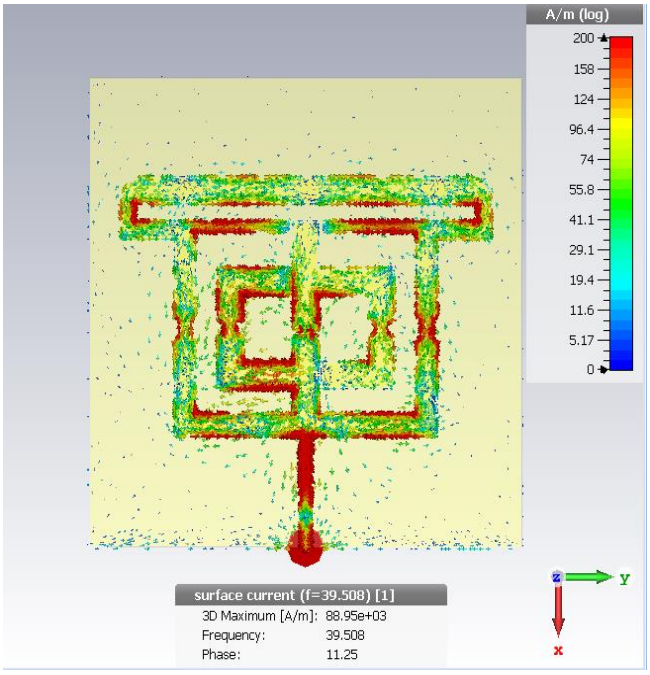

(a)

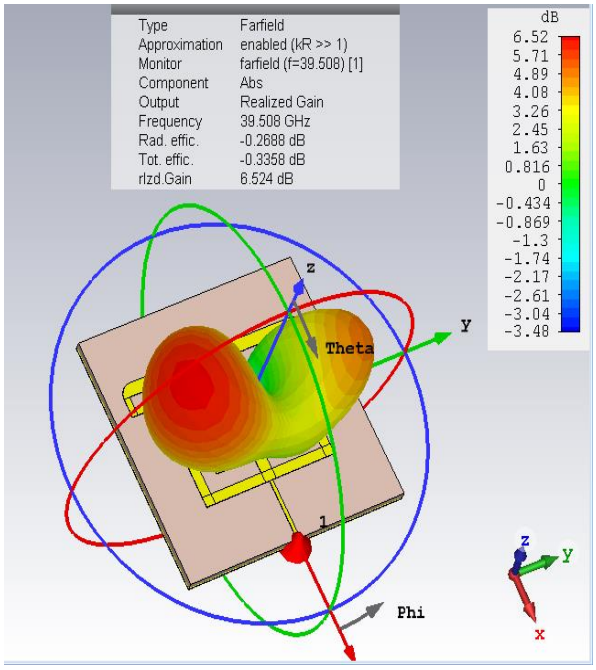

(b)

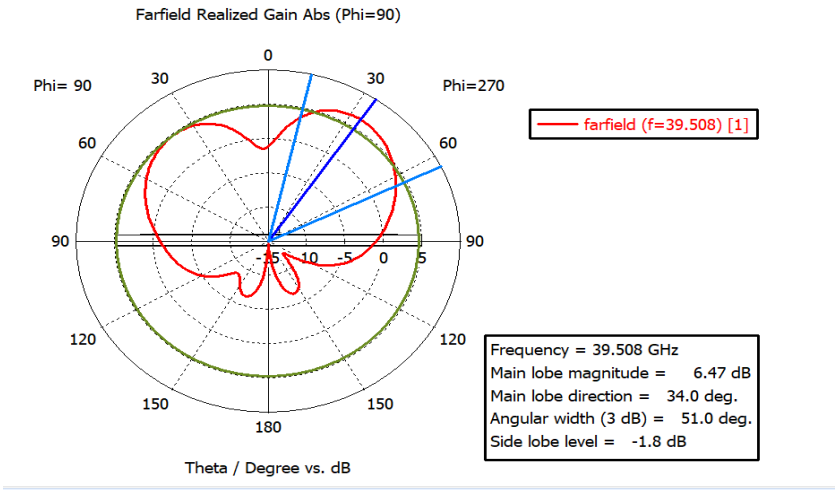

(c)

Figure-3.23: (a) Surface current density (b) 3D radiation pattern (c) polar plot of the radiation pattern at 39.508 GHz

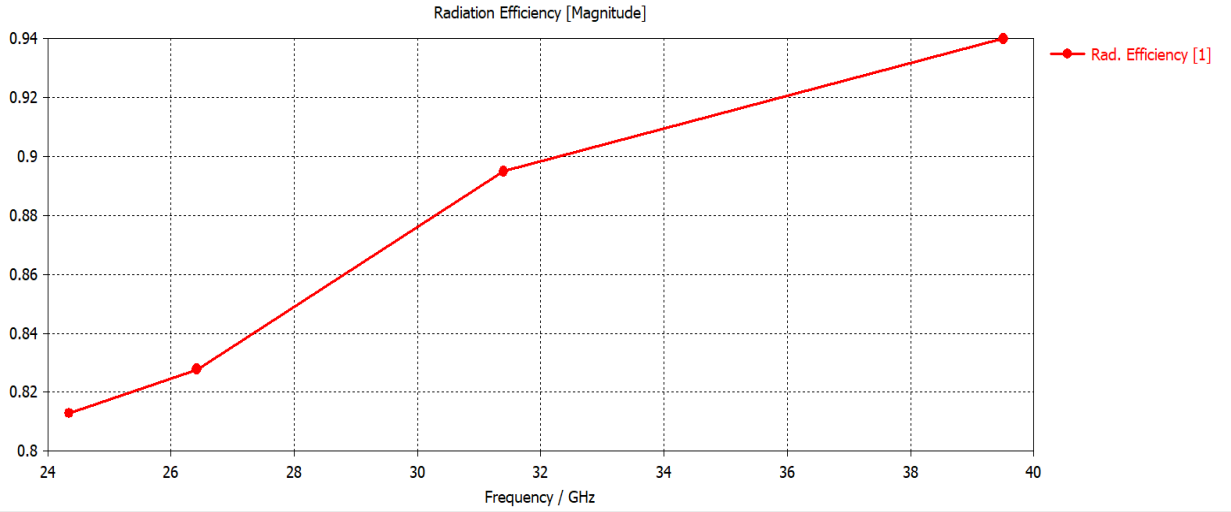

Figure-3.24: Radiation efficiency of the Model-4 antenna

The antenna geometry is shown in figure 3.18 . As we can see from the geometry, all arms of the antenna along the feed line are curved at the center to intensify the surface current at those points. The U stub is also added at the far end of the antenna. With the smooth edge of the antenna the radiation edge becomes narrow and thereby radiation loss is decreased [54]. The radius of outer ring curves are 0.1mm and radius of inner ring curves are 0.15mm. The notch at the center bar along feedline is 0.15mm X 0.15mm in size. From the S11 response in figure-3.19 we can see that there are 4 notable resonances in the mm wave band. All four resonances occurred at 24.346 GHz,26.425 GHz, 31.402 GHz, 39.508GHz. Along with the resonances, there are sizeable bandwidths in the higher 5G band of 39GHz. Bandwidths measured at half power point i.e. -6 dB is shown in table 3.3 . We can see that higher 5G band of 39 GHz has a good

bandwidth of 1.35GHz and following close by is the 31GHz band with a bandwidth 1.22.GHz.Though the 31 GHz band is not dedicated for mm wave 5G communication, little tuning could take this band to 28 GHz, which is the mm wave 5G band. The other 5G band is 26 GHz band, which FCC is planning to designated for 5G, has a bandwidth of 476 MHz . Finally, the 24 GHz band has a bandwidth of 381 MHz.

Table 3.4

-6 dB (1/2 power point) Bandwidth at each radiating band

Frequency range	Bandwidth
24.146 GHz-24.527 GHz	381 MHz
26.166 GHz- 26.642 GHz	476 MHz
30.657 GHz – 31.878 GHz	1.22 GHz
38.848GHz-40.198 GHz	1.35GHz

From the surface current density of the antenna and the corresponding 3D and polar radiation plot we can see a consistent pattern with very high directivity and realized gain. Radiation pattern at all frequency bands consisting of two directional main lobes propagating along +Z direction. At the resonance frequency of 31.402 GHz, the surface current tend to be more intense in one half of the antenna compared to the other half. Hence we have a directed beam with single lobe at 31.402 GHz. This model also has relatively good realized gains of 5.05 dB, 4.07 dB, 5.94 dB, and 6.52 dB at resonance frequencies 24.346 GHz, 26.425 GHz, 31.402 GHz, and 39.508 GHz respectively. This antenna also has an excellent radiation efficiency from

80-94%, depending on the frequency. Overall this could be dubbed as a perfect antenna to be used in a massive MIMO scheme for mm wave 5G communication. This antenna could be suitable for use in conjuction with a 5G chip and a matching network, but at its current dimension it is not suitable for testing with a network analyzer. Most of the commercially available SMK connectors are almost the same size as the Model-4 antenna. As this is a prototype we are proposing here, for the purposes of testing we need to connect it to the VNA. Hence, we modified this Model-4 to accommodate testing needs and fabrication requirements. This brings us to our final design.

Final Model:

The antenna proposed in this stage is the one we have chosen to put to test for a better 5G antenna. This is the combination of experience we gained by running numerous simulations on the structure. It is basically the Model-4 antenna, but printed on a bigger substrate and with a longer feed. These arrangements are made to accomodate the 2.92mm edge launch connector (FMCN1494 by Fairview Microwave). The compact size, maximum operating ceiling of 40GHz, and reasonable price made it suitable for use in our antenna testing. The antenna geometry and all the test results generated from simulation is shown in figures 3.25- 3.30 .

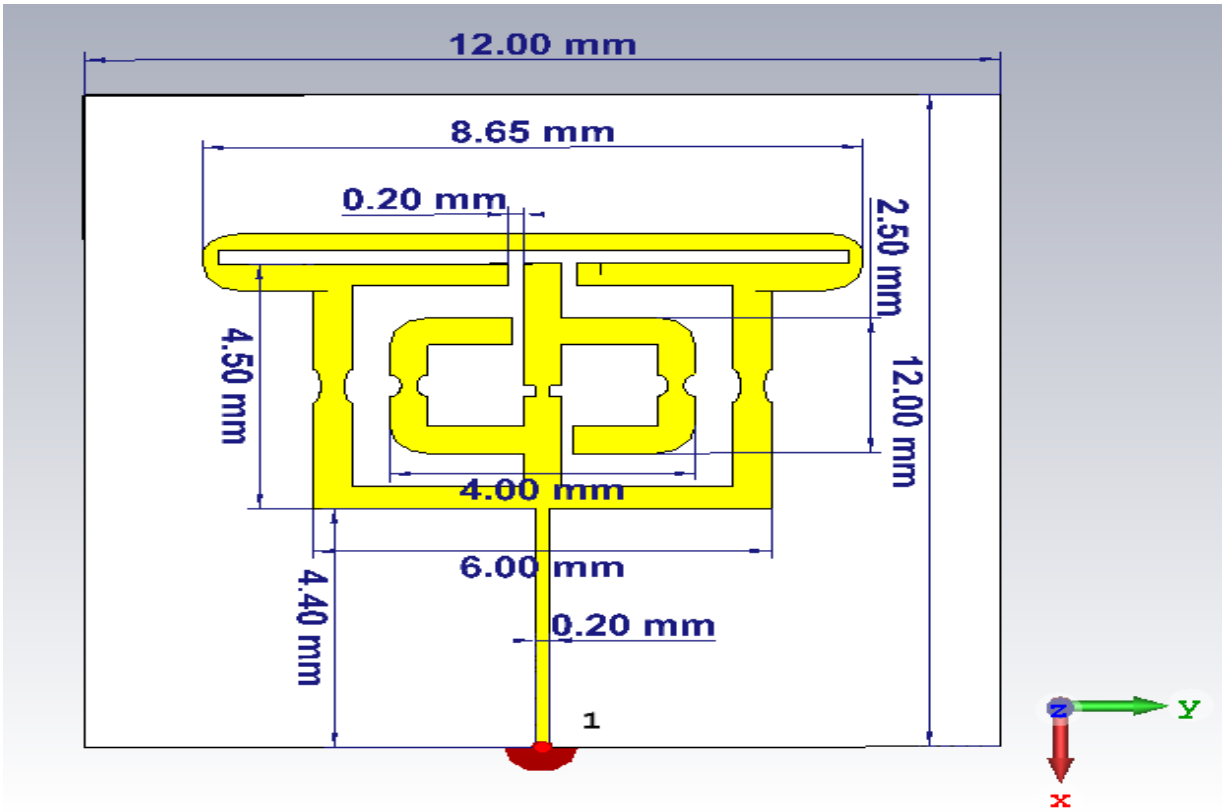

Figure-3.25: Geometry of the proposed 5G mm wave antenna

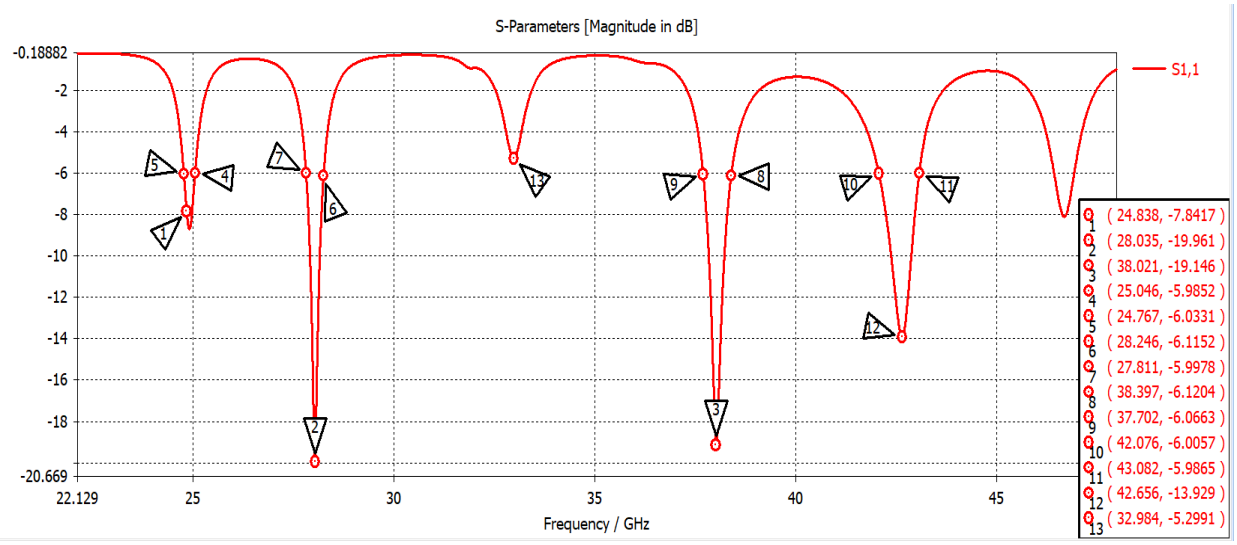

Figure-3.26: S11 response of the proposed Antenna

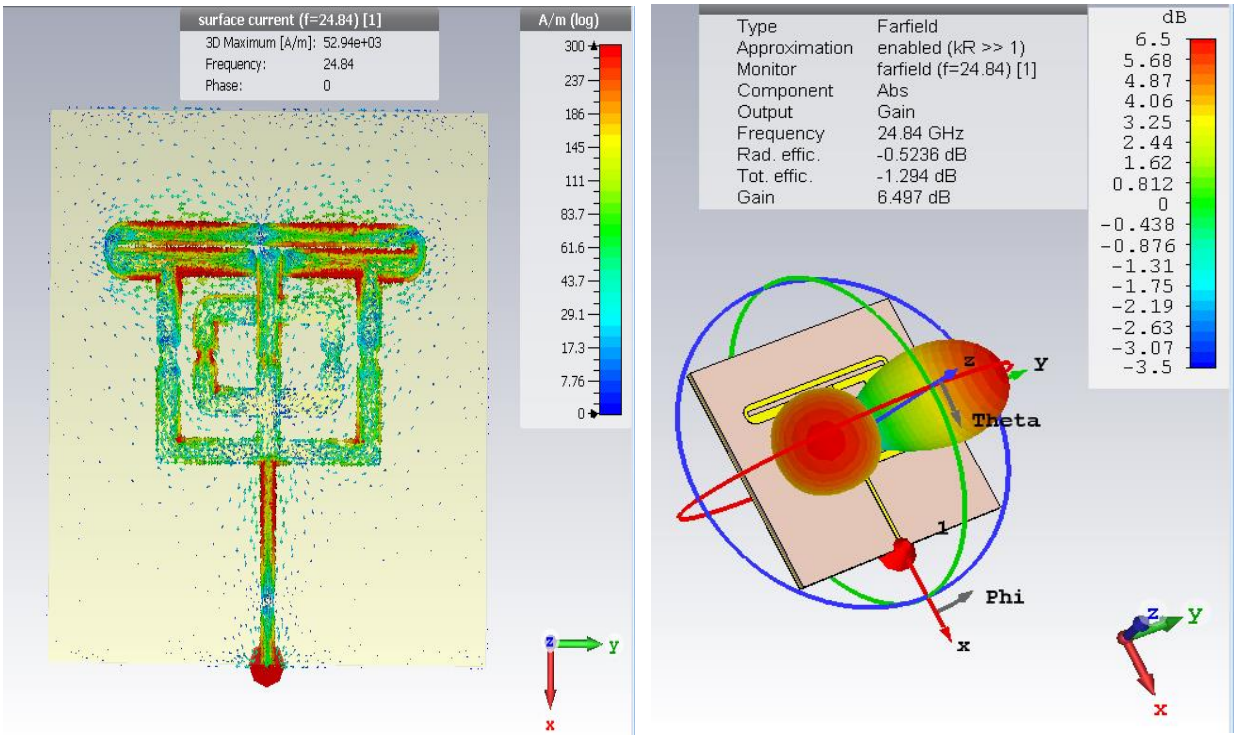

(a) (b)

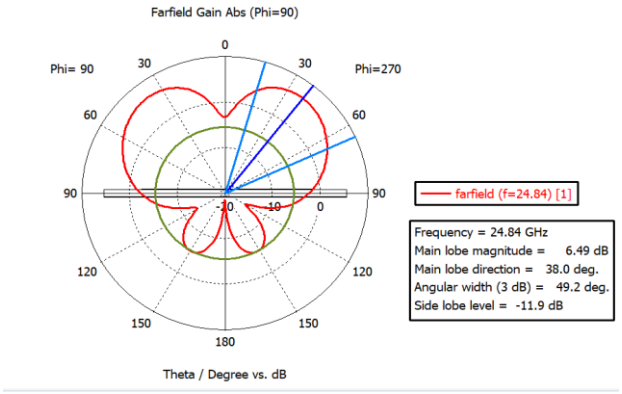

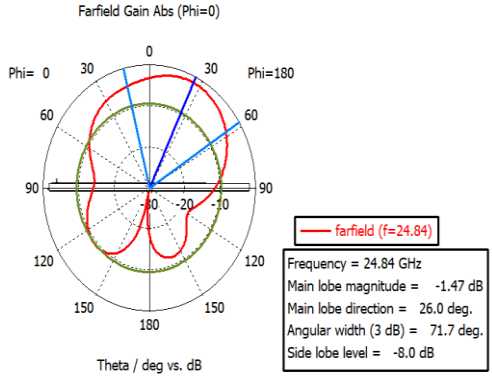

(c) (d)

Figure-3.27: (a) Surface current density (b) 3D radiation pattern (c) polar plot (phi=90°) (d) polar plot (phi=0°) at 24.84 GHz

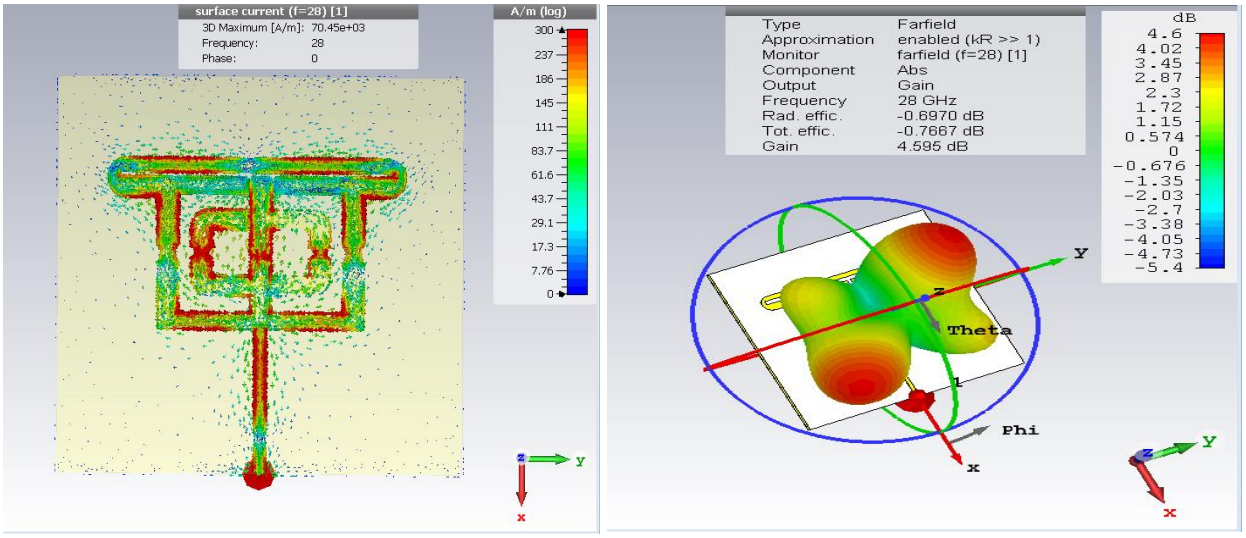

(a) (b)

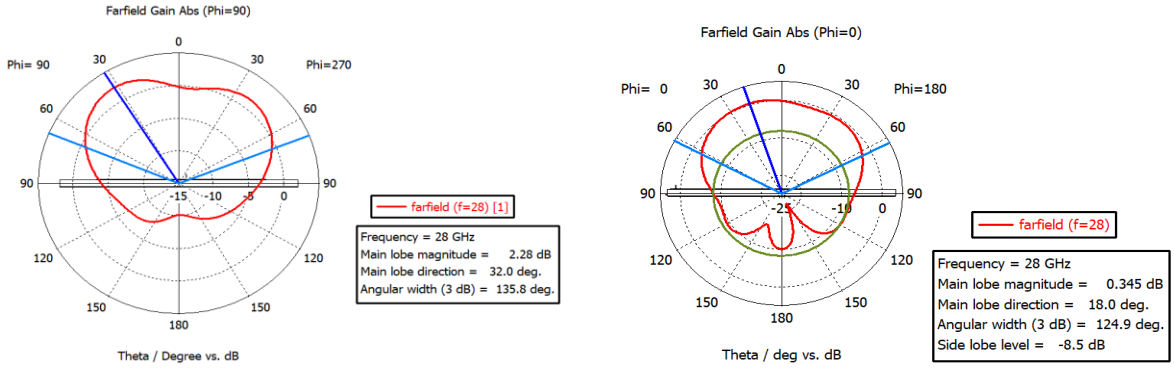

(c) (d)

Figure-3.28: (a) Surface current density (b) 3D radiation pattern (c) polar plot (phi=90°) (d) polar plot (phi=0°) at 28 GHz

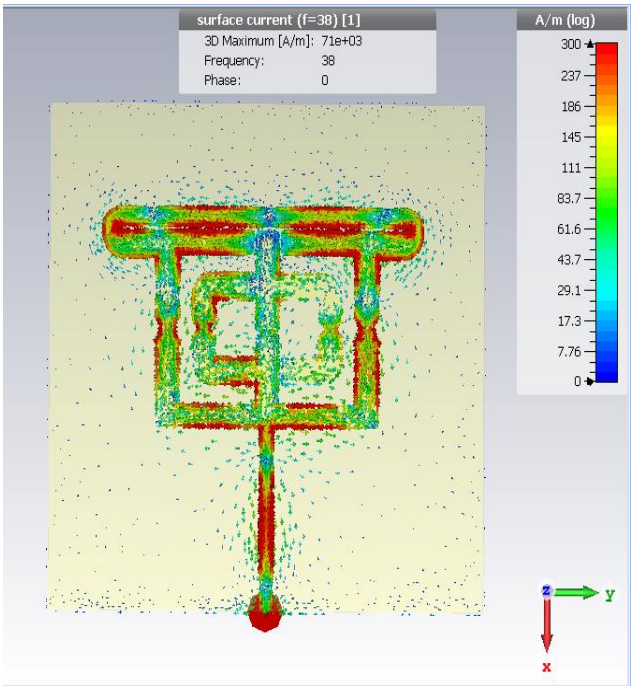

(a)

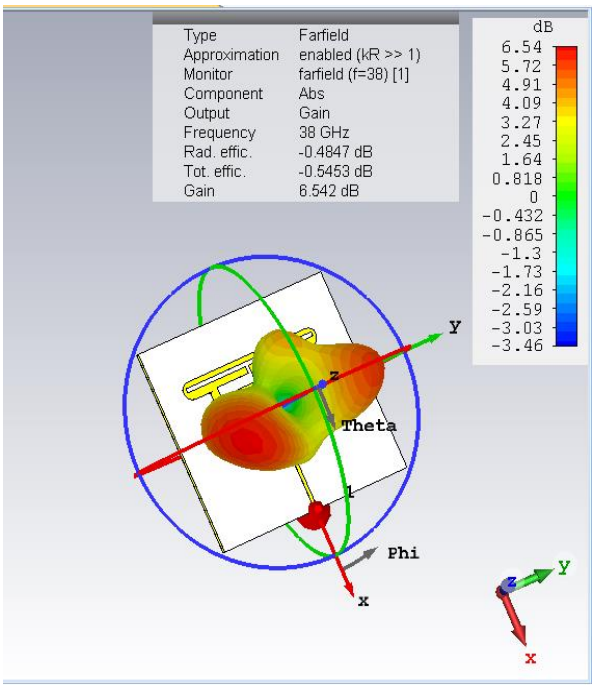

(b)

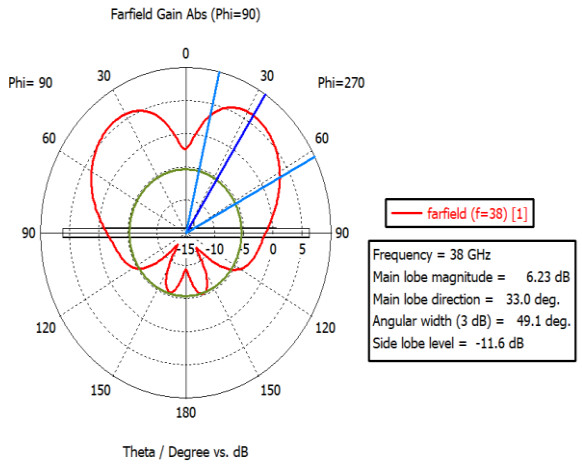

(c)

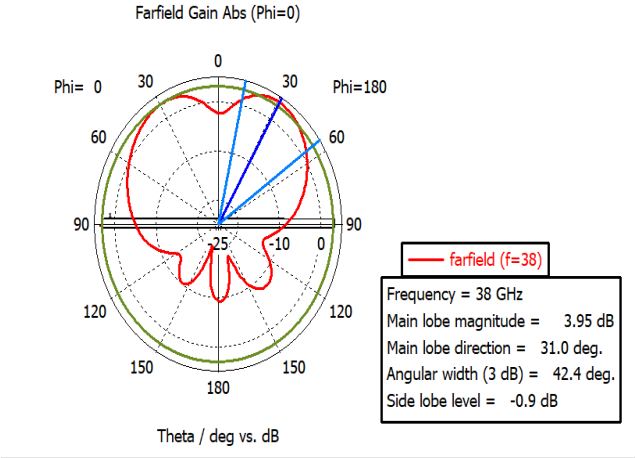

(d)

Figure-3.29: (a) Surface current density (b) 3D radiation pattern (c) polar plot (phi=90°) (d) polar plot (phi=0°) at 38 GHz

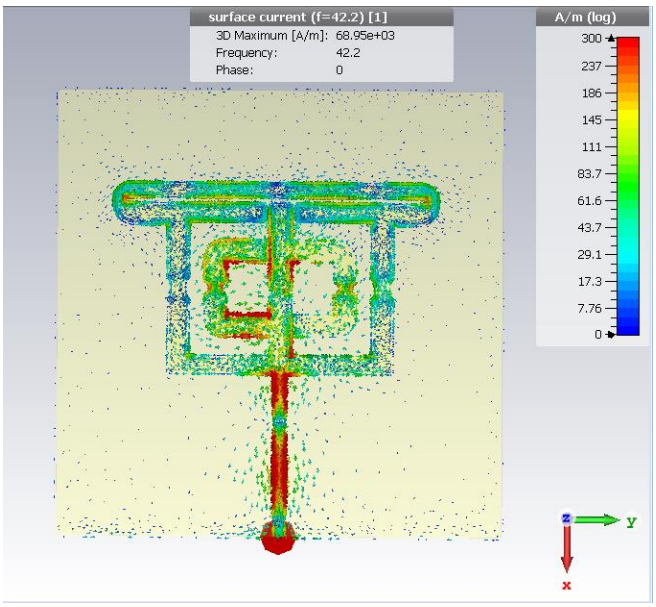

(a)

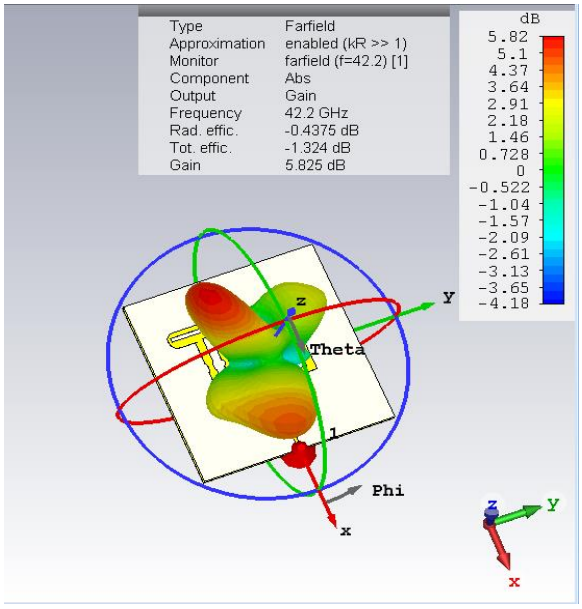

(b)

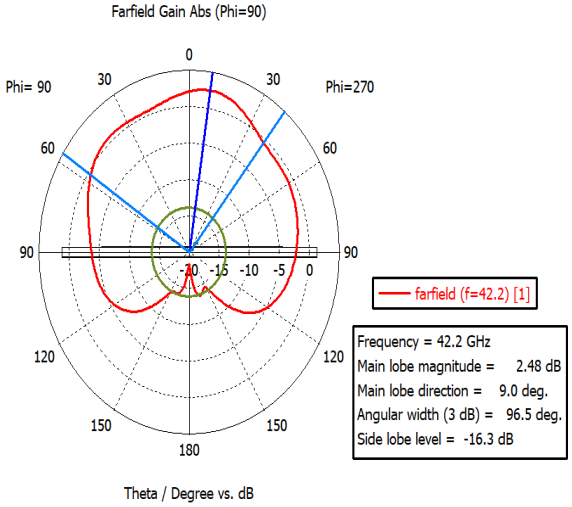

(c)

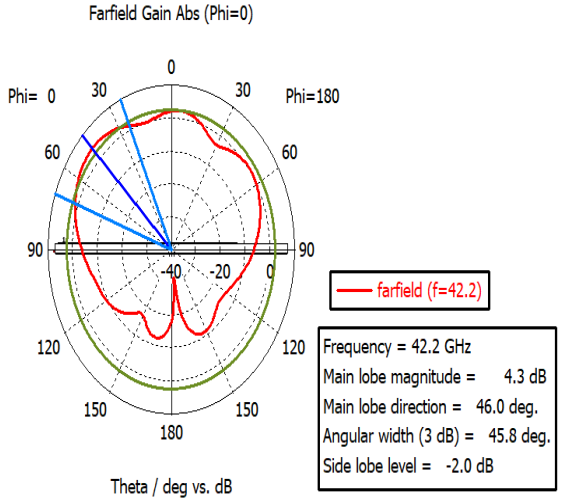

(d)

Figure-3.30: (a) Surface current density (b) 3D radiation pattern (c) polar plot (phi=90°) (d) polar plot (phi=0°) at 42.2 GHz

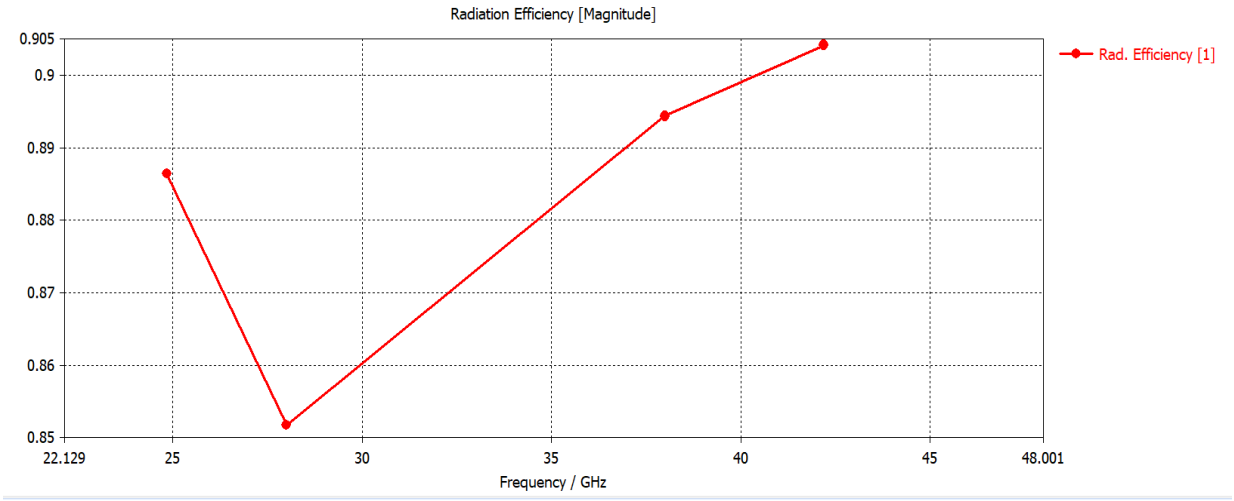

(a)

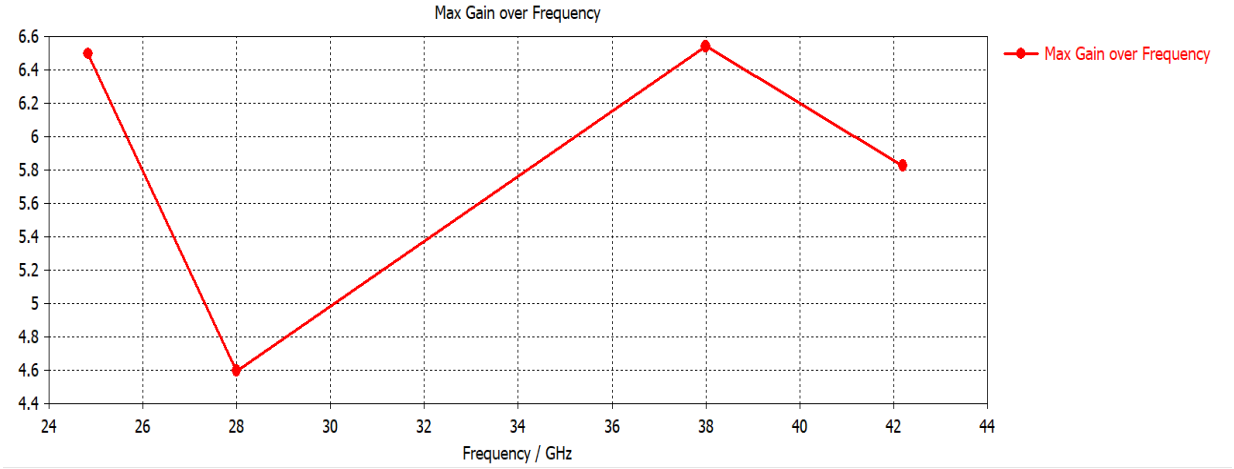

(b)

Figure-3.31: (a)Radiation Efficiency of the proposed antenna over the frequency of interest (b) Max gain over the frequency of interest

From the figure 3.25 we can see the antenna geometry and dimensions. This antenna is fabricated on a comparatively larger substrate than all the previous designs. The substrate is 12 mm X 12mm , and it is being enlarged to accommodate the edge launch connector for testing purposes. The microstrip feed in this design is 4.4mm in length, almost a two time jump from the Model-4 design. Also noticeable is the enhanced smoothing of the edges to reduce radiating edges. The radius of outer ring and inner ring curves are kept same as the Model-4 case. This antenna is simulated using a discrete port with 50 ohms impedance. As we will be using a 50 Ohm edge launch connector for testing purposes, we can consider that 50 Ohm discrete port to be lumped element representation of our SMK connector. The S_{11} response for this particular model is shown in figure 3.26. We can see that there are noticeable resonances at frequencies 24.838 GHz, 28.035 GHz, 38.021 GHz, and 42.656 GHz. Among all these bands the first three resonances are right in the FCC designated 5G band [55]. The finale resonance is in the 42 GHz range, which is being considered by FCC for 5G frequency allocation [55]. The bandwidth for each of these bands are shown in Table 3.4. Here, we are calculating -6dB bandwidth from the S11 response, as it is the half power point.

Table 3.5

-6 dB (1/2 power point) Bandwidth at each radiating band

Frequency range	Bandwidth
24.767 -25.046 GHz	279 MHz
27.811 GHz- 28.246 GHz	435 MHz
37.702 GHz – 38.397 GHz	695 MHz
42.076 GHz-43.082 GHz	1 GHz

We can see from the table 3.3 that this antenna has a fair bandwidth at all of the 5G bands it covers. In a microstrip antenna with complicated structure, there is always a trade off between frequencies excited and bandwidth covered. In this case, the antenna resonates at 4 mm wave 5G bands with suitable bandwidths. We can also see that, this antenna has its greatest mm-wave 5G bandwidth at 42 GHz band, which FCC will soon put to spectrum auctioning along with the 26 GHz band [55].

From surface current distributions and far field plots at figure 3.27-3.30, we can see persistent sharp beams with two directional radiating lobes. From the figures we can see that all the radiation beams are persistent with their surface current distribution. For the 24 GHz case in figure 3.27, one can argue that the beam is not positioned along the most intense surface current distribution path. The answer here is that, along the Y axis of the antenna, the radiating structure is coupled better with the whole structure resonating at once. But along X axis of the antenna only half the structure is excited in each cycle. As a result, even though the absolute result is showing more surface current intensity along X axis, the structure is excited better along Y axis, hence the beams are well positioned along f=90° axis. The beam diversity of this antenna is very apparent from the position of beam at each resonance frequency. At 24.838 GHz the beam is positioned at f=90°. At 28 GHz it's positioned diagonally making the phi approximately 45°. At 38 GHz it's positioned again along f=90°, and at 42.2 GHz, it's positioned along f=0°. So, along with directivity this antenna also provides some nice beam diversity. One can manipulate the direction of beam by clever positioning of many antennas to cover both f=0° and f= 90° axes. The compact profile of the beam could also facilitate better isolation while in use in a massive MIMO system. The simulated radiation efficiency of this antenna is also in the range of 85%-

90% , as shown in the plot of figure- 3.31(a). Along with the high gain it offers in the range of 4.8 dB- 6.5 dB, which is shown in figure- 3.31(b), this could be a better solution for a 5G system, where the signal is prone to absorption and attenuation. The progression of this antenna design is shown through the evolution of S_{11} response in the figure-3.32 below. For perspective, I have marked the resonance points of the final design in the figure. We wrap up this chapter here, and in next chapter we will go through the measurements from the fabricated prototype and how it compares to the simulated results.

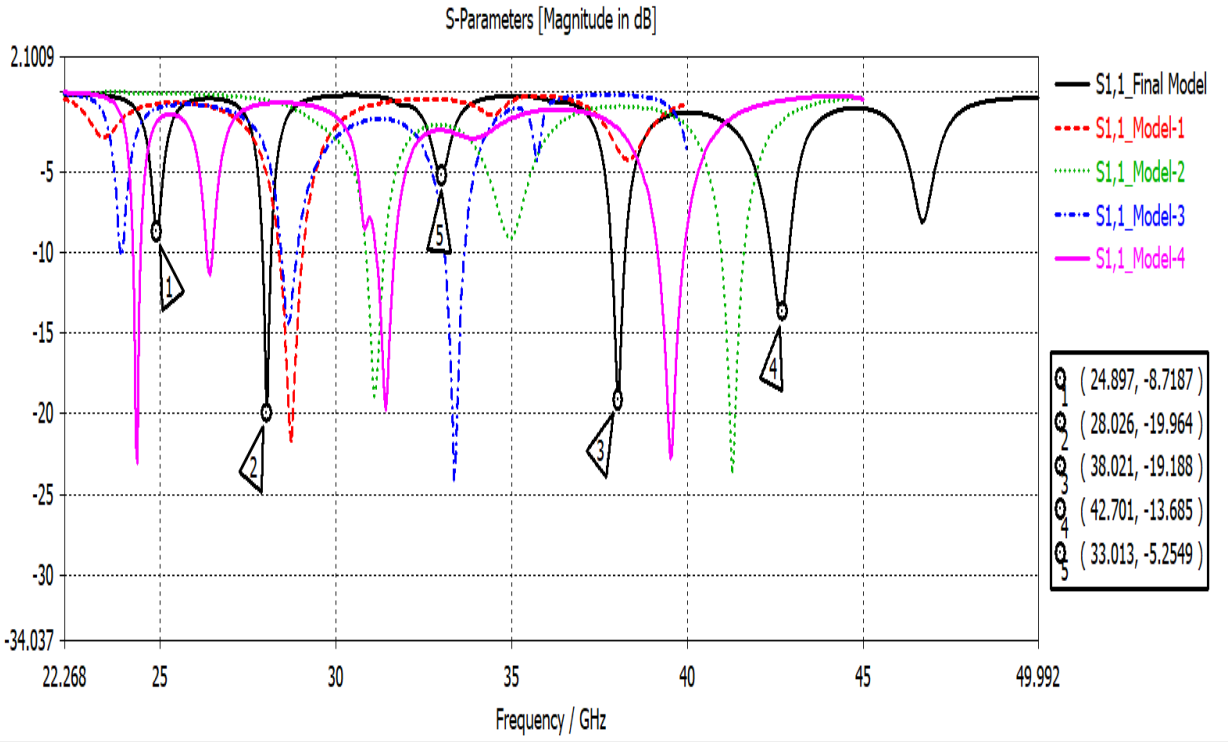

Figure-3.32 : Comparison of S_{11} responses of the 5 models presented

CHAPTER IV

EXPERIMENTAL RESULT AND CONCLUSION

4.1: Experimental Result

In the previous chapter we've described the numerical design and analysis of the new mm wave 5G antenna. Since this is a planar Antenna, it is basically a printed circuit board with a full ground on the back and special trace geometry on the front. The substrate used for printing is Rogers RT Duroid 5880, with a dielectric constant of 2.2 and a loss tangent of 0.0001. The fabricated prototype is shown in figure 4.1 .

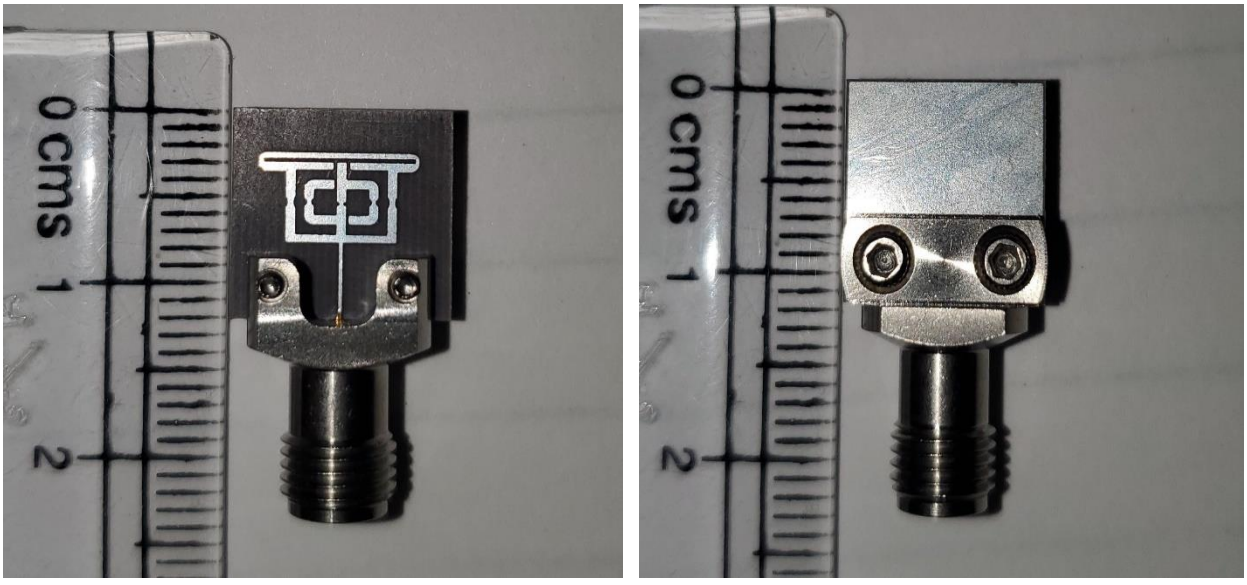

(a) (b)

Figure-4.1: (a) Front view of the proposed antenna (b) Back View of the proposed antenna

For the connector we have chosen lightweight and compact SMK connector FMCN1494. In a practical mm wave system, this type of antenna will be fed by a matching network originating from an oscillator or IC. So the connector won't effect the real life performance of this antenna. To test the antenna an Agilent E8364B vector network analyzer is used. It has a range of 10MHz-50 GHz, and we used it in a single port mode to measure the S_{11} response of the antenna. Since we were lacking a 2.92mm adapter for our 2.92 mm SMK connector, we used an adapter for 2.42mm connector which is rated at 27 GHz. This mismatch at the connector input gave us a shifted S11 response and increased reflection in frequencies expected to have resonances. The result is shown in figure- 4.2.

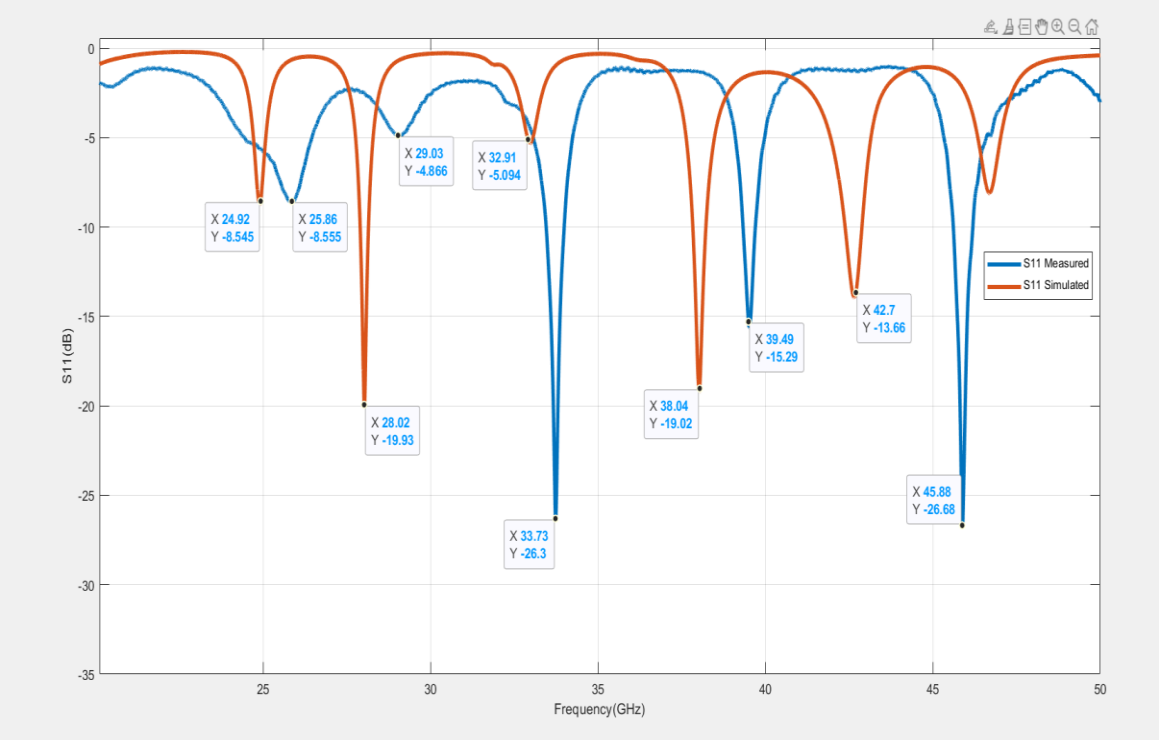

Figure-4.2: Plot of Simulated and measured S_{11} response

From the combined plot of simulated and measured responses, we can see that due to the consequence of the mismatch, there are major shifts in the resonance frequency response of the antenna. The simulated resonance at 24.92 GHz has shifted to 25.86 GHz with almost same level of S_{11} magnitude but bigger -6dB bandwidth. The resonance at 28.02 GHz shifted to 29.03 GHz, but lost significant amount of S_{11} magnitude which is attained by the resonance at 33.73 GHz. In simulation the lowest S_{11} magnitude at 33 GHz range was -5 dB, but as a result of the mismatch it became resonant during experiment. The resonance at 38.04 GHz shifted 39.49 GHz, but it is still in the 5G band. The resonance at 42.7GHz shifted to 45.88 Ghz due to dimension mismatch of the adapter and connector. But even with the mismatch one thing is apparent, this antenna has resonances at frequencies we simulated it for, no matter how little the spike at that frequency is. The point here is the spike at and around that frequency. Now, we will look at the stand alone experimental result and calculate the -6 dB bandwidth of the antenna.

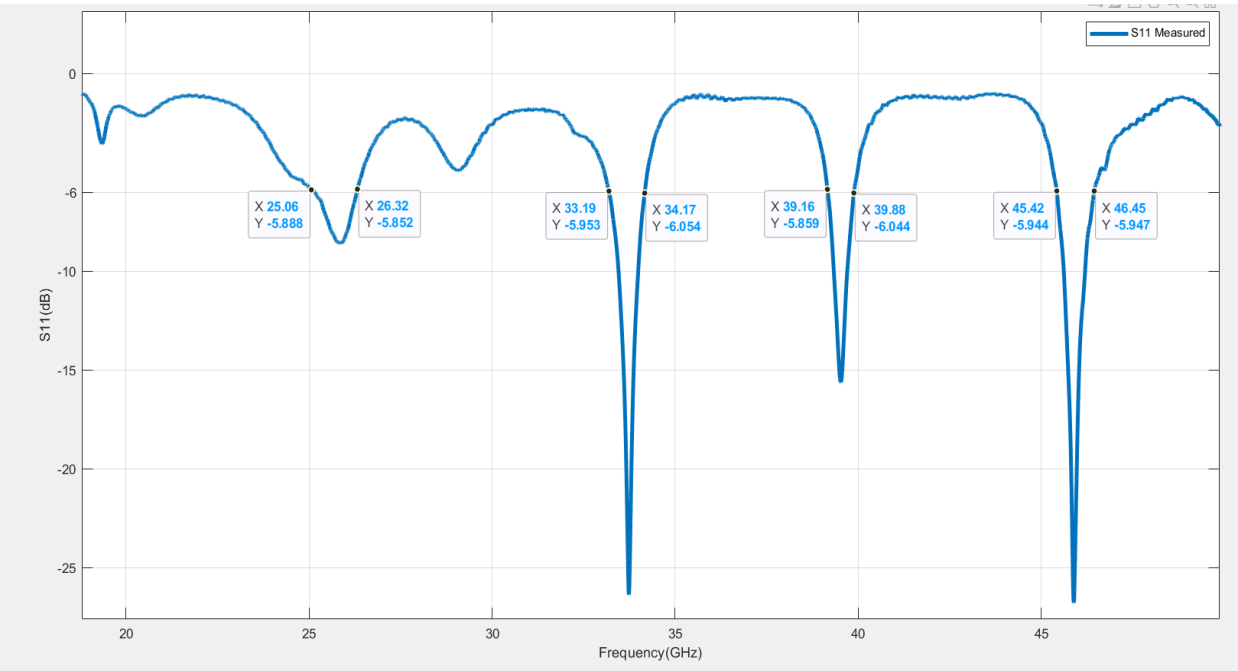

Figure-4.3: Measured S_{11} response with marked datapoints

Table-4.1

-6 dB banwidth and frequency band of the antenna

Frequency Range	Bandwidth
25.06-26.32	1.26 GHz
33.19-34.17	980 MHz
39.16-39.88	720 MHz
45.42-46.45	1.03GHz

We have tested the antenna with an 2.9mm to 2.4mm adapter. The results can be seen in figure-4.4.

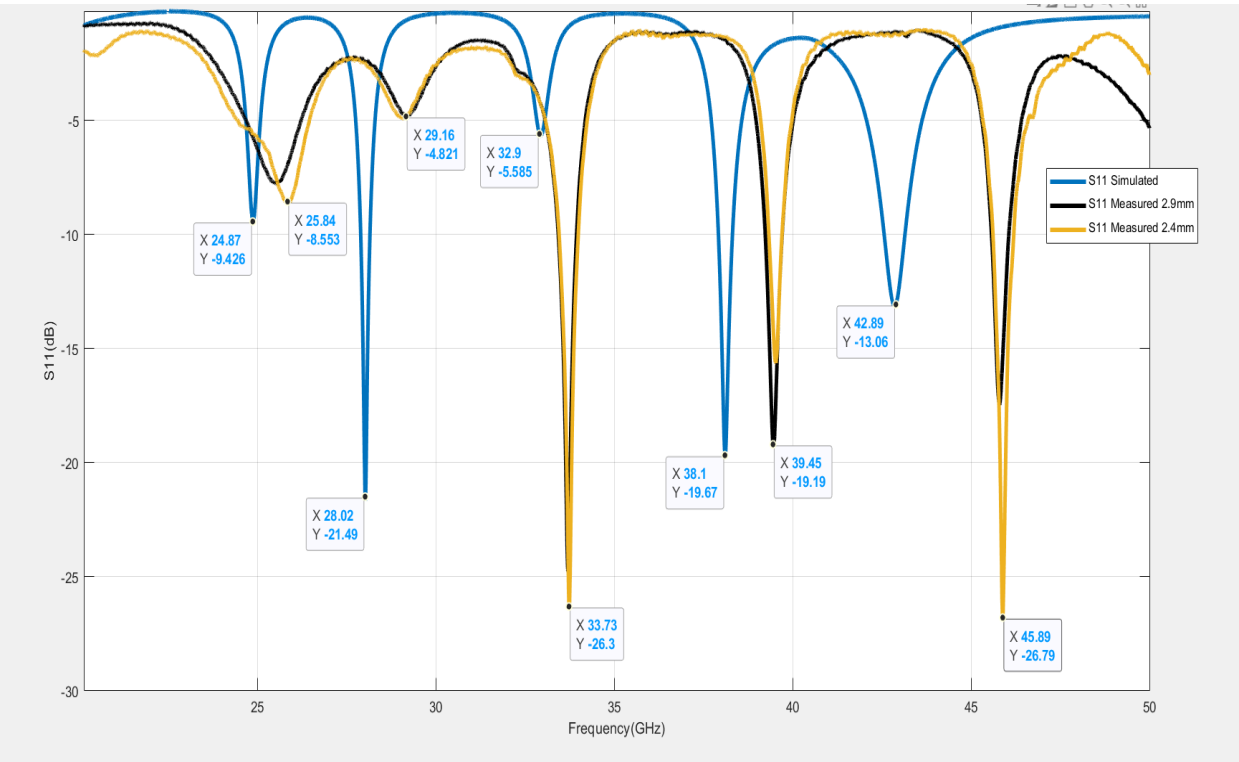

Figure-4.4: Simulated and measured S11 response of the antenna

From the measurements we can see that measurement results are almost same as the 2.4 mm adapter, even though we have used a 2.9mm adapter to connect the antenna to VNA. One reason of this shift could be the lack of modelling the connector. As we considered the connector as a lumped 50 ohm impedance in CST, the size of the connector may have affected the results. As the connector has parts which is connected to ground but placed on the side of the transmitting element, their could be some capacitive coupling and an elongation of the ground plane also could've affected the result. One other thing which could've affected the result is the substrate. If the substrate has a different dielectric constant than the constant it's been simulated for, the result will surely get affected. I believe with a very compact connector we could get a better response from the antenna, as all the resonances can be seen present here. Just not in the exact frequency range.

4.2: CONCLUSION

In this thesis we have proposed a metamaterial inspired 5G antenna that is resonant at four mm wave bands, which are designated for use in mm wave 5G communication by FCC. With its very narrow beam it is suitable for a massive MIMO application, where many antennas are needed to be placed in a close proximity. By perfect positioning of multiple antennas, beam diversity could be created easily, which in turn may reduce the use of beamforming in 5G system. High gain of this antenna will also help in reducing the loss in the channel such as absorption, attenuation, etc. The simulated radiation efficiency of this antenna is in the range of 85-90% . If we consider a deviation of 5-10% in practical measurements, this antenna will still be a good one with a radiation efficiency of 75-80% in practical environment. The compact size of this antenna also makes it suitable for placement in a cellphone or any miniature devices.

REFERENCES

[1] M. M. Hasan, M. R. I. Faruque, and M. T. Islam, "Dual band metamaterial antenna for LTE/bluetooth/WiMAX system," *Sci. Rep.*, vol. 8, no. 1, pp. 1–17, 2018, doi: 10.1038/s41598-018-19705-3.

[2] Y. He and G. V. Eleftheriades, "Metamaterial-inpsired wideband circular monopole antenna," *IEEE Antennas Propag. Soc. AP-S Int. Symp.*, pp. 50–51, 2012, doi: 10.1109/APS.2012.6349423.

[3] W. Liu, Z. N. Chen, and X. Qing, "Metamaterial-Based Low-Pro fi le," vol. 62, no. 3, pp. 1165–1172, 2014.

[4] G. Sri Latha, G. S. N. Raju, and P. A. Sunny Dayal, "Design and Analysis Metamaterial Inspired Wearable Antenna for 2.45GHz ISM Band," *Proc. Int. Conf. Microelectron. ICM*, vol. 2020-Decem, no. Icm, pp. 7–10, 2020, doi: 10.1109/ICM50269.2020.9331772.

[5] H. Cheng *et al.*, "A compact antipodal Vivaldi antenna with metamaterial half-lens for beam control," *J. Phys. D. Appl. Phys.*, vol. 54, no. 20, p. 205104, 2021, doi: 10.1088/1361-6463/abe485.

[6] M. N. Hasan, S. Bashir, and S. Chu, "Dual band omnidirectional millimeter wave antenna for 5G communications," *J. Electromagn. Waves Appl.*, vol. 33, no. 12, pp. 1581–1590, 2019, doi: 10.1080/09205071.2019.1617790.

[7] H. Ullah and F. A. Tahir, "A High Gain and Wideband Narrow-Beam Antenna for 5G Millimeter-Wave Applications," *IEEE Access*, vol. 8, pp. 29430–29434, 2020, doi: 10.1109/ACCESS.2020.2970753.

[8] Z. Chen and Y. P. Zhang, “FR4 PCB grid array antenna for millimeter-wave 5G mobile communications,” *2013 IEEE MTT-S Int. Microw. Work. Ser. RF Wirel. Technol. Biomed. Healthc. Appl. IMWS-BIO 2013 - Proc.*, pp. 13–15, 2013, doi: 10.1109/IMWS-BIO.2013.6756214.

[9] H. Alsaif and M. A. H. Eleiwa, “Compact design of 2 × 2 mimo antenna with super-wide bandwidth for millimeters wavelength systems,” *Symmetry (Basel).*, vol. 13, no. 2, pp. 1–8, 2021, doi: 10.3390/sym13020233.

[10] M. Khalily, R. Tafazolli, T. A. Rahman, and M. R. Kamarudin, “Design of Phased Arrays of Series-Fed Patch Antennas with Reduced Number of the Controllers for 28-GHz mm-Wave Applications,” *IEEE Antennas Wirel. Propag. Lett.*, vol. 15, no. c, pp. 1305–1308, 2016, doi: 10.1109/LAWP.2015.2505781.

[11] P. Mogensen *et al.*, “B4G local area: High level requirements and system design,” *2012 IEEE Globecom Work. GC Wkshps 2012*, no. 3, pp. 613–617, 2012, doi: 10.1109/GLOCOMW.2012.6477644.

[12] P. Mogensen *et al.*, “5G small cell optimized radio design,” *2013 IEEE Globecom Work. GC Wkshps 2013*, no. 3, pp. 111–116, 2013, doi: 10.1109/GLOCOMW.2013.6824971.

[13] P. Mogensen *et al.*, “Centimeter-wave concept for 5G ultra-dense small cells,” *IEEE Veh. Technol. Conf.*, vol. 2015-Janua, no. January, 2014, doi: 10.1109/VTCSpring.2014.7023157.

[14] O. El Ayach, S. Rajagopal, S. Abu-Surra, Z. Pi, and R. W. Heath, “Spatially sparse precoding in millimeter wave MIMO systems,” *IEEE Trans. Wirel. Commun.*, vol. 13, no. 3, pp. 1499–1513, 2014, doi: 10.1109/TWC.2014.011714.130846.

[15] S. K. Yong and C. C. Chong, “An overview of multigigabit wireless through millimeter wave technology: Potentials and technical challenges,” *Eurasip J. Wirel. Commun. Netw.*, vol. 2007, 2007, doi: 10.1155/2007/78907.

[16] G. Hendrantoro, R. J. C. Bultitude, and D. D. Falconer, “Use of cell-site diversity in millimeter-wave fixed cellular systems to combat the effects of rain attenuation,”

IEEE J. Sel. Areas Commun., vol. 20, no. 3, pp. 602–614, 2002, doi: 10.1109/49.995519.

[17] D. Abdorahimi and A. M. Sadeghioon, "Comparison of radio frequency path loss models in soil for wireless underground sensor networks," *J. Sens. Actuator Networks*, vol. 8, no. 2, 2019, doi: 10.3390/jsan8020035.

[18] C. Technology, *Millimeter- Wave Antennas: Configurations and Applications*. .

[19] "FEDERAL COMMUNICATIONS COMMISSION OFFICE OF ENGINEERING AND TECHNOLOGY Bulletin Number 70 Millimeter Wave Propagation: Spectrum Management Implications," 1997.

[20] I. Press and F. Canavero, *MILLIMETER WAVE COMMUNICATION SYSTEMS*. .

[21] G. R. Maccartney, J. Zhang, S. Nie, and T. S. Rappaport, "Path loss models for 5G millimeter wave propagation channels in urban microcells," *GLOBECOM - IEEE Glob. Telecommun. Conf.*, pp. 3948–3953, 2013, doi: 10.1109/GLOCOM.2013.6831690.

[22] R. W. Ziolkowski and E. Heyman, "Wave propagation in media having negative permittivity and permeability," *Phys. Rev. E - Stat. Physics, Plasmas, Fluids, Relat. Interdiscip. Top.*, vol. 64, no. 5, p. 15, 2001, doi: 10.1103/PhysRevE.64.056625.

[23] R. M. Walser, A. P. Valanju, and P. M. Valanju, "Comment on 'extremely low frequency plasmons in metallic mesostructures,'" *Phys. Rev. Lett.*, vol. 87, no. 11, pp. 119701–1, 2001, doi: 10.1103/PhysRevLett.87.119701.

[24] J.B. Pendry, A. J. Holden, D. J. Robbins, and W. J. Stewart, "Magnetism from conductors, and enhanced non-linear phenomena," *IEEE Trans. Microw. Theory Tech.*, vol. 47, no. 11, pp. 2075–2084, 1999.

[25] D. Bílková, "Modern methods of parametric estimation: Estimation using L-moments and TL-moments," *APLIMAT 2015 - 14th Conf. Appl. Math. Proc.*, pp. 53–79, 2015.

[26] O. Altıntaş, M. Aksoy, and E. Ünal, "Design of a metamaterial inspired omega shaped resonator based sensor for industrial implementations," *Phys. E Low-Dimensional Syst. Nanostructures*, vol. 116, no. August 2019, 2020, doi:

10.1016/j.physe.2019.113734.

[27] N. Wongkasem and M. Ruiz, “Multi-negative index band metamaterial-inspired microfluidic sensors,” *Prog. Electromagn. Res. C*, vol. 94, no. June, pp. 29–44, 2019, doi: 10.2528/PIERC19041503.

[28] K. V. Sreekanth *et al.*, “Extreme sensitivity biosensing platform based on hyperbolic metamaterials,” *Nat. Mater.*, vol. 15, no. 6, pp. 621–627, 2016, doi: 10.1038/nmat4609.

[29] M. Aslinezhad, “High sensitivity refractive index and temperature sensor based on semiconductor metamaterial perfect absorber in the terahertz band,” *Opt. Commun.*, vol. 463, p. 125411, 2020, doi: 10.1016/j.optcom.2020.125411.

[30] F. Lu, Q. Tan, Y. Ji, Q. Guo, Y. Guo, and J. Xiong, “A novel metamaterial inspired high-temperature microwave sensor in harsh environments,” *Sensors (Switzerland)*, vol. 18, no. 9, 2018, doi: 10.3390/s18092879.

[31] A. A. Althuwayb, “Enhanced radiation gain and efficiency of a metamaterial-inspired wideband microstrip antenna using substrate integrated waveguide technology for sub-6 GHz wireless communication systems,” *Microw. Opt. Technol. Lett.*, no. November 2020, pp. 1–7, 2021, doi: 10.1002/mop.32825.

[32] H. Li *et al.*, “Directive metamaterial antenna using high impedance surface,” *2004 4th Int. Conf. Microw. Millim. Wave Technol. ICMMT 2004*, pp. 480–482, 2004, doi: 10.1109/icmmt.2004.1411571.

[33] Y. Lee, X. Lu, Y. Hao, S. Yang, J. R. G. Evans, and C. G. Parini, “Directive millimetrewave antennas using freeformed ceramic metamaterials in planar and cylindrical forms,” *2008 IEEE Int. Symp. Antennas Propag. Usn. Natl. Radio Sci. Meet. APSURSI*, no. 1, pp. 28–31, 2008, doi: 10.1109/APS.2008.4619479.

[34] A. Alù and N. Engheta, “All optical metamaterial circuit board at the nanoscale,” *Phys. Rev. Lett.*, vol. 103, no. 14, 2009, doi: 10.1103/PhysRevLett.103.143902.

[35] A. Krasnok, M. Tymchenko, and A. Alù, “Nonlinear metasurfaces: a paradigm shift in nonlinear optics,” *Mater. Today*, vol. 21, no. 1, pp. 8–21, 2018, doi: 10.1016/j.mattod.2017.06.007.

[36] J. B. Pendry, “Negative refraction makes a perfect lens,” *Phys. Rev. Lett.*, vol. 85, no. 18, pp. 3966–3969, 2000, doi: 10.1103/PhysRevLett.85.3966.

[37] F. Qin *et al.*, “Hybrid bilayer plasmonic metasurface efficiently manipulates visible light,” *Sci. Adv.*, vol. 2, no. 1, pp. 1–9, 2016, doi: 10.1126/sciadv.1501168.

[38] D. Schurig *et al.*, “Metamaterial electromagnetic cloak at microwave frequencies,” *Science (80-.).*, vol. 314, no. 5801, pp. 977–980, 2006, doi: 10.1126/science.1133628.

[39] A. Alù and N. Engheta, “Cloaking a sensor,” *Phys. Rev. Lett.*, vol. 102, no. 23, 2009, doi: 10.1103/PhysRevLett.102.233901.

[40] A. Alipour, A. Mir, and A. Farmani, “Ultra high-sensitivity and tunable dual-band perfect absorber as a plasmonic sensor,” *Opt. Laser Technol.*, vol. 127, no. February, p. 106201, 2020, doi: 10.1016/j.optlastec.2020.106201.

[41] H. Li, Y. Li, L. Chang, W. Sun, X. Qin, and H. Wang, “A Wideband Dual-Polarized Endfire Antenna Array With Overlapped Apertures and Small Clearance for 5G Millimeter-Wave Applications,” *IEEE Trans. Antennas Propag.*, vol. 69, no. 2, pp. 815–824, 2020, doi: 10.1109/tap.2020.3016512.

[42] I. Lima De Paula *et al.*, “Cost-Effective High-Performance Air-Filled SIW Antenna Array for the Global 5G 26 GHz and 28 GHz Bands,” *IEEE Antennas Wirel. Propag. Lett.*, vol. 20, no. 2, pp. 194–198, 2021, doi: 10.1109/LAWP.2020.3044114.

[43] M. A. Ashraf, O. M. Haraz, and S. Alshebeili, “Compact size enhanced gain switched beam conformal antipodal tapered slot antenna system for 5G MIMO wireless communication,” *2015 IEEE 11th Int. Conf. Wirel. Mob. Comput. Netw. Commun. WiMob 2015*, pp. 613–618, 2015, doi: 10.1109/WiMOB.2015.7348019.

[44] Z. Gan and Z. H. Tu, “Dual-Mode Conjoint Patch-Pair for 5G Wideband Patch Antenna Array Application,” *IEEE Antennas Wirel. Propag. Lett.*, vol. 20, no. 2, pp. 244–248, 2021, doi: 10.1109/LAWP.2020.3046759.

[45] O. M. Dardeer, H. A. Elsadek, H. M. Elhennawy, and E. A. Abdallah, “Single-fed dual wideband filtenna for 4G/5G mobile applications,” *Int. J. RF Microw. Comput.*

Eng., no. December 2020, pp. 1–12, 2021, doi: 10.1002/mmce.22616.

[46] K. Liu, S. Yang, S. W. Qu, Y. Chen, M. Huang, and J. Hu, "A low-profile wide-scanning fully metallic lens antenna for 5G communication," *Int. J. RF Microw. Comput. Eng.*, no. December 2020, pp. 1–8, 2021, doi: 10.1002/mmce.22584.

[47] W. Lee, Y. K. Hong, H. Won, M. Choi, N. S. Jeong, and J. Lee, "Dual-band (5G millimeter-wave and dedicated short-range communication) stacked patch antenna for advanced telematics applications," *Microwave and Optical Technology Letters*, vol. 61, no. 5. pp. 1381–1387, 2019, doi: 10.1002/mop.31737.

[48] S. Science, N. Series, and G. Crater, "Metamaterials and Negative Refractive Index Author (s): D . R . Smith , J . B . Pendry and M . C . K . Wiltshire," vol. 305, no. 5685, pp. 788–792, 2015.

[49] X. Chen, T. M. Grzegorczyk, B. Wu, J. Pacheco, and J. A. Kong, "ɨ 2 ʿ 1 +," vol. 016608, no. July, pp. 1–7, 2004, doi: 10.1103/PhysRevE.70.016608.

[50] S. Roy and U. Chakraborty, "Metamaterial Based Dual Wideband Wearable Antenna for Wireless Applications," *Wirel. Pers. Commun.*, vol. 106, no. 3, pp. 1117–1133, 2019, doi: 10.1007/s11277-019-06206-3.

[51] D. K. Misra, *Radio-Frequency and Microwave Communication Circuits: Analysis and Design: Second Edition*. 2004.

[52] M. V. Schneider, "Microstrip Lines for Microwave Integrated Circuits," *Bell Syst. Tech. J.*, vol. 48, no. 5, pp. 1421–1444, 1969, doi: 10.1002/j.1538-7305.1969.tb04274.x.

[53] M. N. Hasan, S. Chu, and S. Bashir, "A DGS monopole antenna loaded with U-shape stub for UWB MIMO applications," *Microwave and Optical Technology Letters*, vol. 61, no. 9. pp. 2141–2149, 2019, doi: 10.1002/mop.31877.

[54] N. E. Lindenblad, "Slot antennas," *Proc. IRE*, vol. 35, no. 12, pp. 1472–1479, 1947, doi: 10.1109/JRPROC.1947.234572.

[55] "America's 5G Future | Federal Communications Commission." https://www.fcc.gov/5G (accessed Apr. 25, 2021).

BIOGRAPHICAL SKETCH

Mohammad Ashif Hossain Chowdhury received his B.Sc. in Electrical and Electronic Engineering from Chittagong University of Engineering and Technology, Bangladesh in 2013. He joined Dr. Heinrich Foltz's research group at UTRGV in 2019 with 'Presidential Graduate Research Assistantship' award. Before joining UTRGV he had been working at Bangladesh Atomic Energy Commission as an Engineer. His research interest is in the field of applied electromagnetics, optics, plasmonics, high frequency electronics etc. Along with his research in applied electromagnetics, he also worked on programming ARM microcontrollers for a device developed at the UTCRS (University Transportation Center for Railway Application), during summer 2020. He was awarded a Master of Science in Engineering in Electrical Engineering from the University of Texas Rio Grande Valley in May of 2021. He will be joining the University of Utah as a PhD student in the ECE department from fall 2021. He can be reached at ashif.baec@gmail.com.